THE EFFECT OF NITROGEN AND TITANIUM ON THE TOUGHNESS OF HIGH STRENGTH SAW WELD DEPOSITS

by

Stephen W. Stanko

B.S.M.E., UNITED STATES NAVAL ACADEMY
(1980)

SUBMITTED TO THE DEPARTMENTS OF MATERIALS SCIENCE AND ENGINEERING AND OCEAN ENGINEERING IN PARTIAL FULFILLMENT OF THE REQUIREMENTS FOR THE DEGREES OF

MASTER OF SCIENCE IN MATERIALS ENGINEERING

and

NAVAL ENGINEER

at the

MASSACHUSETTS INSTITUTE OF TECHNOLOGY

May 12, 1989

Signature of author Stephen W. Stanko
Department of Ocean Engineering
May 12, 1989

Certified by Thomas W. Eagar
Professor Thomas W. Eagar
Thesis Supervisor

Approved by B F Tibbitts
Professor Barry F. Tibbitts
Thesis Reader

Accepted by A. Douglas Carmichael
Professor A. Douglas Carmichael, Chairman
Department Graduate Committee
Department of Ocean Engineering

Accepted by Samuel M. Allen
Professor Samuel M. Allen, Chairman
Department Committee on Graduate Students
Department of Materials Science and Engineering

89 10 10 138

THE EFFECT OF NITROGEN AND TITANIUM ON THE TOUGHNESS OF HIGH STRENGTH SAW WELD DEPOSITS

by

Stephen W. Stanko

Submitted to the Departments of Materials Science and Engineering and Ocean Engineering on May 12, 1989 in partial fulfillment of the requirements for the degrees of Master of Science in Materials Engineering and Naval Engineer.

ABSTRACT

This thesis involves the study of nitrogen and titanium additions during submerged arc welding of HY-100. By comparing the properties of butt-welded HY-100 plate under various levels of nitrogen and titanium contamination, quantitative conclusions about the effects of these elements were achieved. The ultimate goal of this work was to further the development of consumables and procedures for joining high strength steels.

In this endeavor, ten butt-welded HY-100 sample plates were produced using the submerged arc welding process. With the exception of incremental increases in the nitrogen and titanium concentrations, the welding parameters were held constant for all the test welds. Evaluating and quantifying these compositional variations required comprehensive metallographic examinations, chemical analyses and mechanical testing.

Nitrogen was shown to degrade the weld deposit toughness, as measured by the ductile-to-brittle transition temperature, at a rate of +14°C for every 0.01 weight percent increase. Examination of the microstructure revealed that this degradation was primarily the result of a sharp increase in coarse ferrite with aligned martensite-austenite-carbide constituent at the expense of fine acicular ferrite, and a significant increase in the amount of M-A constituent. This investigation supports the contention that nitrogen acts in the same manner as carbon by segregating to carbon-enriched areas; thus, effectively increasing the amount of M-A present and enhancing its embrittling influence.

Similarly, titanium above 0.009 weight percent was shown to degrade toughness. In this case, the DBTT increased at a rate of +11°C for every 0.01 weight percent increase in titanium. Examination of the microstructure revealed that this degradation was predominantly due to a sharp increase in ferrite with aligned M-A-C which exhibited a particularly high degree of crystallographic orientation and veining. In addition there was a substantial increase in embrittling inclusions which were believed to degrade toughness through precipitation and dispersion hardening effects.

It is concluded that for the welding of high strength steels, nitrogen concentrations need to be held as low as possible. In this regard, it may prove beneficial to use better argon shielding methods for steelmaking and vacuum degassing during SAW electrode production in order to achieve these lower levels of nitrogen. Furthermore, titanium concentrations should be held below 0.01 weight percent while the exact concentration needs to be based on a balance with boron, nitrogen, aluminum and oxygen.

Thesis Supervisor: Dr. Thomas W. Eagar
Title: Professor of Materials Engineering

Thesis Reader: Capt. Barry F. Tibbitts
Title: Professor of Ocean Engineering

TABLE OF CONTENTS

List of Figures

List of Tables

ACKNOWLEDGMENTS

I would first like to express my deep gratitude and appreciation to Professor Thomas Eagar. His unbounded encouragement and valued guidance throughout this work has been of crucial importance.

Secondly, I would like to acknowledge the financial support of this research which was provided by the Office of Naval Research and David Taylor Research Center, United States Department of the Navy. This includes the generous donation of materials and technical support provided by David Taylor Research Center. In this regard, special thanks goes to Paul Holsberg and Gene Franke for their enthusiastic advice, technical support and assistance at every turn.

I am grateful for the assistance and friendship offered by all the staff and members of the welding group. This includes special mention of Bruce Russell, Julie Putnam and Irvin Puffer who provided needed help in the weld preparation phase of this work. All of these people provided invaluable help when most needed.

A special thanks goes to my wife, Patty, and my son, Leo, for their patience, love and support throughout my years at M.I.T. It is to them that I dedicate this thesis.

Lastly, I would like to express a deep appreciation to my parents for the wise advise, abundant love and support they have always given me.

CHAPTER 1

INTRODUCTION

1.1 Overview

The negative effects of nitrogen on increasing the hardness and lowering the toughness of HY-100 and higher strength steels has become of particular interest to the U.S. Navy in recent years. Application of these steels to naval construction has expanded the awareness of the sensitivity of these higher strength steels to notch toughness.

The increased effect of nitrogen on notch sensitivity is partially due to the modern use of desulfurization technology in the production of these steels. Since sulfur is a surfactant, it reduces nitrogen pick-up during steelmaking by competing for surface sites on the liquid pool with the net impact of raising the level of nitrogen in the base metal. Additionally, it is known that the detrimental effects of nitrogen are greater in higher strength steels. As a result, the control of nitrogen becomes more important as the strength of naval construction steels increase.

During welding, dilution of small amounts of nitrogen from the parent plate and from consumable sources into the weld can have a marked effect on microstructure and toughness. Atmospheric nitrogen is also introduced into the weld pool. A recent study [11] has shown that there are three basic mechanisms for atmospheric nitrogen contamination. These include absorption on the heated plate and filler metal before the flux becomes molten, direct atmospheric entrainment into the welding arc due to the electromagnetic pressure of the arc plasma and transport from contaminated flux. The negative impact on weld toughness from this source of contaminating nitrogen

can be of particular concern especially in shielded metal arc welding (SMAW). However, in the case of the submerged arc welding (SAW) process, the high deposition rate of this process is believed to minimize the exposure of the weld pool to contaminating gases. Thus, it is anticipated that atmospheric nitrogen contamination using the SAW process is insignificant.

Through the use of metallographic examination, the impact of nitrogen on toughness can be clarified when the influence of this impurity is correlated to the microstructural details. Previous research shows significant correlation between the ferrite grain size and the notch toughness of the weld. As the nitrogen content in the weld increases, the grain size becomes coarser. Additionally, there is a tendency toward grain boundary fracture and nitrogen compound precipitation with the increasing presence of nitrogen and nitride forming elements.

In submerged arc weld deposits of lower strength steels, the toughness has been improved by increasing the content of acicular ferrite and decreasing the content of polygonal ferrite. This is achieved through an ideal balance of titanium and boron in titanium-boron bearing welding consumables. One hypothesis proposed by Japanese investigators indicates that segregation of nitrogen in the weld metal promotes the formation of martensite-austenite (M-A) constituent which is believed to be an initiation site for cleavage fracture. By reducing or combining the free nitrogen in the weld deposit, the fraction of M-A constituent may be reduced and toughness improved.

Improving the toughness of welds in high strength steels involves reducing the contamination of the molten weld pool by nitrogen and in developing toughness enhancing welding consumables. In this regard, the Al-Ti-O-B-N balance must be closely controlled in order to optimize weld metal toughness. Future research is needed in developing consumables to accommodate wide ranges of nitrogen content in high strength steel weldments.

1.2 Proposed Work

A total of ten butt-welded, 3/4 inch thick, HY-100 sample plates were produced using the submerged arc welding process which was slightly modified by using an auxiliary argon shielding device to minimize contamination from air trapped in the flux burden. These welds were produced in accordance with MILSPEC requirements [1] which specified various SAW parameters for HY-100 steel. The first two sample plates were baseline plates produced without introducing any contamination. The next four sample plates contain various levels of nitrogen contamination which was obtained by introducing a manganese nitride powder in the weld groove. The following three sample plates were prepared with a constant level of nitrogen contamination and varying amounts of titanium contamination which was obtained by introducing titanium powder in the weld groove. Finally, the last plate attempted to achieve a 3.5:1 stoichiometric weight percent ratio of titanium/nitrogen contamination. The welding characteristics (current, voltage, travel speed, etc.) were held constant for all sample plates. In addition to the preparation of the welds, this research also required preparation for metallography, chemical analysis of each weld, interpretation of the microstructures and mechanical testing of the weld metal.

This research involved considerable lab work in preparation and evaluation of the welds. The plate, flux, and consumable electrode, each with low initial nitrogen contents, were provided by DTRC. Welding of the plates, preparation for metallography and microstructure evaluation were done at MIT. Chemical analysis was performed by LUVAK labs. Mechanical test specimens were prepared and broken at DTRC and evaluated at MIT.

CHAPTER 2

LITERATURE SURVEY

2.1 HY-100 Steel

HY-100 steel is a low carbon low alloy steel quenched and tempered to achieve a yield strength of 690 MPa.

It contains principal additions of Ni, Cr, Mo, and V and has a compositional range overlapping, but slightly higher than, that of HY-80 steel [2]. The higher strength of the HY-100 alloy is achieved by adjustments in the tempering temperature. Like HY-80, the quench and tempered microstructure of HY-100 steel consists of a bainitic-martensitic duplex structure. The elemental composition of the HY-100 steel plate used in this investigation is tabulated in Table 3.1.

2.2 The SAW Process

A significant portion of the cost of ship construction is attributed to welding operations. In recent years, the cost of ship construction has been substantially reduced by the cost effectiveness of the highly automated, high speed and high deposition rate submerged arc welding process. From the welder's standpoint, this is an attractive process due to the covered arc, reduced fume generation, and tolerance of joint inconsistencies.

Figure 2.1 shows the SAW process used in this investigation. As shown in this figure, the typical SAW setup was modified by adding an auxiliary argon gas shielding

device. The auxiliary argon shielding was used to displace air trapped in the flux burden thus minimizing, as much as possible, the introduction of hydrogen, nitrogen and oxygen from the atmosphere. By applying an electric arc to the workpiece, a molten pool of metal is formed beneath it. As illustrated, a portion of the flux blanket is melted into the puddle. The portion of the flux that is melted serves initially to protect the molten metal from the atmosphere and later to control the shape of the weld bead.

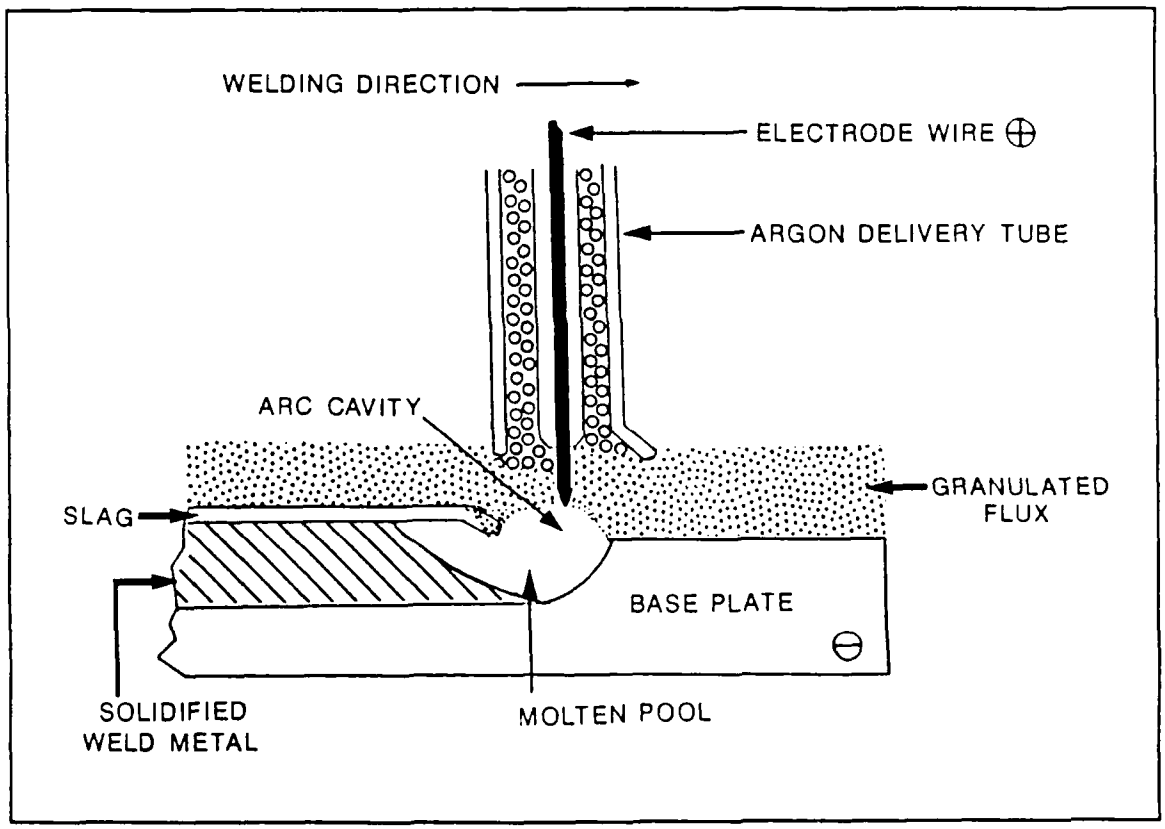

Figure 2.1 The SAW setup with an auxiliary argon shielding modification.

The most important property in evaluating the quality of high strength steel welds produced by the SAW process is the fracture toughness of the weld metal. This is most strongly influenced by carefully controlling the chemical composition and

thermal cycling of the weldment.

With regard to the SAW process, some of the key welding parameters that must be closely controlled in order to optimize fracture toughness include:

CONSUMABLE COMPOSITION
JOINT GEOMETRY
JOINT PREPARATION
VOLTAGE
CURRENT
TRAVEL SPEED
ELECTRODE STICKOUT
PREHEAT/INTERPASS TEMPERATURE
NUMBER OF PASSES
ELECTRODE FEED RATE

This study has strived to normalize all the welding parameters that influence the fracture toughness of the weld metal with the exception of the chemical composition. By systematically varying the chemical composition of nitrogen and titanium, it is hoped that their influence on the fracture toughness of HY-100 weldments can be quantified. This can not be accomplished unless a firm understanding of the impact of microstructural details on fracture toughness is achieved.

2.3 The Microstructure of HY-100 Steel Welds

HY-100 weld metal microstructural features are considered to have the most significant effect on the weld metal fracture toughness.

Weld metal microstructural development is complex but in simple terms may be considered dependent on chemical composition, cooling rate, austenite grain size and inclusion content [3]. In simplistic terms, upon weld metal cooling, equiaxed ferrite grains nucleate and grow from prior austenite grain boundaries (grain boundary ferrite). This is followed by the intragranular, inclusion assisted, nucleation of fine acicular ferrite. Finally, carbon-enriched regions between the acicular ferrite laths, or adjacent to grain boundary ferrite, may either transform to ferrite carbide aggregates or martensite, or may remain, untransformed, as retained austenite (microphases) [4].

In order to better understand this complex process, the following is a more detailed general discussion of the types of microstructures found in HY-100 weld metal. These microstructures are discrete in terms of the guidelines proposed by Hoekstra et al [5]. They have done much work in defining the microstructural constituents of high strength steel weld metal as summarized below.

2.3.1 Microstructural Features

PRIMARY microstructure develops during solidification and usually results in a cast structure exhibiting columnar grains. The length axis of these grains are parallel to the direction of the temperature gradient during solidification. Sometimes a dendritic substructure can be observed inside the columnar grains. Occurrence of this substructure is accompanied by segregation phenomena. During solidification δ-ferrite is formed first, followed by austenite at slightly lower temperatures. The austenitic (cast) structure is usually regarded as the primary microstructure, which is maintained during cooling until the $\gamma-\alpha$ transition is reached. During the $\gamma-\alpha$ transformation the secondary microstructure develops. Often, one of the transformation products is grain boundary ferrite, which marks the original austenitic grains. The primary microstructure therefore remains recognizable in as-deposited weld metal, particularly at moderate magnifications (up to 100X) [5].

SECONDARY microstructure of HY-100 weld metal develops on cooling during the $\gamma - \alpha$ transformation. Depending on cooling rate and chemical composition, several constituents may form. Although there is much ambiguity about nomenclature, the nomenclature proposed by Abson and Dolby [7] is generally accepted and is used here. The most important structural constituents are grain boundary ferrite, polygonal ferrite, ferrite with aligned M-A-C, acicular ferrite, martensite, and M-A microconstituent as described by Table 2.1.

Table 2.1 Description of weld metal microstructural constituents [6].

CONSTITUENT	DESCRIPTION	PREVIOUS DESCRIPTION
(PRIMARY FERRITE)		
Grain boundary ferrite	Veins or polygonal grains associated with austenite boundaries.	Proeutectoid ferrite, ferrite veins, blocky ferrite, polygonal ferrite, ferrite islands.
Intragranular polygonal ferrite	Polygonal grains found intragranularly larger than 3 times the surrounding ferrite laths or grains.	
Acicular ferrite	Widmanstatten ferrite grains found intragranularly. Also isolated laths of high aspect ratio.	Acicular ferrite.
Ferrite with aligned M-A-C	Two or more parallel laths of ferrite, where their aspect ratio is greater than 4:1.	Ferrite side plates, upper bainite, feathery bainite, lamellar product.
Martensite	Colony size must be larger than surrounding ferrite or grains.	Martensite laths.
(Microphase) M-A microconstituent	Blocky or needle-like microphase consisting of retained austenite, lath martensite, and twinned martensite.	Ferrite-carbide aggregate, martensite, lath ferrite, high C martensite.

Some of the other popular descriptions for these microstructural features are presented in Table 2.2.

Table 2.2 Review of microstructural terminology used for high strength steel weld metals [3].

Dube C A Aaronson H I Cochrane R C	Widgery D J	Abson D J	Others	Japanese researchers
Allotriomorphic (polygonal) ferrite	Proeutectoid ferrite	Grain boundary ferrite	Proeutectoid ferrite, Grain boundary ferrite	Proeutectoid ferrite, Grain boundary ferrite
	Polygonal ferrite	Polygonal ferrite, blocky ferrite	Polygonal ferrite	
		Ferrite islands	Polygonal ferrite	
Primary and secondary ferrite sideplates	Lamellar component (products)	Ferrite with aligned M-A-C, Upper bainite	Ferrite sideplates, Lath ferrite	Ferrite sideplates, Lath like ferrite
Intragranular ferrite plates	Acicular ferrite	Acicular ferrite, Fine bainitic ferrite	Acicular ferrite, Needle like ferrite, Fine grained ferrite	Acicular ferrite
Lath martensite, Twinned martensite, Retained austenite, Upper (occasionally lower) bainite	Martensite	Martensite, M-A constituent	Martensite, M-A constituent, Lath ferrite	Martensite, M-A constituent, High C martensite, Upper bainite

An example of these microstructural details are shown in figure 2.2.

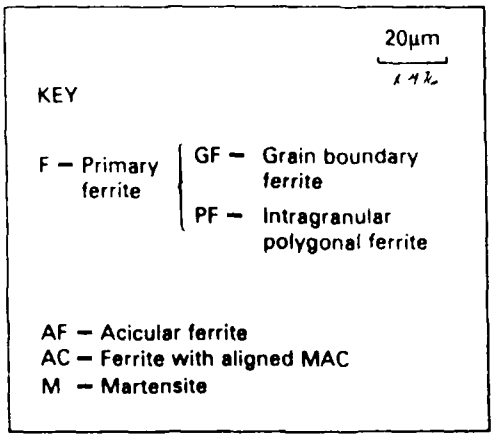

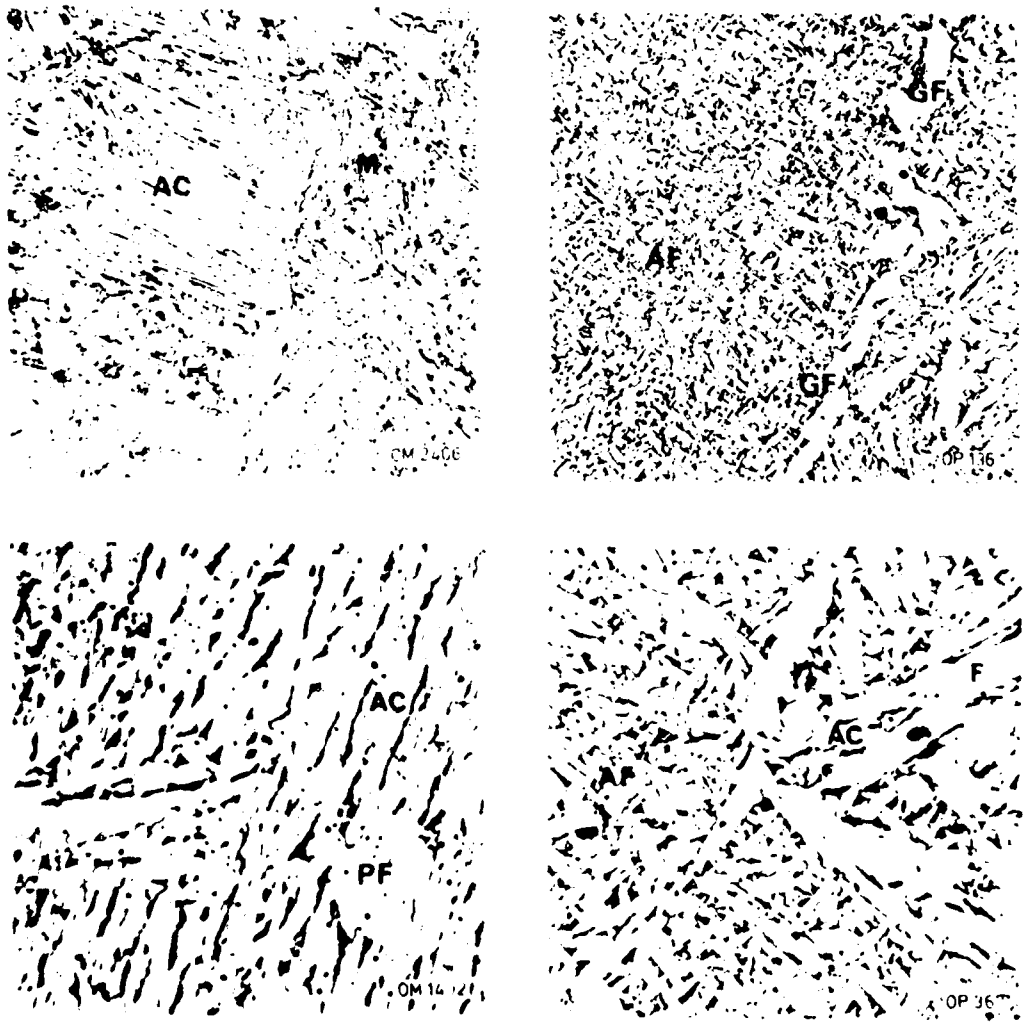

Figure 2.2 Examples of microstructural constituents found in HY-100 weld metal [6].

Grain boundary ferrite "GF" forms along prior austenite grain boundaries where the original austenite grains remain recognizable. Grain boundary ferrite is often described as proeutectoid ferrite. However, this description is misleading because other constituents (e.g. ferrite side plates) were originally also proeutectoid phases.

Polygonal ferrite "PF" is a microstructural constituent which occurs in the form of course ferrite islands inside the prior austenite grains. Polygonal ferrite has been described as intragranular grain boundary ferrite.

Ferrite with aligned M-A-C "AC" appears in a cross sectional view as long needles with an aspect ratio of at least 20:1. This microstructural constituent grows from grain boundary ferrite into the original austenite grain as packets of parallel plates. In addition, isolated packets of ferrite side plates can sometimes be seen inside the original austenite grains. In most cases, these features are attached to grain boundary ferrite. These observations also indicate that ferrite side plates have a real plate like structure, rather than needle or lath like, and are separated from each other by low angle grain boundaries. Abson and Dolby [7] describe these ferrite side plates as ferrite with aligned M-A-C (martensite, austenite, and/or carbide). This description indicates more clearly the composition of this structural constituent, but does not say anything about its morphology. In the literature [5], ferrite with aligned M-A-C is also called (upper) bainite, ferrite side plates or Widmanstatten ferrite. The first description is incorrect because ferrite with aligned M-A-C develops at higher temperature than the bainite start temperature.

Acicular ferrite "AF" always occurs in the interior of the original austenite grains. According to Hoekstra et al [5], it is characterized by:

-Fine grains (0.5-5.0 μm) with aspect ratios from about 3:1 to 10:1.

-High angle boundaries between the ferrite grains.

-High dislocation density of about 10^{14} lines/m^2.

-Absence of twin formation.

Another constituent is lath ferrite, which is an intragranular austenite transformation product resembling lower bainite. It is found among acicular ferrite or side plate structures. Unlike ferrite side plates, lath ferrite is not attached to grain boundary ferrite.

In addition to these major constituents, pearlite, martensite, and retained austenite may also occur in high strength weld metal, usually in very small amounts.

TERTIARY microstructure is the final microstructural feature to be discussed. In a multilayer deposit with each layer composed of a number of beads, each successive bead tempers previous ones. Consequently the secondary microstructure will partly be heated into the γ-region. This extra transformation results in formation of tertiary microstructure, consisting of more or less equiaxed grains which are coarser at higher austenization temperatures. This means that in the tertiary microstructure a distinction can be made between coarse grained and fine grained regions. It is clear that the tertiary microstructure will not appear in a one bead deposit.

2.3.2 Relationship Between Microstructure and Notch Toughness

The microstructure of as-deposited ferritic weld metal has a direct relationship with notch toughness. Research has shown, [5], that the notch toughness transition temperature varies as ln $(1/\sqrt{d})$, where d represents the average size of the ferrite grains. A similar relationship has been found between notch toughness transition temperature and average size of prior austenite grains. These findings imply that grain refinement of weld metal is beneficial to toughness. One cause of decrease in austenite grain size is the presence of non-metallic inclusions. Because of their pinning effect it is clear that higher inclusion contents reduce the austenite grain size and therefore favor higher temperature transformation products [5].

The inclusions themselves influence fracture in the ductile mode. It is well known that the upper shelf energy of the Charpy V-notch transition curve is controlled by the nucleation, growth and coalescence of microvoids at inclusions. Fewer inclusions produce a larger dimple size on a ductile fracture surface because of the smaller number of inclusions available to initiate microvoid coalescence. This leads to a higher upper shelf energy of the transition curve because larger dimple size is associated with higher energy absorption. It appears that the number, morphology, type and size distribution of inclusions available to initiate microvoid coalescence are more important in influencing upper shelf energy than volume fraction [43].

Tweed and Knott [4] claim that sites for brittle fracture initiation are also associated with non-metallic inclusions. Their model involves initial plasticity in grain boundary ferrite, plasticity induced inclusion fracture and crack growth under the combined effect of dislocation pile-up and crack tip stress fields.

Each different constituent of the secondary microstructure has its own influence on the notch toughness. Once again, Hoekstra et al [5] is helpful in defining these influences as described below.

Grain boundary ferrite is normally considered detrimental to toughness because it is coarse grained compared with acicular ferrite. From several observations [5] it appears that cracks in ferritic weld metal normally propagate along grain boundary ferrite, a process which is intensified by the presence of brittle pearlitic structures along grain boundaries.

Polygonal ferrite, like grain boundary ferrite, is detrimental to toughness because of its coarse grain size.

Ferrite with aligned M-A-C, like grain boundary ferrite, is also detrimental to toughness. This is linked with the presence of precipitated carbides, retained austenite and martensite along the ferrite plates. Moreover, the ferrite plates are separated by low angle grain boundaries, causing a much larger effective grain size.

Acicular ferrite can be considered as a constituent promoting toughness. In general, the ductile-brittle transition temperature is found [5] to decrease linearly with the amount of acicular ferrite. The favorable influence of acicular ferrite on toughness is primarily caused by fine grain size (0.5 μm-5 μm). Furthermore, acicular ferrite is characterized by favorable dislocation density and absence of twin formation, which lead to plastic deformation rather than cleavage. The chance of cleavage is further reduced by the presence of high angle grain boundaries between mutual grains, since these boundaries impede crack propagation. Investigations have shown, [5], that nucleation of various ferrite morphologies is aided by non-metallic inclusions. In particular, oxygen rich inclusions of a certain type and size are associated with the intragranular formation of acicular ferrite, because of their small lattice disregistry with ferrite-iron. It appears that at intermediate oxygen levels, notch toughness of weld metal is high because of the presence of fine acicular ferrite structures.

Martensite and retained austenite also adversely influence the toughness of ferritic weld metal.

In summary, toughness is favored by the presence of acicular ferrite, whereas toughness is unfavorably influenced by the presence of all the other previously described microstructural constituents.

2.3.3 Factors Influencing Microstructure

The microstructure of ferritic weld metal is determined mainly by chemical composition and thermal history.

CHEMICAL COMPOSITION

The chemical composition of weld metal is determined by the composition of consumables and base material, and the degree of dilution. Physical and chemical reactions in the liquid phase; for example, absorption of hydrogen, nitrogen, and oxygen from the environment, and oxidation of some alloying constituents also play

an important role. The influence of alloying elements on microstructure appears to originate from a displacement (complete or partial) of the CCT (continuous cooling transformation) diagram to shorter or longer times. Alloying elements which cause formation of more acicular ferrite and less grain boundary ferrite and ferrite with aligned M-A-C are beneficial to toughness. In unalloyed and low alloyed ferritic weld metal such formation is achieved if the CCT diagram is displaced towards longer times. However, it is worth noting that too large a displacement may cause the formation of martensite and retained austenite due to the deposit becoming over alloyed for the prevailing level of dilution and cooling rate [5].

In this context, the CCT diagram is often used to denote the transformations that occur in weld metal samples which experience continuous cooling. Figure 2.3 shows a typical CCT diagram for submerged arc welds. As this diagram indicates, there are a number of possible transformation products which appear in the sample at ambient temperature. Furthermore, the amount of each constituent is strongly controlled by the cooling rate.

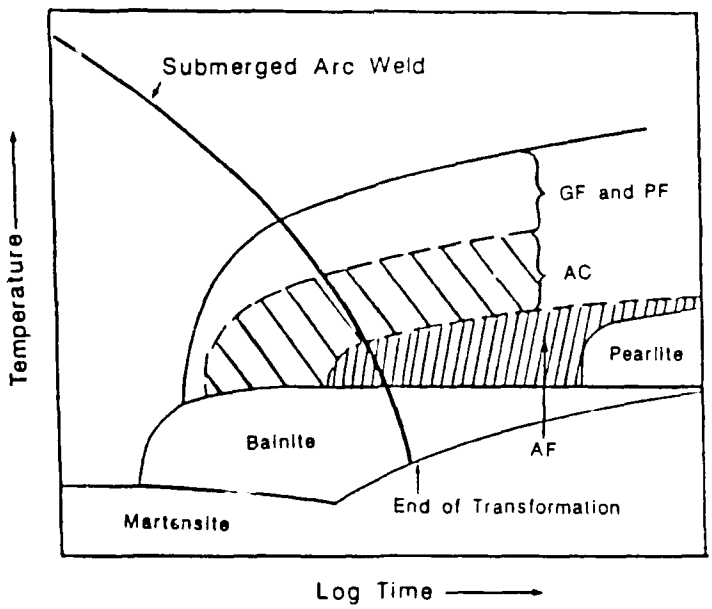

Figure 2.3 CCT diagram for typical SAW steel welds [8].

For the cooling curve experienced in this investigation, the final structure observed consists of a mixture of:

1. Acicular ferrite
2. Ferrite with aligned M-A-C
3. Grain boundary ferrite
4. Polygonal ferrite

According to Lancaster [8], these transformation products are formed as the SAW weld cools below the A_3 temperature. The slow cooling rate of the SAW deposits typically results in ferrite nucleating and growing efficiently from the grain boundaries and moving into the austenite behind a planar front. The redistribution of carbon is relatively efficient at this slow cooling rate. As the temperature decreases, carbon continues to diffuse into the austenite with the growth of grain boundary and polygonal ferrite. Subsequently, the remaining austenite undercools to a temperature where only ferrite needles can break through the carbon solute barrier. Lancaster [8] states that these needles, known as ferrite with aligned M-A-C or Widmanstatten side plates, have the Kurdjumov-Sachs orientation relationship with the austenite. Growth of the ferrite needles is rapid since solute is efficiently redistributed to the sides of the growing tip, thus avoiding solute pile-up problems. On further cooling below A_1, acicular ferrite is formed and carbon-enriched regions between the ferrite needles transforms to cementite or pearlite. Acicular ferrite is a more equiaxed transformation product and its growth is facilitated by the presence of a high density of nucleation sites. At faster cooling rates there is the opportunity for bainitic and martensitic constituents to form.

In addition to the nucleation and growth rates, Lancaster [8] also contends that the final volume fraction of the various transformation products depends on the density and dispersion of nucleation sites, the overlap of diffusion fields from adjacent products and the impingement of adjacent volumes.

Refocusing on the CCT diagram, the transformation characteristics in this investigation are believe to be strongly affected by the compositional changes in the weld metal.

Some elements help to stabilize the austenite (austenite formers) and other stabilize ferrite (ferrite formers). Included in the first category is nitrogen and included in the latter category is titanium. However, the exact mechanism by which these elements affect the austenite-ferrite transformation and thus the C-curve behavior is complicated. Lancaster [8] believes this is due to the tendency of these elements to exhibit partitioning at the austenite-ferrite interface. Regardless, the influence of these elements on the CCT diagram is well documented [8].

Specifically, austenite stabilizers such as nitrogen tend to inhibit transformations, pulling the C-curves towards longer transformation times. Looking at figure 2.3 (CCT diagram) we can see that this results in an increase in ferrite with aligned M-A-C and bainite at the expense of acicular ferrite.

Conversely, strong carbide or nitride forming elements (ferrite stabiiizers) such as titanium promote transformations, pulling the C-curves to shorter transformation times. This tends to suppress grain boundary and polygonal ferrite, but not acicular ferrite or bainite. Worth noting; however, is that inclusions, if present in sufficient number and size, also tend to promote the nucleation of acicular ferrite.

Apart from their effect on the CCT diagram, alloying and contaminating elements also influence mechanical properties by such mechanisms as solid solution hardening, precipitation hardening or ageing. For many alloying elements there is an optimum concentration related to maximum toughness. However, finding the optimum levels is difficult because the optimum level of one element is often influenced by the level of others. This implies that the different effects are not usually additive. A discussion of the interdependent relationships experienced by nitrogen and titanium is presented in subsequent sections of this chapter.

THERMAL HISTORY

The thermal history of a weld is characterized by fast heating and relatively fast cooling. During heating metal is melted, during cooling it solidifies. The cooling procedure is particularly important for the resulting microstructure and depends on many factors already mentioned; such as the welding current, arc voltage, travel speed, consumable properties, preheat temperature and joint geometry.

According to Hoekstra et al [5], cooling in the solid state can be characterized by two parameters; the austenization time parameter denoted as t(1200 ℃-800 ℃) and the transformation time parameter denoted as t(800 ℃-500 ℃). At constant chemistry, the austenization parameter determines final grain size of the austenite. The transformation parameter, $t_{8/5}$, helps determine the nature and distribution of the transformation products. For example; in figure 2.3 (CCT diagram), by increasing t(800 ℃-500 ℃) the amount of acicular ferrite decreases while the amount of grain boundary ferrite increases, accompanied by a deterioration in toughness.

Since the cooling rates for all 10 test welds were carefully normalized, there was not expected to be any noticeable differences between the welds due to thermal cycling variations. In this regard, variations among the welds due to thermal effects was considered negligible, and the thrust of this work only concentrated on the variations due to composition changes.

2.4 Influence of Nitrogen

The primary aim of this work is to identify and quantify the ways in which nitrogen contamination influences the properties of HY-100 welds produced by the SAW process. To fully understand the role of nitrogen requires, at a minimum, a comprehensive review of the literature regarding the sources of nitrogen contamination in the SAW process and the mechanisms by which nitrogen influences the microstructure and mechanical properties.

2.4.1 Sources of Nitrogen

Nitrogen is present in steel as an impurity and directly affects base plate and HAZ properties. Additionally, through dilution, it directly affects weld metal metallurgy and mechanical properties. It is not usually a deliberate alloying addition in modern high strength steel weld deposits. However, it is picked up from the environment and from impurities in the consumables used in the welding process. Atmospheric nitrogen may be introduced into the weld puddle during welding with the amount being a function of the welding process and flux being used.

Plate nitrogen contents vary with the steel making process, the slagging practices and the alloy content of the steel. Characteristic values (from a historic viewpoint) as presented by Gray et al [9] are:

Basic Open Hearth (BOH)	0.005-0.008%
Basic Electric Arc (EAF)	0.009-0.012%
Basic Oxygen Furnace (BOF)	0.005-0.007%

Potentially detrimental effects of nitrogen have come into focus during the past decade due to the adoption of desulfurization technology on a broad scale. Sulfur is a surfactant and reduces nitrogen pick-up when present in normal amounts, thus desulfurization during steelmaking can lead to an acceleration of the nitrogen pick-up process. This has resulted in nitrogen contents in steel creeping upward (to as high as 0.015-0.018 weight percent in the worst cases) from the traditionally expected levels [9].

Measures taken to reduce nitrogen contents have involved development of steelmaking practices and oxygen blowing techniques that reduce the turn-down level of nitrogen, improve ladle refining techniques that limit exposure to the atmosphere, and allow removal of nitrogen by vacuum decarburization or gas injection procedures [9]. Alloying or gettering with titanium has also been practiced but there are negative aspects connected with this approach as will be discussed in section 2.5.

In addition to nitrogen introduced into the weld pool from the base plate and from consumable sources, nitrogen can be picked up during the welding process itself. Eagar [10] has studied this phenomena for various weld processes, as shown in figure 2.4. He concludes that of the various flux shielded welding processes, the SAW process has the least pick-up of nitrogen for a given oxygen content.

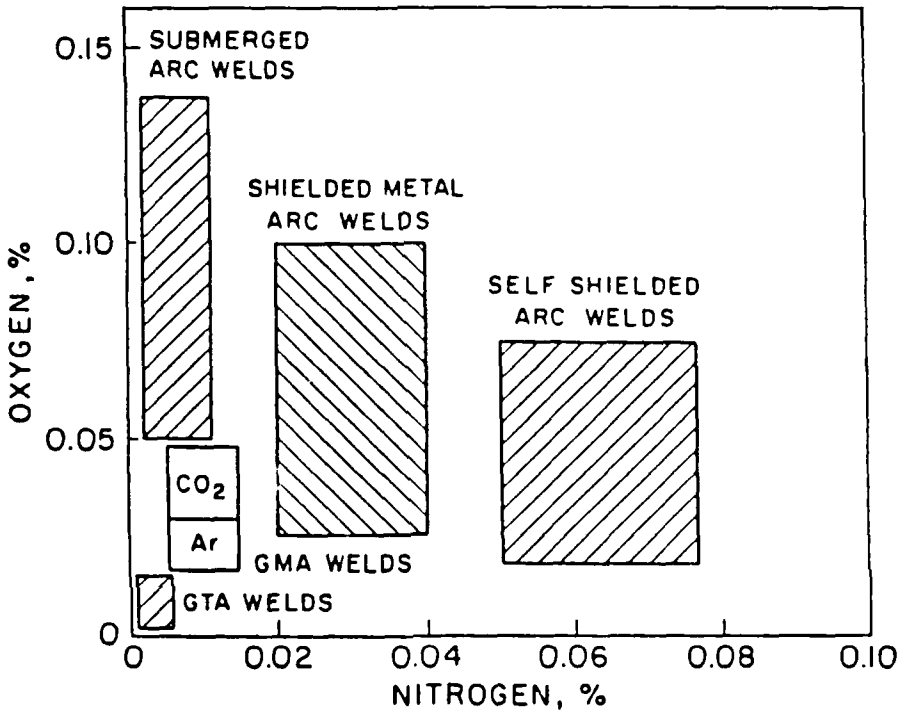

Figure 2.4 Oxygen and nitrogen levels expected from several arc welding processes [10].

With respect to the SAW process, the basic mechanisms for free nitrogen contamination include absorption on heated plate and filler metal before the flux becomes molten, direct atmospheric entrainment into the welding arc due to the electromagnetic pressure of the arc plasma, and transport from contaminated flux [11].

Major heat sources for the electrode in submerged arc welding are anodic heating (under direct current reverse polarity) and joule heating from the electrode's resistance. Heating of the base plate in front of the weld puddle is caused principally by

conduction. Since the rate at which heat diffuses through the base plate close to the weld pool is greater than the arc travel speed, there will be at some distance ahead of the weld, heated base plate unprotected by melted flux.

The arc generates a pressure differential between the region of high current density near the electrode tip and the region of low current density close to the workpiece. This pressure drop, due to elcctromagnetic forces, is able to draw atmospheric gas directly into the arc cavity.

Finally, the flux itself may be contaminated during its manufacture due to absorption of atmospheric nitrogen.

According to Lancaster [12], the amount of nitrogen absorbed in arc welding increases with the partial pressure of nitrogen in the arc atmosphere and with the amount of oxygen. Specifically, he reports that the saturation level for nitrogen in a 1600 ℃ environment is approximately equal to the equilibrium solubility at one atmosphere pressure which equates to 0.045 percent by mass. In the case of a 50% N_2-50% O_2 air atmosphere, the amount dissolved rises to 0.16% [12] which indicates that nitrogen dissociation in the arc plasma can produce supersaturation of the liquid steel pool.

Bhadeshia et al [13], have developed an equation relating nitrogen activity in liquid steel to the concentration of nitrogen. They contend that nitrogen is a diatomic gas, so that its activity in liquid steel a_N varies with the square root of the partial pressure of nitrogen p_N in the gas which is in equilibrium with the liquid steel.

$$a_N = K \times p_N \qquad (2.1)$$

Here K is a proportionality constant which depends on temperature. The concentration of nitrogen x_N is related to the activity by the relation:

$$a_N = f \times x_N \tag{2.2}$$

In this equation, f is the activity coefficient given by:

$$\log_{10}\{f\} = \sum_i (x_i \times e_i) \tag{2.3}$$

The quantity x_i is the concentration in weight percent of an element "*i*" in the liquid steel, and e_i is the corresponding Wagner interaction parameter between the element concerned and nitrogen, for dilute solutions. The activity coefficient thus represents the influence of other alloying additions on the solubility of nitrogen in dilute liquid steel.

The results of their study [13] shows that most of the nitrogen in the arc derives from the nitrogen in the wire consumable used. Additionally, of all the welding parameters, the welding current most significantly influences the nitrogen concentration in cases where the molten weld pool is exposed to the atmosphere. Specifically, in this case of welding without shielding the weld pool, an increase in the welding current usually decreases the weld nitrogen concentration. An example of this effect is shown in figure 2.5. This figure also shows that when adequate shielding is provided, the variations in current have little influence on the nitrogen pick-up.

Bhadeshia et al [13] conclude their study with the contention that the nitrogen concentrations in diluted submerged arc weld deposits can be estimated as a function of the electrode nitrogen concentration, base metal nitrogen concentration, and of the alloy content of the weld deposit. There is only a very small contribution from air trapped in the flux burden.

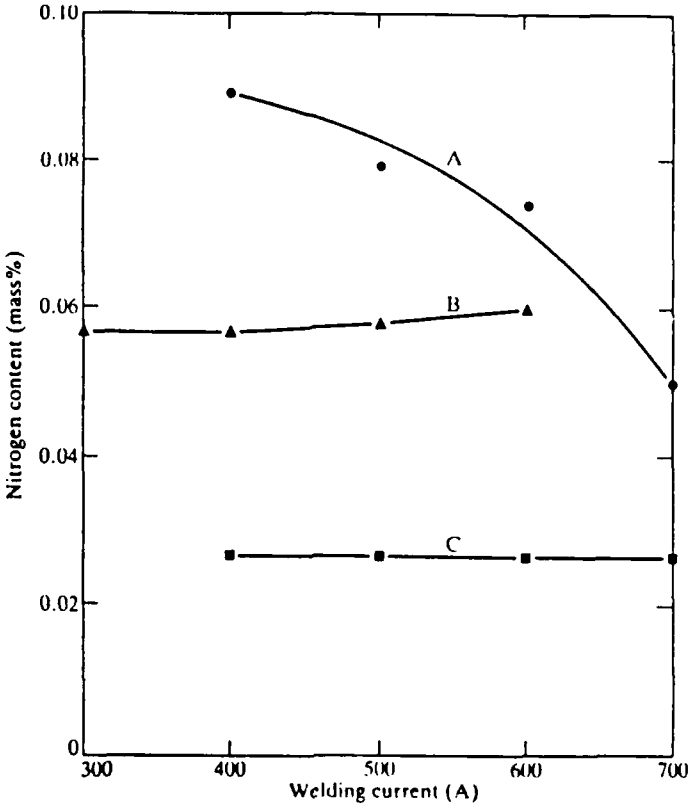

Figure 2.5 The nitrogen content of transferring drops in self-shielded, flux-cored DC arc welding: curve A, with iron powder core; curve B, rutile core; curve C, $CaCO_3$-CaF_2 core plus Al and Mg [12].

2.4.2 Nitrogen's Effect on Microstructure and Mechanical Properties

The toughness of submerged arc weld deposits is improved by increasing the content of acicular ferrite and decreasing the content of polygonal ferrite [14].

Nitrogen, either directly or indirectly, plays an important role in the above mechanism. However, there have been few investigations of the influence of nitrogen content on the mechanical properties and microstructure of high strength weld deposits, and the few results are often contradictory. For example, Mori et al [15] indicated that a change in the total nitrogen content of the deposit from 45 to 93 ppm had no effect on weld metal microstructure, while Okabe et al [16] observed a decrease in

acicular ferrite content when the nitrogen content was increased from 29 to 78 ppm. Nakanishi [17] and Oldland [18] contend that in these weld deposits, a higher nitrogen content is associated with a higher content of martensite-austenite (M-A) microphase, not with changes in acicular or polygonal ferrite content. Finally, Den-Ouden et al [19] and Horii and Maiaki [20] have suggested that the detrimental influence of increasing the nitrogen content on the toughness of weld metal is not related to changes in the microstructure or weld chemistry, but that free nitrogen is itself the main factor controlling weld toughness.

According to Lancaster [12], nitrogen is damaging in two ways; first by causing porosity, and secondly by embrittling the weld deposit.

Porosity appears when the nitrogen content exceeds approximately 0.045% by mass, as shown in figure 2.6. This would be expected from the saturation effect discussed earlier.

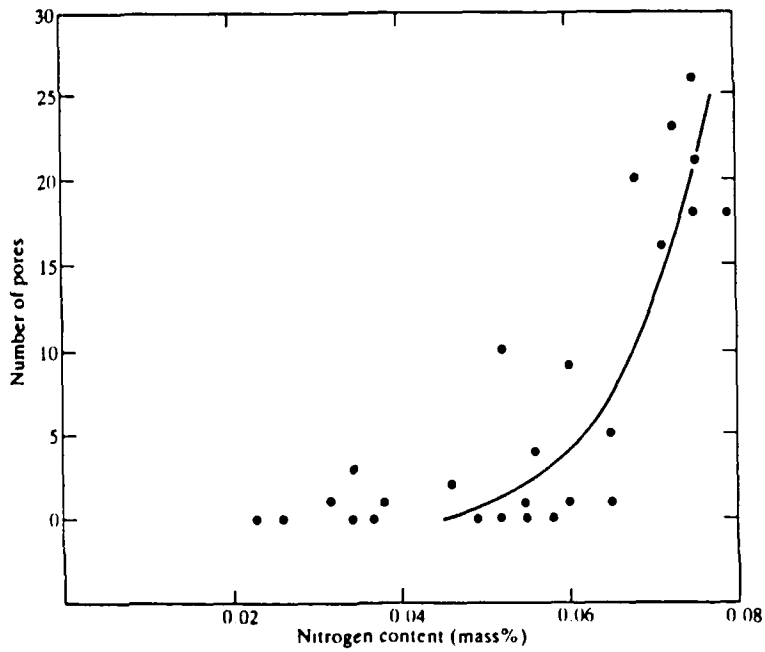

Figure 2.6 The number of pores in the fractured surface of a tensile testpiece as a function of nitrogen content; self-shielded flux-cored welding of carbon steel [12].

Nitrogen has a severely embrittling effect on weld metal. Deoxidants normally added to welding filler materials are usually adequate to combine with nitrogen to form non-embrittling nitrides. However, these deoxidants, such as aluminum and titanium, are themselves embrittling if present in excessive quantity.

Additionally, nitrogen in high strength steel may be responsible for strain-age embrittlement. Lancaster [12] discusses this phenomena in terms of nitrogen-bearing steel. He states that if a nitrogen-bearing steel is subject to plastic strain and simultaneously or subsequently heated at a temperature of about 200 ℃, the notch ductility is reduced. Prior to World War II a number of welded bridges were erected in Belgium and Germany using steel made by the air-blown Bessemer process, and therefore of high nitrogen content. Several such bridges failed by brittle fracture, and these failures were ascribed to strain-age embrittlement. Subsequent testing has shown that if a small crack forms adjacent to the weld boundary and is then strained and reheated by successive weld passes, the tip of the crack can be sufficiently embrittled to initiate a brittle fracture. The root passes of a multipass weld are similarly strained and reheated, and this may also lead to a degree of embrittlement. Strain-age embrittlement may be prevented or at least reduced by the addition of strong nitride-forming elements such as aluminum or titanium [12].

The detrimental effect of free nitrogen on HAZ and weld deposit toughness is well documented [9,14,21,22]. Gray et al [9] states that free nitrogen has been shown to increase the Charpy V-notch transition temperature +23 ℃ per 0.001 weight percent rise in nitrogen. However, in general, the detrimental effects of free nitrogen are difficult to quantify due to the interactions with aluminum, titanium, boron, and other elements. To a large extent, nitrogen is always free after welding except in the presence of titanium. TiN is stable up toward the melting point of steel and hence inhibits grain growth of austenite [21]. In this context, TiN can be used as a austenite-grain stabilizer in the coarse grain zone; in other words, as a grain refiner.

Of key importance is the fact that the Ti/N ratio should be ≤ 3.5 in order to avoid weldment embrittlement due to titanium carbide precipitation. Further discussion on the role of titanium will follow this section.

A literature review by Gray et al [9] has shown that nitrogen increases hardness as shown in figure 2.7.

Additionally, the literature survey by Gray et al [9] has shown that nitrogen lowers Charpy shelf energy as shown in figures 2.8, 2.9, and 2.10. In the same context, they have shown that nitrogen raises the fracture appearance transition temperature (FATT) as shown in figure 2.11.

Finally, Gray et al [9] concludes that a high nitrogen content leads to an increased percentage of proeutectoid ferrite and deterioration of notch toughness, as shown in figure 2.12.

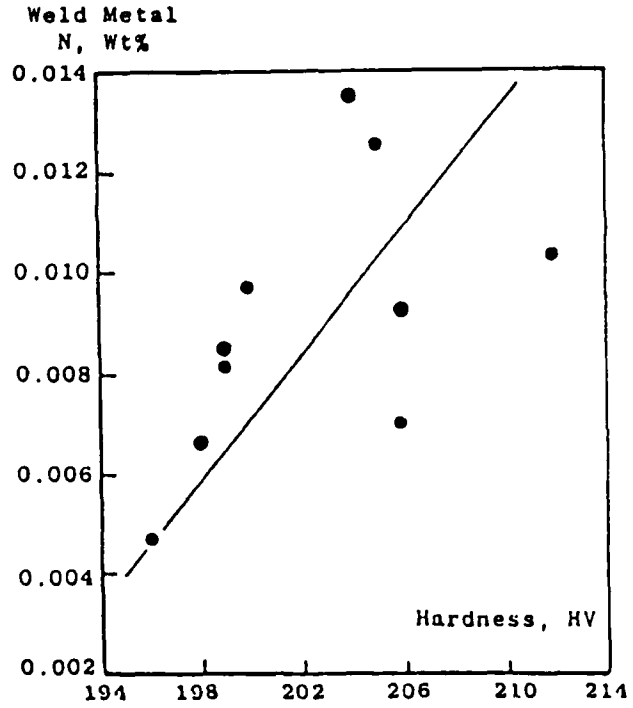

Figure 2.7 Variation in hardness with weld metal nitrogen content [9].

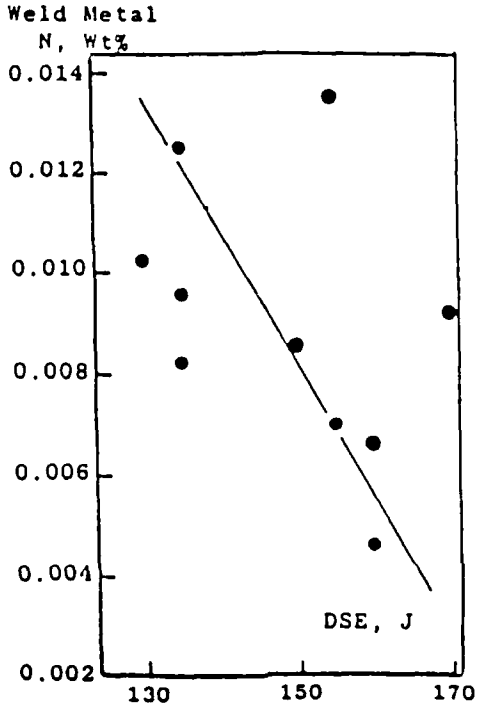

Figure 2.8 Variations in ductile shelf energy with weld metal nitrogen content [9].

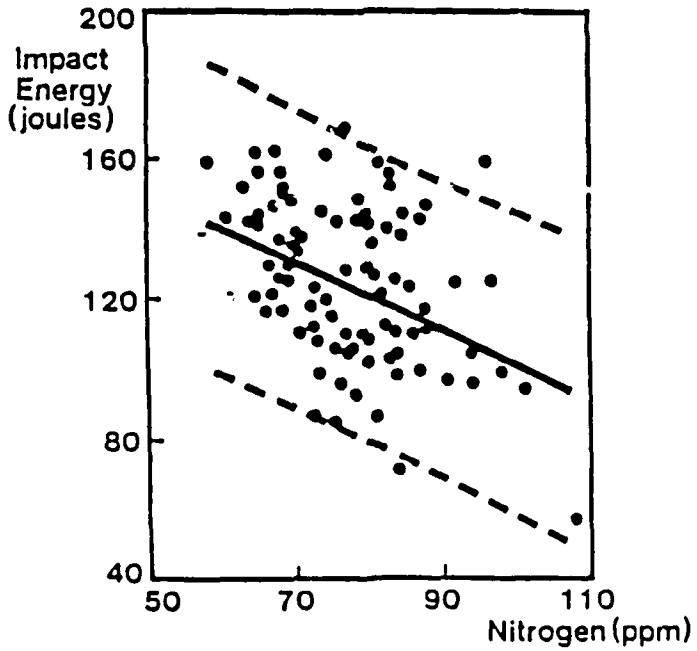

Figure 2.9 Weld centerline Charpy values versus weld metal nitrogen content [9].

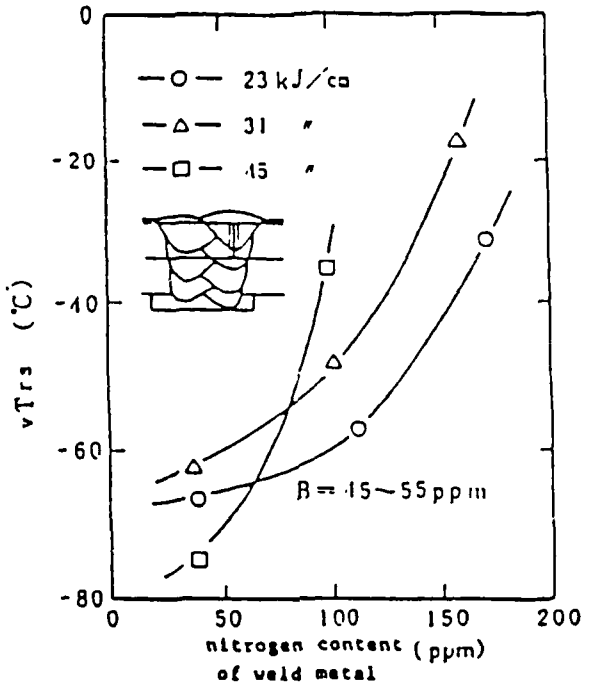

Figure 2.10 Effect of nitrogen content and heat input on notch toughness of weld metal (as welded) [9].

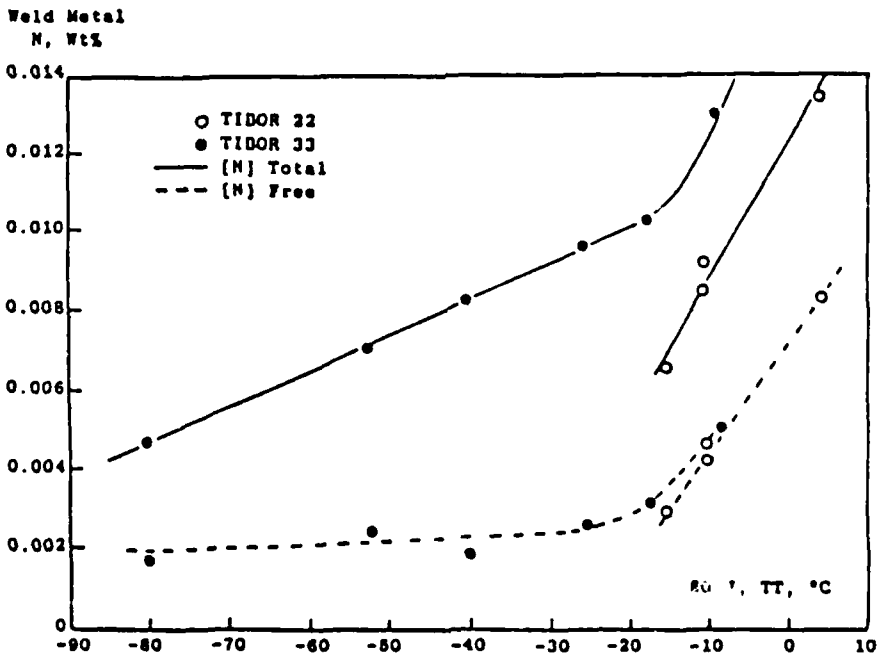

Figure 2.11 Variations in 80 J transition temperature with weld metal nitrogen content [9].

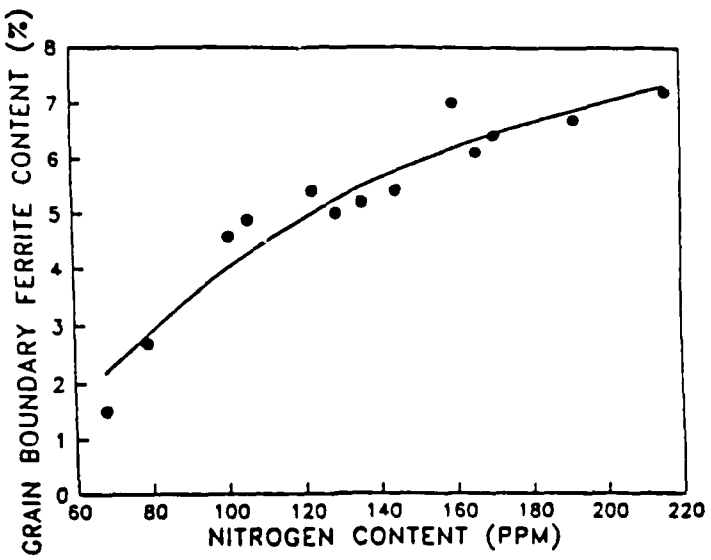

Figure 2.12 Effect of weld nitrogen content on proeutectoid ferrite content [9].

This literature review has revealed that there exists a certain amount of ambiguity about the mechanisms by which nitrogen influences the weld metal properties. With this in mind, the following broad conclusions are considered valid and seem to best characterize nitrogen's role in this regard.

1. Nitrogen concentrations in diluted submerged arc weld deposits can be estimated as a function of the wire nitrogen concentration, base metal nitrogen concentration and the alloy content of the weld. There is only a very small contribution from air trapped in the flux [13].

2. In the case of multipass weld deposits, where the dilution is extremely low, the toughness properties of welds will be consistently high provided major changes in deposit nitrogen content are not produced by welding procedure modifications. If deposit nitrogen content is raised due to employment of higher travel speeds, higher current, or inadequate control of flux burden height, the toughness properties will be reduced [23].

3. Free (i.e., uncombined) nitrogen dramatically increases HAZ and weld metal Charpy V-notch transition temperature at the rate of +23 ℃ per 0.001 weight percent nitrogen according to Gray et at [9]. It is desirable therefore to reduce nitrogen content to as low a level as possible in steels that are to be welded with high heat inputs.

4. As the total nitrogen content in the deposit is increased, higher weld metal titanium contents are required to maintain optimum toughness (at any given deposit oxygen, aluminum and boron content) [14]. When deposit aluminum, nitrogen, boron, titanium and oxygen contents are balanced such that no excess oxygen, nitrogen and titanium are available after TiN and TiO formation, optimum toughness occurs. Presently, there is a need for consumables to be properly formulated to accommodate wide ranges of base plate nitrogen contents.

5. Above a certain level (70 ppm according to Lau et al [14]), increasing the nitrogen content decreases the acicular ferrite content, increases the primary ferrite and ferrite with aligned M-A-C content, and increases the soluble nitrogen levels.

6. Nitrogen is an austenite stabilizer which inhibits transformations, pulling the C-curves (on the CCT diagram) towards longer times to transformation. This tends to promote the formation of ferrite with aligned M-A-C and bainite at the expense of acicular ferrite. The net result is a detrimental effect on weld metal toughness [8].

7. Additionally, nitrogen embrittles the weld and reduces toughness due to interstitial solid solution hardening and strain age hardening effects. At high levels of nitrogen contamination, 0.045% by mass, weld metal porosity degrades the mechanical properties of the weld [12].

8. There are several mechanisms proposed in the literature to explain the means by which nitrogen influences the mechanical properties and microstructure. In addition to those mechanisms already addressed, it seems likely that nitrogen segregates in the same manner as carbon to further promote the formation of M-A constituent which

embrittles the weld and lowers the fracture toughness. A complete discussion of M-A constituent influence on weld metal mechanical properties and microstructure is presented in section 2.6.

2.5 Influence of Titanium on Weld Metal Microstructure and Properties

The balance of evidence indicates that additions of titanium to high strength steel weld metal improves its toughness and that the improvements are due to a refinement of the microstructure [24].

In this context, Snyder and Pense [25] have suggested that small titanium additions up to an optimum level of about 0.04 weight percent can have a beneficial effect on the toughness of submerged arc weld metal. However, toughness appears to be continuously reduced by titanium additions greater than 0.04 weight percent indicating that high dilution welding processes such as SAW may develop low toughness weld deposits when used on base metals containing high titanium [25]. The point here is that there is an optimum range of titanium which will produce maximum toughness in weld metals, and that this range will depend upon the exact chemical composition of the weldment in question.

In particular, it has been observed that increasing the titanium content of submerged arc welds increases the proportion of acicular ferrite, but that the effect is a function of overall deoxidation in the weld. In other words, the effect of titanium depends upon the amount of aluminum, silicon, manganese, oxygen, boron and nitrogen in the weld pool prior to solidification [22].

Titanium most often combines with oxygen to form titanium oxide (TiO) which promotes intragranular nucleation of acicular ferrite. This process is attributed to an advantageous crystallographic orientation between the nucleated ferrite and the nucleating agent [26]. Similarly, titanium nitride particles (TiN) have been shown to promote the formation of acicular ferrite [26]. TiN and TiO particles are believed

to serve as nucleating sites for Mn, Si, Ti and Al oxides which together form the weld metal inclusions. Thus, with more TiN and TiO formation, more inclusions nucleate and there are then more initiation sites for acicular ferrite formation.

In welding steel, titanium is often added with boron with the intent that titanium nitride precipitates will reduce the amount of free nitrogen in the weld metal, thus preventing boron nitride (BN) formation and allowing boron to segregate easily into prior austenite grain boundaries. The solute boron segregated at the austenite boundaries seems to suppress nucleation of primary ferrite by a mechanism not yet fully understood [26].

However, Matlock and Edwards [27] have suggested that titanium and boron interact to improve the microstructure as follows. The precipitation of TiN or titanium-bearing oxides allows free boron to segregate to the prior austenite grain boundaries due to suppression of boron compound precipitation. Boron segregation to the austenite grain boundaries lowers the grain boundary surface energy and thus suppresses the nucleation of grain boundary ferrite. Moreover, the titanium-bearing precipitates serve as nucleation sites for intragranular acicular ferrite. Similarly, Oladipupo [21] proposes that titanium additions improve toughness by forming stable precipitates which restrict austenite grain growth during weld thermal cycling and promote transformation to smaller bainite colonies and introduce some fine polygonal ferrite grains. Matlock and Edwards [27] conclude that improvements in toughness from titanium additions are due to 1) the reduction in the amount of grain boundary ferrite, 2) the reduction in free nitrogen in the matrix, and 3) the increase in the volume fraction of acicular ferrite. These suggestions seem correct in light of the present knowledge concerning crack propagation in primary ferrite, interstitial solute dislocation interactions, and the interaction between propagating cracks and high angle boundaries.

In Matlock and Edward's study [27], the acicular ferrite volume fractions in high strength steel weld metal are plotted against their titanium concentrations, figure 2.13. These data imply that titanium concentrations of 0.04 weight percent or more

may assist the formation of a large fraction of acicular ferrite, (this is based on aluminum contents less than 0.04 weight percent). Although titanium can not be assumed to be the only important microalloying element, this figure suggests that it is important for the promotion of acicular ferrite. Worth noting is that some work, such as that by Dorschu and Lesnewich [46], showed that the optimum titanium concentration is actually much lower. Specifically, they showed that the optimum Charpy energy absorption at -60°F in 140 ksi steel weld metal occurred at a titanium concentration of 0.01 weight percent. Additionally, above 0.02 weight percent titanium, there was a steep drop in the absorption energy [46].

Thus, titanium is beneficial in neutralizing the negative effects of free nitrogen. As deposit nitrogen content is increased, higher weld metal titanium contents can be used to maintain optimum toughness values (at any given deposit oxygen content) [23]. When titanium and oxygen contents are in balance such that the remaining Ti/N weight percent ratio is approximately 3.5, then toughness is optimum. This is because titanium has neutralized the negative effects of nitrogen on toughness by forming TiN. Additionally, no excess titanium is available to precipitate as titanium carbides and thus embrittle the weld metal.

It has been shown by Burkhardt et at [23], that optimum toughness properties occur when a critical oxygen/titanium ratio of around 1:1 is attained during submerged arc welding. For any given welding consumable combination, the titanium content required in excess of this oxygen/titanium ratio depends on the total nitrogen content, i.e., on the titanium content needed to tie up soluble nitrogen as TiN. This requirement to tie-up free nitrogen is necessary if optimum toughness properties are to be achieved.

However, any factor that affects titanium content available for TiN formation will also affect toughness properties. The plate aluminum content is important since aluminum's deoxidation capability will free titanium from its deoxidation role and promote TiN formation. Thus higher nitrogen levels can be tolerated, with respect to optimum weld metal toughness, when the aluminum content is increased [23].

Grong and Matlock [28] have suggested that optimum toughness in submerged arc welding (SAW) occurs when the Al/O_2 ratio is 28:1. They explained this effect via an optimum distribution of aluminum inclusions, i.e., by means of optimum intergranular acicular ferrite nucleation.

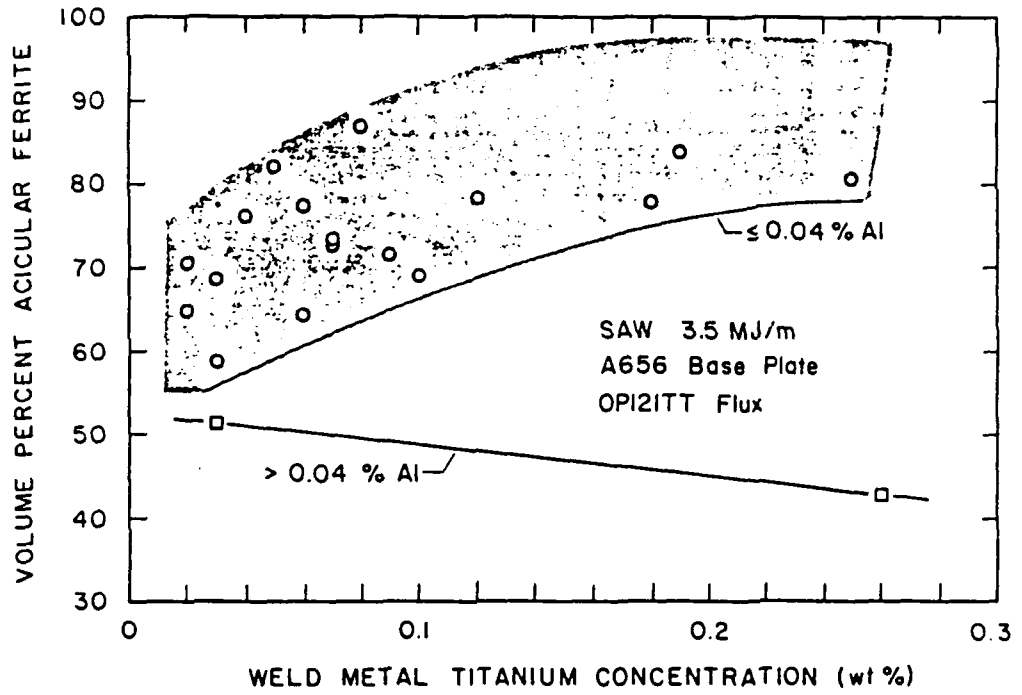

Figure 2.13 The volume percent acicular ferrite plotted as a function of the weld metal titanium concentration. Note that the effect of titanium changes depending on the aluminum concentration [27].

Based on this literature survey of the influence of titanium on weld metal microstructure and properties, the following broad conclusion are reached:

1. It has been suggested [25 and 27] that titanium levels up to 0.04 weight percent can have a beneficial effect on toughness by refinement of the microstructure. However, some authors [46] contend that the optimum titanium level is actually a much lower 0.01 weight percent.

2. Titanium is a ferrite stabilizer which promotes transformations, thus pulling the C-curve to shorter transformation times. This tends to suppress polygonal and grain boundary ferrite; but, not acicular ferrite [8]. However, at excessive titanium levels, the C-curve can be pulled to transformation times which promote ferrite with aligned M-A-C and bainite at the expense of acicular ferrite. Additionally, titanium forms TiO and TiN which initiate inclusions. These inclusions, if present in sufficient number and size, promote the nucleation of acicular ferrite.

3. The interplay of titanium and nitrogen during welding critically affects final weld metal toughness properties. By controlling the amount of titanium so as to produce only TiO and TiN and thus avoiding brittle carbides, the fracture toughness of the weld metal can be enhanced [23].

4. The Al-Ti-O-B-N balance must be closely controlled in order to optimize weld metal toughness.

5. Consumable requirements and specifications should be reviewed to insure nitrogen levels are consistent with weld metal chemistries containing aluminum, titanium, boron, oxygen, and nitrogen [9].

2.6 Role of M-A Constituent on Fracture Toughness of HY-100

As previously discussed, the loss of toughness due to increased nitrogen content is most often attributed to the coarsening of the structure at the expense of a fine acicular ferrite microstructure. The influence of microstructural details; such as the volume percent of acicular ferrite, primary ferrite, and ferrite with aligned M-A-C, have been widely investigated. However, the affect of microconstituents on weld metal toughness has not been made clear. Recently though, some researchers [29] have proposed that martesite-austenite (M-A) constituent has a significant affect on fracture toughness as shown in figure 2.14.

Biss and Cryderman [30] did a study of several hot-rolled, low-carbon, bainitic steel plates. Their study indicated that, in these steels, the M-A constituent increased as a result of adding increased amounts of interstitial hardenability-promoting elements such as nitrogen. Easterling [41] proposes that these elements increased the stability of carbon-enriched austenite regions that formed as a result of partial transformation to bainitic ferrite, suppressed the nucleation of cementite, and caused the formation of regions of high-carbon martensite, surrounded by retained austenite.

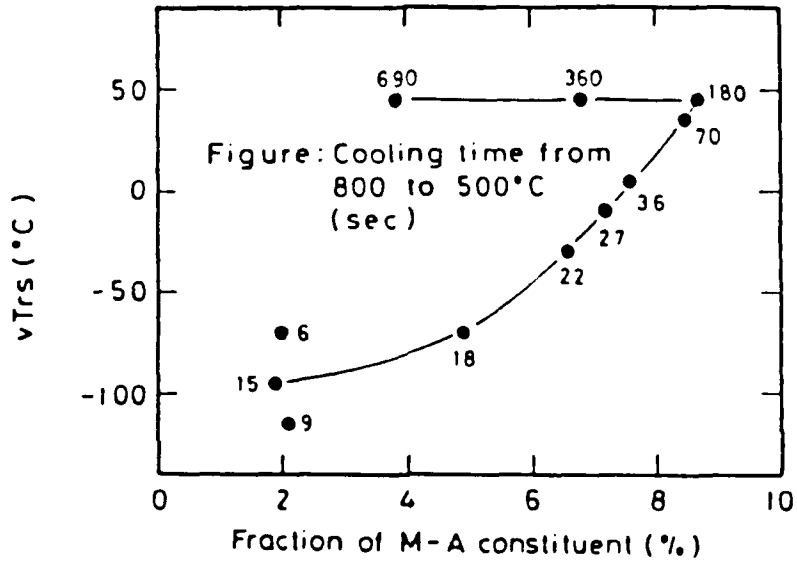

Figure 2.14 Relations between fraction of M-A constituent and vTrs (half size specimens) [29].

In this context, this investigation attempts to correlate an increase in the content of M-A in the weld metal with an increase in nitrogen content. Such a correlation provides a fresh perspective with regard to the mechanisms by which nitrogen reduces fracture toughness. In order to better understand the role this constituent plays in controlling weld metal properties, the following discussion of its characteristics is presented.

Ikawa et at [29] suggest the following process for the formation of M-A constituent. On cooling from the austenite state, bainitic ferrite is formed and the remaining austenite becomes stable. This is because of the carbon enrichment caused by the growth of bainitic ferrite. This enrichment is completed at about 400 ℃-450 ℃, and the carbon content of the remaining austenite reaches 0.5-0.8 weight percent. Cooling further, some part of this austenite decomposes into ferrite and carbide, in the temperature range of 300 ℃-350 ℃. If cooling is rapid enough, this decomposition does not happen. Consequently, the undecomposed austenite transforms into lath and twin martensites at lower temperature, and a small amount of austenite is retained.

In high strength steels, M-A constituent is referred to as the island regions composed of high carbon martensite and retained austenite surrounded by bainitic ferrite which forms in the heating cycle with medium cooling rate. In recent years, M-A has been taken into account as one of the main factors which causes deterioration of the HAZ toughness of high strength steel welded with high heat input. Many works have been devoted to investigating the structure of M-A and its effect on strength and toughness. Most of the work done before 1981 was summarized in a review paper. But until recently the mechanisms by which M-A deteriorates the HAZ and weld metal toughness have not been identified. Some authors [29 and 31] put forward the hypothesis that cracks initiated at the interface between M-A and ferrite due to stress concentration, but there is no evidence to prove this hypothesis.

Chen et at [31] have done much work in this area. They propose several mechanisms, based on the temperature of the weld deposit, by which M-A influences the fracture behavior.

In the case of moderately high temperature; due to heavy deformation of the ferrite matrix, high stress concentrates on the boundary of M-A and makes it crack or debond. With increasing strain, the cracks grow to voids and further develop to deep holes. Finally, the main crack forms and propagates by lateral growing and coalescence of deep holes due to internal necking which ultimately leads to rupture of the specimen [31].

Conversely, at low temperature, the presence of blocky islands of brittle M-A gives rise to concentration and triaxiality of stress at the point near the boundary between the M-A and the ferrite matrix which causes the ferrite matrix to cleavage crack. The main crack propagates by a sequence of similar processes and leads to catastrophic fracture of the specimen. The central effect which controls the fracture process at low temperature is the size of the M-A islands. The larger the size of these islands, the smaller the load to make the new crack nucleus initiate [31].

Based on this literature survey of the role of M-A on weld metal properties, the following broad conclusions are reached:

1. M-A constituent is formed from the austenite in which carbon has been condensed up to 0.5-0.8 weight percent on continuous cooling. This constituent consists of twinned martensite, lath martensite, and retained austenite [29].

2. Rapid loss of toughness with an increased cooling time is caused by appearance and increase of M-A constituent [29].

3. The extent of the harmful effect of M-A constituent on toughness decreases as cooling time increases [31].

4. Nitrogen is believed to act in the same manner as carbon by segregating to carbon-enriched areas; thus, effectively increasing the amount of M-A constituent present and enhancing the embrittling influence of M-A constituent.

5. The steels containing higher levels of M-A constituent are found to have poorer impact properties, higher tensile strength and lower yield strength to tensile strength ratios than normal bainitic steels (which have low levels of M-A constituent) [30].

CHAPTER 3

EXPERIMENTAL TECHNIQUES

3.1 Experimental Design

The welds in this investigation were made at optimum welding parameters as proposed by Franke [47] and in strict accordance with MILSPEC requirements [1]. The intent in this experiment was to normalize all factors influencing the quality of the welds produced such that only the influence of specific compositional changes can be quantified. Subsequently, the welds produced were subjected to comprehensive chemical, metallographic, and mechanical testing in order to evaluate the impact of nitrogen and titanium on the weld metal fracture toughness and to explore the mechanisms behind this behavior.

3.2 Materials

The base plate used in this analysis consisted of 0.75 inch HY-100 steel while the backing bars and run on/off tabs were 0.5 inch HY-100 steel. This steel was made to military specification, MIL-S-16216J, by United States Steel Corporation. The chemical composition of this steel is shown in Table 3.1 along with the MILSPEC requirements.

Table 3.1 Chemical composition of HY-100 steel base plate, weight percent.

ELEMENT	HY-100 PLATE	MIL-S-16216J REQUIREMENTS
C	0.174	0.10-0.22
S	0.008	0.002-0.020
O	0.002	-----
N	0.0061	-----
Mn	0.28	0.10-0.45
P	0.006	0.020 max
Si	0.24	0.12-0.38
Ni	2.70	2.67-3.57
Cr	1.35	1.79-1.86
Mo	0.50	0.27-0.63
Cu	0.16	0.25 max
Ti	0.003	0.02 max
Al	0.021	-----
V	0.002	0.03 max
B	0.003	-----
H (ppm)	1.9	-----

The military specifications, MIL-E-23765/2D [1], authorizes use of MIL-120S-1 electrode for qualifying HY-100 welds in the horizontal fillet and flat position only. The MIL-120S-1 electrode was 0.093 inch diameter Linde 120, heat #120022. The composition of this wire and its specification requirements are listed in Table 3.2.

The flux was Navy-approved Oerlikon OP121TT, Lot#1131. This flux is a fully basic, agglomerated flux sized to the Tyler mesh range 8x48. The flux basicity is documented to be 3:1. The flux composition is shown in Table 3.3.

The shielding was 100% pure argon gas which was flooded over the flux bed at 10 psig.

Table 3.2 Chemical composition of welding electrode, weight percent.

ELEMENT	L-TEC 120 HEAT #120022	MIL-120S-1 MIL-E-23765/2D
C	0.073	0.10 MAX
S	0.006	0.01 MAX
O	0.003	-------
N	0.005	-------
Mn	1.590	1.40-1.80
P	≤0.004	0.01 MAX
Si	0.330	0.25-0.60
Ni	2.200	2.00-2.80
Cr	0.280	0.60 MAX
Mo	0.470	0.30-0.65
Cu	0.015	0.30 MAX
Ti	0.014	0.10 MAX
Al	0.030	0.10 MAX
V	≤0.001	0.03 MAX
B	0.0029	-------
H (ppm)	2.600	-------

Table 3.3 Oerlikon OP121TT flux composition, weight percent.

COMPOUND	WEIGHT PERCENT
FeO	1.48
PbO	0.13
TiO_2	0.65
MnO	0.63
CaF_2	24.55
CaO	10.65
K_2O	0.50
MgO	23.67
P_2O_5	0.22
Al_2O_3	19.19
SiO_2	14.12
NaO_2	0.69
Loss on Ignition	3.50

3.3 Welding Procedures and Parameters

Ten butt-welded, 3/4 inch thick, HY-100 sample plates were produced using the submerged arc welding process with auxiliary argon shielding to exclude atmospheric nitrogen. Various levels of nitrogen and titanium composition were obtained by introducing nitrated manganese powder (Mn_2N-Mn_4N) and/or titanium powder (Ti) in the weld groove prior to each welding pass.

The SAW setup shown in figure 3.1 included a Linde V1-800 CV/DC power supply (not shown in the figure) with a UCC-8 controller, a Linde EH-10 wire feeder head, and a Union Carbide "J" governor controlling the welding travel speed.

In accordance with MIL-E-23765/2D [1], the joint geometry, figure 3.2, includes a 45° "V" joint with a 0.5 inch root gap. A 0.5 inch by 2.0 inch backing bar was tack welded under the joint. The test plate was 14 inches wide and 25 inches long which insures that three dimensional cooling rates were consistent between the test welds.

The surfaces of both the base plates and backing bars were ground smooth to remove rust, paint, and scale. The test welds were held in place by four "C" clamps.

All welding passes were deposited at a nominal heat input of 55 KJ/in (98% arc efficiency) which was accomplished by using a welding current of 400 amps, welding voltage of 33 volts, and a travel speed of 14.11 in./min. The polarity was DCRP (electrode positive). The preheat and interpass temperatures were maintained at 250 °F. These welding parameters meet the requirements of MIL-E-23765/2D [1] and are believed to be optimum parameters as indicated by Franke [47].

Temperature measurements of the plate were accomplished by using an embedded thermocouple positioned 0.25 inches from the weld pool centered on the plate's length. Voltage was verified with a calibrated digital voltmeter and welding current was monitored with a shunt resistor (800A-50MV). Electrode travel speed was controlled using a Union Carbide "J" governor which, through a calibrated DC motor, provided the needed 14.11 in./min travel speed. The welding current was controlled indirectly

Figure 3.1 The SAW setup used in this investigation.

by adjusting the electrode feed rate to a nominal value of 50 in./min. The electrode extension was maintained at 0.625 inches which is a sufficient length to prevent contamination due to melting of the contact tip.

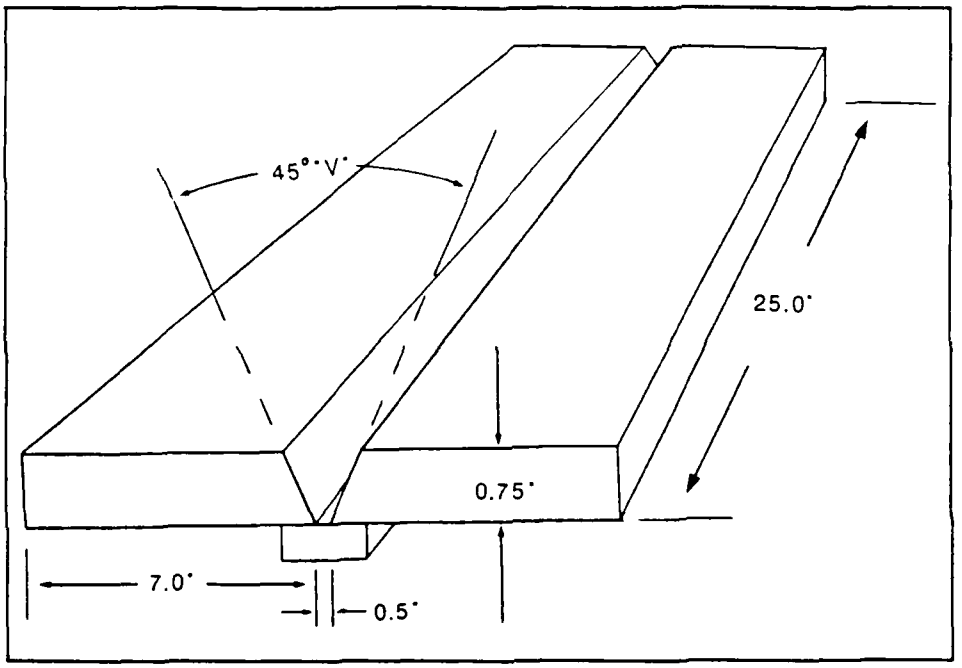

Figure 3.2 The test plate joint geometry in accordance with MIL-E-23765/2D.

All weld passes were completed using pure argon gas which was flooded over the flux bed at 10 psig. The argon gas was used to displace air trapped in the flux thereby reducing, as much as possible, the introduction of hydrogen, nitrogen and oxygen from the atmosphere. However, as the literature survey revealed, the amount of contamination from air trapped in the flux burden was negligible. Thus, the benefit in using argon shielding to minimize air contamination was considered to be very small.

All the above welding parameters were closely monitored in order to normalize the influence of these parameters among the ten test welds. Of special concern in this regard was the desire to achieve identical cooling rates among all ten test welds.

3.4 Testing and Evaluation

After preparation of all the welds, each test weld was sectioned for chemical composition analysis, metallographic examination, hardness evaluation, and mechanical testing.

3.4.1 Chemical Analysis

The chemical composition was determined from 30 gram samples of all-weld metal cut from the center of each test weld. Chemical analyses were performed by LUVAK Labs located in Boyston, Massachusetts. The results are tabulated in weight percent with the exception of hydrogen which is recorded in PPM. The methods used by LUVAK Labs to quantify compositions are shown in Table 3.4.

Table 3.4 Methods used in determining chemical composition.

SPECIES	METHOD
CARBON	Combustion/Infrared
SULFUR	Combustion/Automatic Titration
OXYGEN	Inert Gas Fusion
NITROGEN	Inert Gas Fusion
HYDROGEN	Vacuum Hot Extraction
METALS	Plasma Emission Spectro-graphic Analysis

From the results of the chemical analyses the carbon equivalent for each weld was calculated.

3.4.2 Metallographic Examination

From the center of each test weld, two transverse specimens were sectioned. One transverse sample was mounted in bakelite in preparation for microscopic examination while the second sample remained unmounted in preparation for macro-analysis.

Both samples were ground on successive emery paper to 600 grit; followed by polishing on a 9 μm diamond paste wheel; then on a 1 μm diamond paste wheel; and finally, on a polishing wheel using Struers OP-S. In-between each grinding and polishing step, the specimens were ultrasonically cleaned in methanol rinsed, and blown dry.

The unmounted specimens were prepared for macro-analysis of the overall integrity of the weld; including bead geometry, gross defect documentation and observation of each pass in the weld. Macroscopic etching was done using a 2% nital solution.

3.4.2.1 Optical Microscopy

Polished specimens were etched in 2% nital solution for examination of the weld metal microstructure. This solution effectively shows the acicular ferrite, ferrite with aligned M-A-C, grain boundary ferrite, and polygonal ferrite microstructures; however, microphases such as M-A constituent were not seen by this method. The optimum etching time was 10 seconds using a swabbing technique. Examination was performed with a Nikon Inverted Microscope EPIPHOT-TME at magnifications of 100X, 200X, 400X, and 1000X. Photographs were taken on types 52 and 55 Polaroid film at various magnifications using an attached Polaroid camera.

Using Vickers microhardness indentations as markers, a carefully selected 150 μm x 150 μm location of each specimen was photographed at 1000X and pieced together into a montage. These areas were photographed for both the unetched and etched condition for quantitative analysis of the inclusions and microstructural features respectively.

Since it is desirable to correlate the impact of the M-A microphase on the fracture toughness of these welds, a significant effort was spent on identifying this high carbon microphase. Several etching techniques were tried, as shown in table 3.5, including 2% nital, followed by a heated 4% picral solution. It is believed that the low carbon content of the weld metal prevents this microphase from being easily etched. However, using the two step electrolytic etching technique described in Table 3.5, the M-A microphase was discernable at high magnification on the SEM and a quantitative point count to determine the volume percent of this phase was achieved.

Table 3.5 Metallographic etchants used to reveal microstructural features [32].

ETCHANT	COMPOSITION	USES
Nital	2-5 ml nitric acid and 95-98 ml methanol for 2% and 5% nital respectively. Etching time: approx. 10 seconds.	For carbon steels; gives maximum contrast between pearlite and a ferrite or cementite network; reveals ferrite boundaries; differentiates ferrite from martesite.
Picral	4 g picric acid, 100 ml methanol and 4 drops 17% zephiran chloride (wetting agent). Etching time: Heat and etch for approx. 1 minute.	For all grades of carbon steel; annealed, normalized, quenched, quenched and tempered, spheroidized, austempered.
Sodium metabisulfite	8 g $Na_2S_2O_5$ and 100 ml distilled water. Etching time: approx. 20 seconds.	Darkens as-quenched martensite.
Marshall's reagent	100 ml water, 8 g oxalic acid and 5 ml sulfuric acid. Etching time: approx. 5 seconds.	Uniform ferrite grain boundary etch for low-carbon or electrical steels.
(Two step electrolytic) 1. EDTA 2. Picric	 5 g EDTA (ethylenediamine tetraacetic acid), 0.5 g sodium fluoride and 100 ml water. Etching condition: 3V, 3 sec. 5 g picric acid, 25 g sodium hydroxide and 100 ml water. Etching condition:6V, 30 sec.	Best method for observing the M-A constituent in low carbon steel. By this method, M-A constituent is embossed and carbides are depressed, in the matrix of ferrite.

3.4.2.2 Scanning Electron Microscopy

After completing optical examination, the same 150 μm x 150 μm location of each 2% nital etched weld specimen was examined with a Cambridge Scanning Electron Microscope under an accelerating voltage of 20KV. Qualitative and quantitative analysis was done at magnifications of 1000X, 5000X, 10000X, and 12000X. Once again, this was done by piecing together micrographs into a montage which provided a sufficiently large sample area of the weld so as to produce statistically significant results. These areas were also photographed for both the unetched and etched condition for quantitative analysis of the inclusions and microstructural features respectively.

Quantitative metallography was done using a J.C. Loebl Magiscan Image Analyzer for inclusion quantification and manually using a point counting method for microstructural composition analysis. From this analysis, inclusion size, shape, and number were determined as was the volume percent acicular ferrite, ferrite with aligned M-A-C, grain boundary ferrite, polygonal ferrite and M-A constituent. The prior austenite grain size was also determined. This required repolishing and etching with 5% nital to better define the grain boundaries. However, even with this etching technique, only a few grains from each weld could be identified.

Additionally, an energy dispersive X-ray spectrometer was used to qualitatively determine the composition of inclusions (greater than 1.5 μm in size) found on the etched surface of the welds.

Finally, the Cambridge Scanning Electron Microscope was used to observe the fracture surfaces of selected Charpy V-notched impact specimens. Mean fracture paths were measured and correlated with volume fractions of microstructural constituents present.

3.4.3 Mechanical Tests

The remaining portions of the test plates were sent for mechanical testing to David Taylor Research Center located in Annapolis, Md. From each test weld, two all-weld-metal tensile specimens and an average of 14 transverse Charpy V-notched specimens were machined and broken in strict accordance with MIL-E-23765/2D [1]. From the test plates, the tensile specimens were taken from the ends and the Charpy V-notched specimens were taken from the center as shown in figure 3.3.

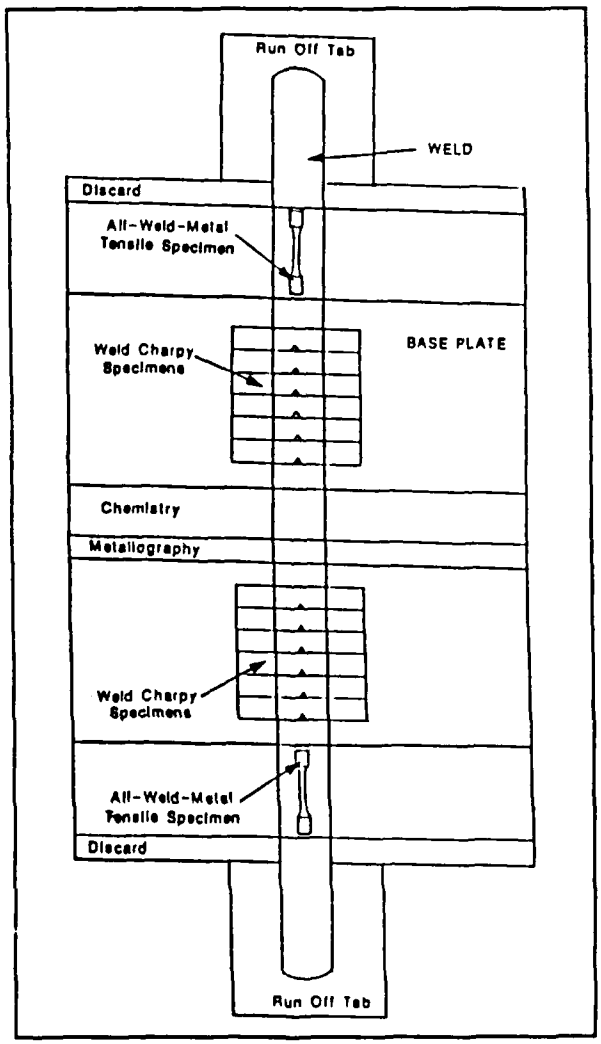

Figure 3.3 Test plate and specimen location.

Additionally, using the polished microscopy specimens from the optical and SEM examination, Vickers microhardness scans were conducted for each weld sample.

3.4.3.1 Hardness Test

Hardness test were performed on the polished microscopy specimens using a Vickers Microhardness Tester. Diamond Pyramid Hardness (DPH) values were obtained using a constant load of 200 grams and an indentation time of 12 seconds. Microhardness scans at 0.5 mm separation between indentations were made on the microscopic specimens from top to bottom "V" and across the middle portion "H" of each transverse weld section as shown in figure 3.4 below.

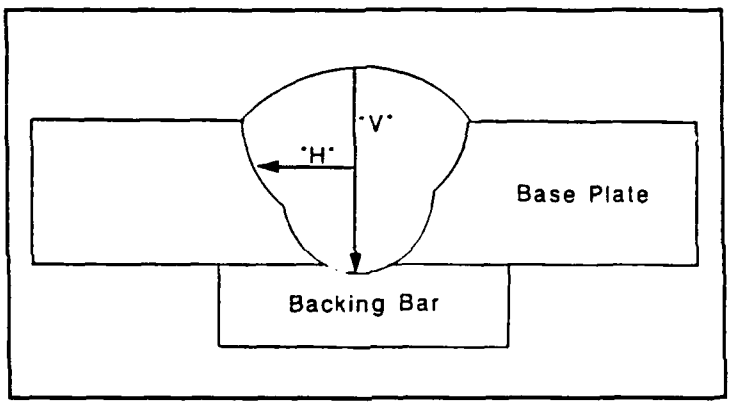

Figure 3.4 Microhardness scans used in evaluating hardness of the HY-100 steel SAW specimens.

3.4.3.2 Tensile Test

Two sub-sized, 0.357 inch, all-weld metal tensile specimens were machined as shown in figure 3.5. The specimens were tested at room temperature using a Baldwin Universal tensile machine at a crosshead speed of 0.02 in./min.

From each tensile specimen, the ultimate tensile strength (UTS), 0.2 percent yield strength (0.2% YS), percent elongation (%EL), and percent reduction in area (%RA) were measured.

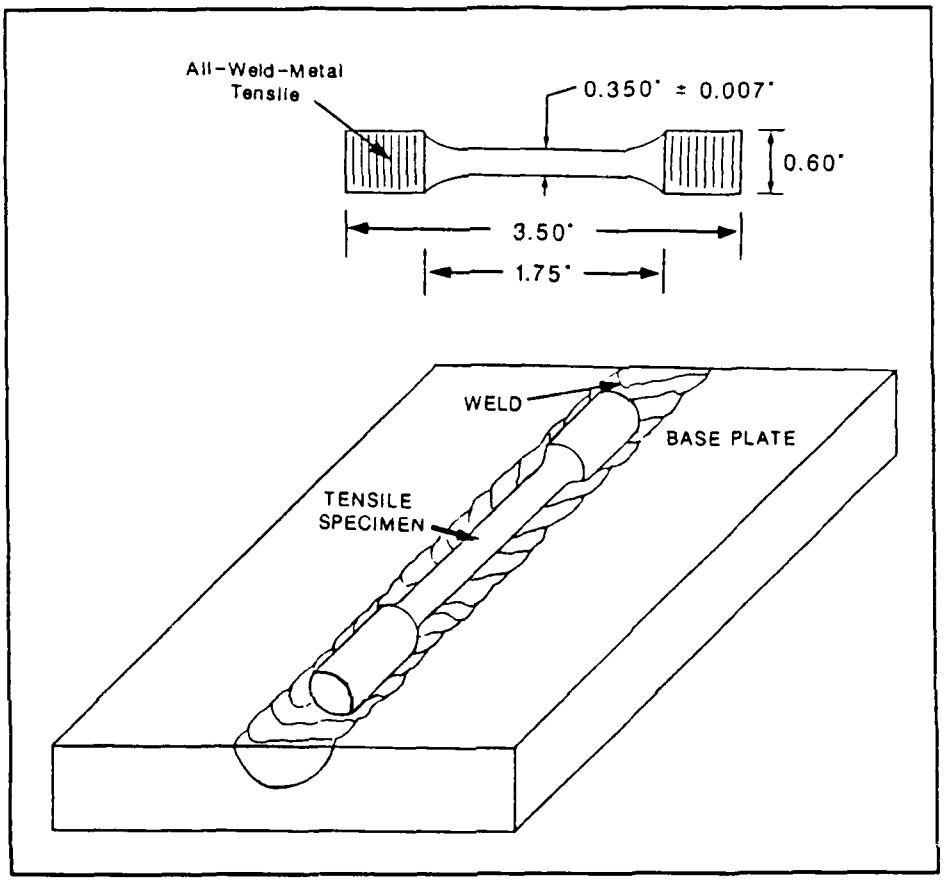

Figure 3.5 Subsized all-weld-metal tensile specimens used in this investigation.

3.4.3.3 Charpy Test

An average of 14 full sized transverse Charpy V-notched specimens per weld were machined 1.0 mm below the plate surface and notched in the through thickness direction along the weld centerline as shown in figure 3.6.

Impact properties for the Charpy specimens were obtained at the test temperatures of -180 °F, -120 °F, -60 °F, 0 °F, 60 °F, 120 °F and 180 °F with all test conducted within a tolerance of ±3 °F. In accordance with MIL-E-23765/2D [1], the required average Charpy V-notch energy at -60 °F is 45 ft-lbs and at 0 °F is 60 ft-lbs. In order for each weld to meet MILSPEC qualifying standards, the average value at the two specified test temperatures must be equal to or greater than these minimum values and no two specimens can have values below the minimum values specified. Temperatures other than the two required by the MILSPEC were used to help identify the upper and lower shelves.

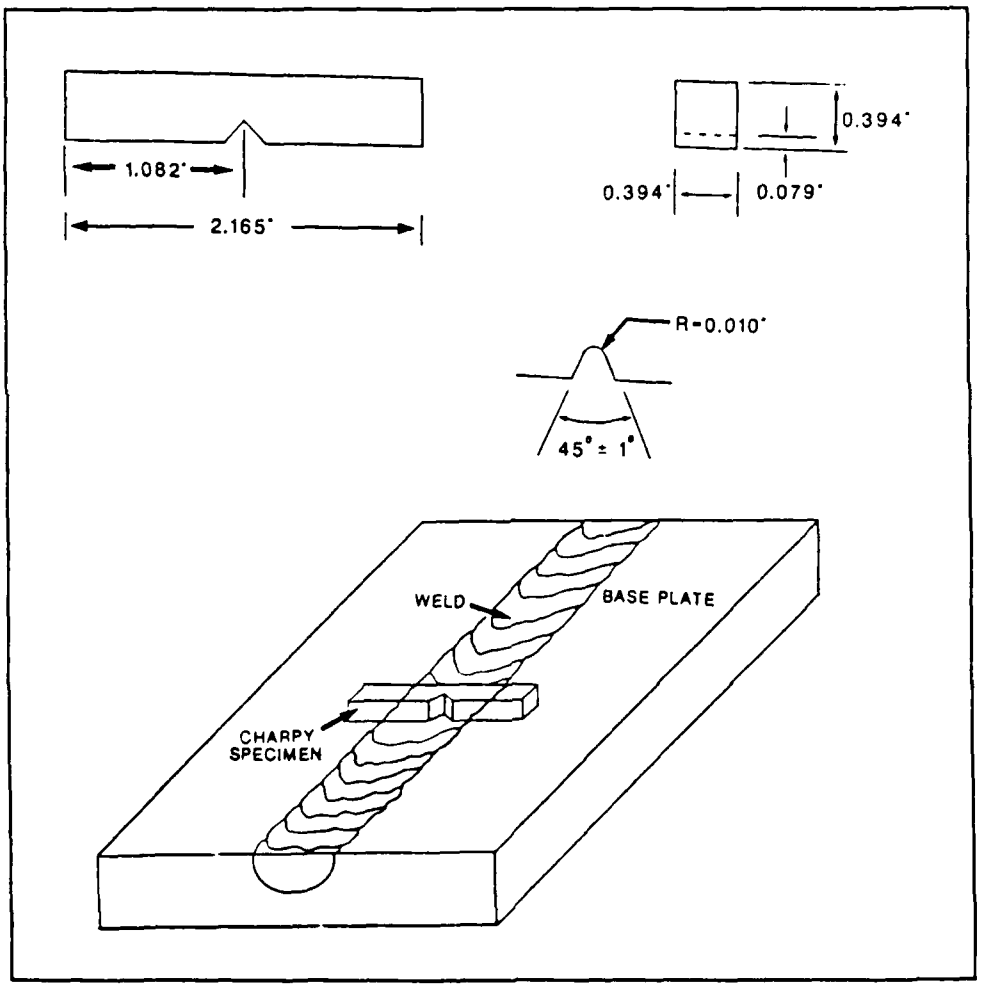

Figure 3.6 Full sized Charpy test specimens used in this investigation.

CHAPTER 4

RESULTS AND DISCUSSION

4.1 Evaluation Criteria

As chapter 3 indicated, quantifying the influence of nitrogen and titanium on the fracture toughness of HY-100 is a complex problem.

The initial effort at quantifying the influence of these compositional changes on the microstructures and properties of the weld metal involved using correlation coefficients and slopes to fit the observed data. The slope, based on a linear least squares fit for the data, provided an indication of the magnitude of influence on the weld metal characteristics in response to variations in nitrogen or titanium content. The correlation coefficient defined a confidence level which was based on how well the data points correlated with the linear least squares fit.

However, this method for evaluating the data was abandoned for several reasons. First, there were only a maximum of six data points for each plot which did not give statistical significance to the least squares fit or correlation coefficient. Secondly, the influence of nitrogen and titanium variations on the weld metal characteristics cannot be accurately modelled by a linear, exponential, or any similar type of line fitting. For these reasons, the slopes and correlation coefficients for the plotted data were not considered representative of the actual conditions that existed within the welds. After further thought, it was decided that the best method for presenting the observed data was in a tabular and a graphical format with a qualitative discussion of the results. For the plots in this chapter, if a general trend could be illustrated,

a solid line connecting the data points was used to highlight the trend. In those plots where no trend was obvious, the data points were plotted without a connecting line to avoid confusion.

In this regard, the following weld metal characteristics were investigated in order to quantify the influence of nitrogen and titanium compositional variations within the weld:

CHEMICAL COMPOSITION

Carbon Equivalent Index, CE (IIW)

Carbon Equivalent Index, Pcm (Ito-Bessyo)

METALLOGRAPHY

Volume Percent Acicular Ferrite, AF

Volume Percent Ferrite with Aligned M-A-C, AC

Volume Percent Grain Boundary Ferrite, GF

Volume Percent Polygonal Ferrite, PF

Volume Percent Martensite-Austenite Constituent, MA

Prior Austenite Grain Size, L_γ

Area Percent Inclusions: including size, morphology, and composition

MECHANICAL

Vickers Microhardness, DPH

0.2% Offset Yield Strength, σ_y

Ultimate Tensile Strength, σ_t

Charpy V-notch Energy, C_v

Ductile-to-brittle transition temperature, DBTT

Mean Fracture Length (from fractography), L_f

4.2 Chemistry

The success of this work hinged on the ability to achieve incremental nitrogen and titanium compositional variations among the test welds, while holding the fractional compositions of all the other elements within tight tolerances. As discussed in chapter 3; in addition to thermal cycling, compositional variations play a major role in the production of weld metal microstructure and in controlling the mechanical properties.

Incremental nitrogen and titanium variations were achieved in this experiment. The influence of these compositional variations are discussed in the following sections of this report.

4.2.1 Chemical Analysis

The results of the chemical analyses for all ten test welds, the base plate, and the LTEC 120 wire are shown in Table 4.1. The average concentration and standard deviation for each element, accept nitrogen and titanium which were varied systematically, are also presented.

Welds number #1 and #2 were baseline welds which represent the typical chemistry for the materials and procedures specified in chapter 3.

Welds #3 through #6 show incremental increases in the weight percent nitrogen which were achieved through manganese nitride powder additions. The recovery of nitrogen was very close to the target compositions that were desired indicating that full recovery of the nitrogen from the manganese nitride powder occurred. This resulted in fairly uniform incremental increases from 0.005 weight percent nitrogen (baseline) up to 0.033 weight percent nitrogen. Additionally, compositional variations

Table 4.1 Summary of chemical compositions in the weld metal, base plate and wire, weight percent.

ELEMENT (wgt %)	LTEC 120S WIRE	BASE PLATE	WELD #1	WELD #2	WELD #3	WELD #4	WELD #5	WELD #6	WELD #7	WELD #8	WELD #9	WELD #10	Average Welds #1-#10	SDEV Welds #1-#10
C	.073	.174	.066	.086	.082	.070	.062	.068	.081	.067	.080	.066	.0728	.00252
S	.006	.008	.010	.008	.003	.004	.006	.003	.007	.007	.004	.004	.0056	.00067
O	.003	.002	.029	.029	.029	.031	.031	.028	.033	.029	.023	.029	.0291	.00048
N	.005	.006	.005	.005	.007	.012	.018	.033	.005	.005	.005	.017	---	---
Mn	1.59	.28	1.40	1.49	1.40	1.53	1.59	1.66	1.46	1.51	1.51	1.62	1.517	.02206
P	.004	.006	.011	.019	.030	.012	.010	.021	.022	.010	.016	.022	.0173	.00183
Si	.33	.24	.39	.66	.57	.45	.50	.56	.58	.49	.65	.66	.5510	.02493
Ni	2.20	2.70	2.23	2.44	2.49	2.41	2.46	2.42	2.35	2.49	2.27	2.47	2.409	.02114
Cr	.28	1.35	.43	.45	.49	.49	.49	.48	.42	.39	.47	.52	.4930	.01080
Mo	.47	.50	.46	.50	.53	.50	.48	.50	.49	.50	.54	.50	.5000	.00467
Cu	.015	.160	.027	.034	.036	.034	.032	.034	.026	.029	.035	.041	.0328	.00115
Ti	.014	.003	.009	.009	.009	.009	.009	.010	.014	.020	.037	.014	---	---
Al	---	.021	.017	.015	.019	.020	.017	.016	.018	.021	.016	.014	.0173	.00059
V	.001	.002	.004	.003	.004	.004	.004	.003	.004	.004	.004	.004	.0040	.00007
B	.003	.003	.003	.004	.005	.003	.003	.005	.003	.004	.004	.006	.0040	.00027
H (ppm)	1.3	1.9	0.4	0.7	0.4	0.7	0.7	0.4	0.4	0.7	0.9	0.7	.6600	.06933

among all the other elements present in the weld metals were negligible. This allowed analysis of the influence of nitrogen variations on weld metal characteristics to proceed without the complicating influence of other elemental variations.

Welds #7 through #9 show incremental increases in the weight percent titanium which were obtained through titanium powder additions. Once again, actual compositional variations achieved were very close to the target increments due to full recovery of titanium from the titanium powder additions. The compositional variations were uniformly incremental from 0.009 weight percent titanium (baseline) up to 0.037 weight percent titanium. Furthermore, compositional variations among the other elements present were negligible as before.

Finally, **weld #10** attempted to achieve a Ti/N ratio of 3.5:1. As Table 4.1 shows, this was not obtained. This was most likely due to inhomogeneous mixing of the manganese nitride powder and the titanium powder which had slightly incompatible mesh sizes. The net result is a Ti/N ratio closer to 1:1. However, relative to the baseline compositions, the increase in the weight percent nitrogen was much greater than the increase in weight percent titanium.

As the rest of this chapter will illustrate, the weight percent variations in nitrogen and titanium were sufficient to cause significant variations in weld metal microstructural characteristics and mechanical properties.

4.2.2 Carbon Equivalent

The carbon equivalent provides a useful measure for assessing the maximum hardness and cold cracking susceptibility of welds in high strength steels.

One method often used to quantify the effect of alloy elements in weld metal is to relate the transformation products to a combined hardenability index such as the effective carbon equivalent.

The most popular carbon equivalent, CE (IIW) is defined by Suzuki [33] as:

$$CE(\%) = C + \frac{Mn}{6} + \frac{(Cu+Ni)}{15} + \frac{(Cr+Mo+V)}{5} \qquad (4.1)$$

In this equation, compositions are in weight percent.

This index is most accurate for slow cooling rates ($t_{8/5}$ longer than 10 seconds), which represents the cooling rate experienced in these SAW welds. However, for evaluating the cold cracking susceptibility of low carbon content steels with less than 0.18% carbon, a carbon equivalent as formulated by Ito and Bessyo, Pcm, has been used. Although this was initially used as a cold cracking parameter, it has been used successfully to determine the relative hardenability of various steels. According to Fleck [26], the Ito-Bessyo carbon equivalent is an indicator of the microstructure developed in weld metal if the titanium level is greater than approximately 0.0045 weight percent, which is much lower then the titanium levels observed in these test welds.

Pcm is defined by Suzuki [33] as:

$$Pcm(\%) = C + \frac{Si}{30} + \frac{(Mn+Cu+Cr)}{20} + \frac{Ni}{60} + \frac{Mo}{15} + \frac{V}{10} + (5 \times B) \qquad (4.2)$$

Once again, compositions are in weight percent.

Values for CE (IIW) and Pcm are shown in Table 4.2. Although both indexes are shown, the Ito-Bessyo (Pcm) carbon equivalent is used in the subsequent comparative analysis.

Figure 4.1 shows the Pcm carbon equivalent plotted against the weight percent nitrogen and figure 4.2 shows the Pcm carbon equivalent plotted against the weight percent titanium. As anticipated, there is no influence of nitrogen or titanium on the carbon equivalent for these welds.

With regard to carbon equivalent indexes, it seems appropriate that a CE index needs to be developed to take into account the role of nitrogen and titanium on cold cracking susceptibility and hardening of weld metal. Although this investigation quantified the influence of nitrogen and titanium, more detailed work beyond the scope of this thesis needs to be accomplished to adequately address a CE index which includes both nitrogen and titanium. Maybe this work will serve as a basis for such an investigation.

Table 4.2 Summary of carbon equivalent indexes for wire, base plate and welds.

DESCRIPTION	CE (IIW)	Pcm
LTEC 120S	0.6359	0.26085
BASE PLATE	0.7818	0.66500
WELD #1	0.6488	0.25609
WELD #2	0.6898	0.30100
WELD #3	0.6885	0.27733
WELD #4	0.6867	0.27660
WELD #5	0.6879	0.27267
WELD #6	0.7043	0.29433
WELD #7	0.6655	0.28287
WELD #8	0.6654	0.27501
WELD #9	0.6882	0.29665
WELD #10	0.7086	0.30195

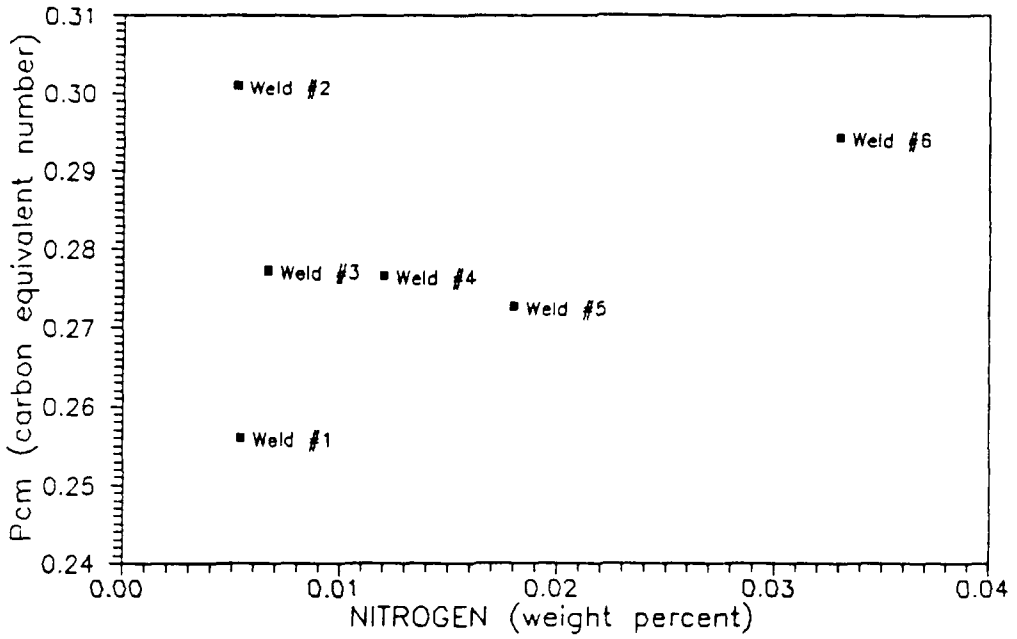

Figure 4.1 Weight percent nitrogen versus Pcm carbon equivalent number.

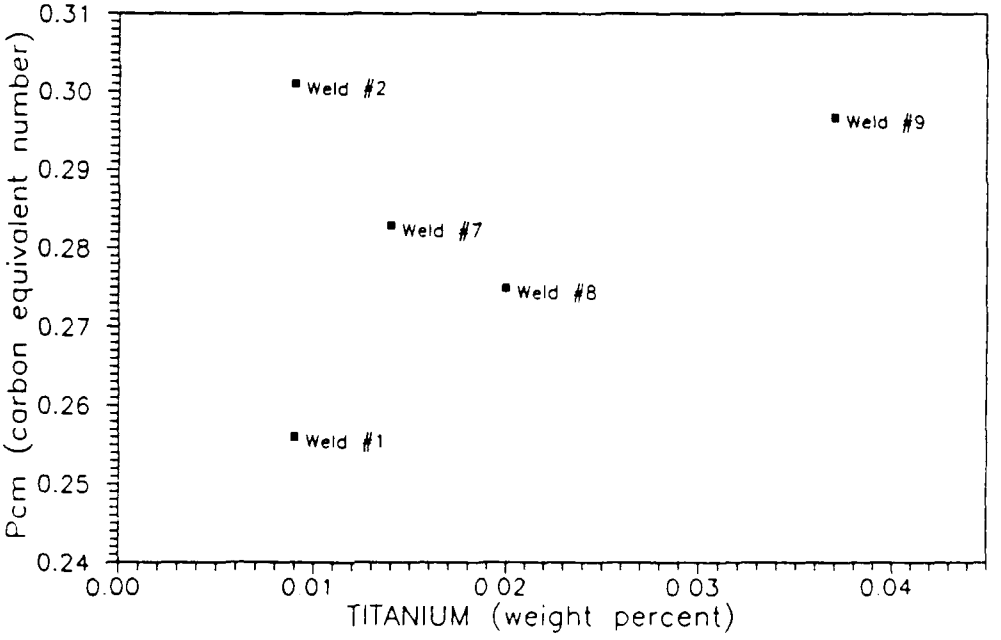

Figure 4.2 Weight percent titanium versus Pcm carbon equivalent number.

4.3 Microstructure

Next to mechanical testing, the quantification of the microstructural features of the weld provides the best estimate of the mechanical properties of the joint. By quantifying the influence of nitrogen and titanium on the microstructural details of the welds, several objectives are realized. First, the mechanisms by which nitrogen and titanium influence the microstructural details and mechanical properties are further enlightened. This contributes to the level of knowledge which is needed to improve consumables and techniques for welding high strength steels. Secondly, the volume fractions of the various microstructural constituents are correlated with the mechanical properties. This provides a data base useful for estimating the mechanical properties of similarly prepared high strength SAW weld deposits; where the estimate would be based on the amounts of titanium and nitrogen present and on the microstructural features observed in the weld.

Quantifying the microstructural features and correlating these features with the mechanical properties was an important part of this investigation. In this regard, a good portion of this work was spent investigating the various microstructural details of the weld deposits. The results of this analysis are presented in the following sections.

4.3.1 Weld Metal Macro-Analysis

Figure 4.4 shows macrographs for all ten welds at a magnification of 4.5X. From these macrographs, one can observe the bead geometry, number of passes, primary solidification structure, dilution, and microstructural characterization of each test weld.

As figure 4.4 illustrates, an important issue is that of choosing the area in each test weld at which qualitative and quantitative metallography is to be performed. It is crucial for comparing microstructural features among the welds that these areas be representative of the same thermal cycling. In this respect, the metallographic analyses were focused at the weld centroid and at a point located approximately 80 percent of the distance from the root to the top of the capping pass. This position is illustrated in figure 4.3. At this point in all the welds, the microstructure had been thermally cycled once by the capping pass thereby insuring that the influence of thermal cycling in this study was normalized. Comparing the macrographs shows that all the welds have basically the same tertiary details at this selected location.

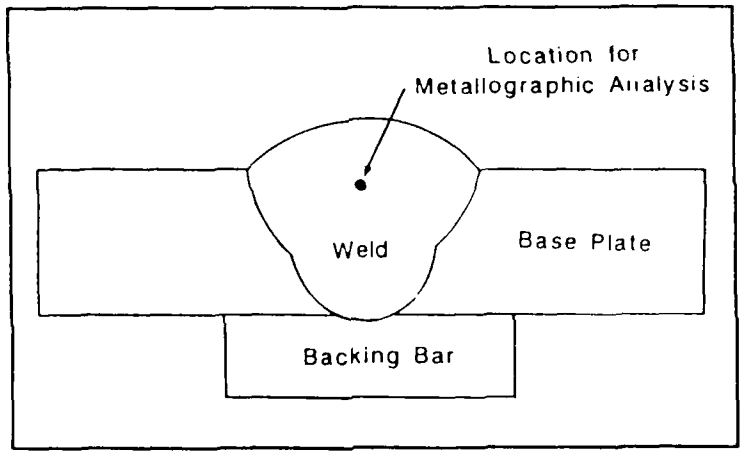

Figure 4.3 A schematic diagram which shows the location on each weld sample where qualitative and quantitative metallography were performed.

4.3.2 Weld Metal Microstructural Analysis

The resulting microstructures of the experimental weldments are presented at 400X (optical) in figure 4.5, at 1000X (SEM) in figure 4.6 and at 5000X (SEM) in figure 4.7. As shown in figure 4.5, the microhardness indentations outline the location

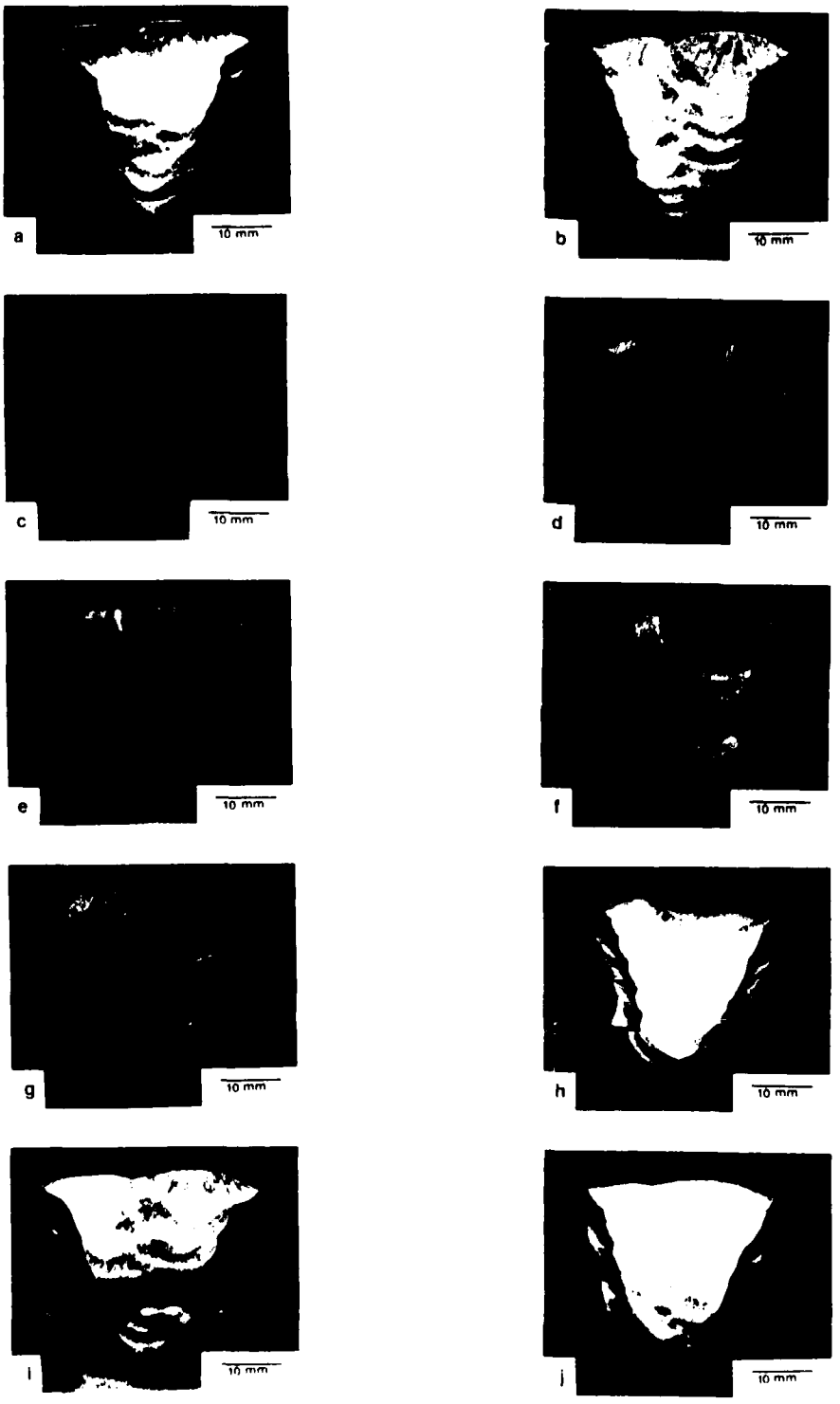

Figure 4.4 Optical macrographs at 4.5X magnification showing the tertiary microstructure. 2% nital etch. a) weld #1, b) weld #2, c) weld #3, d) Weld #4, e) weld #5, f) weld #6, g) weld #7, h) weld #8, i) weld #9, j) weld #10.

of the 150 μm by 150 μm square selected for metallographic examination. Detailed microstructural analyses were carried out at this location on all of the specimens to identify phases and morphologies.

During quantitative metallography for the ferritic phases, each region examined was classified as either fine interlocking laths of acicular ferrite "**AF**", blocky polygonal ferrite "**PF**", grain boundary ferrite "**GF**", or ferrite plates separated by lines of microphase. This latter constituent was identified in chapter 3 as ferrite with aligned M-A-C (martensite, austenite, or carbide) "**AC**".

As chapter 3 addressed, the process by which these microstructural features form is complex and there are many variables which influence the transformations. However, in simplified terms, this HY-100 weld metal microstructure was formed upon cooling when equiaxed ferrite grains nucleated and grew from prior austenite grain boundaries (grain boundary ferrite). This was followed by the intragranular, inclusion-assisted, nucleation of fine acicular ferrite. Finally, carbon-enriched regions between the acicular ferrite laths, or adjacent to grain boundary ferrite, either transforms to ferrite carbide aggregates or martensite, or remains, untransformed, as retained austenite (microphases).

As shown in figures 4.5 through 4.7, a large volume fraction of acicular ferrite and ferrite with aligned M-A-C were produced in all the weldments. The next most prominent microstructures formed, as shown in these figures, were intragranular polygonal ferrite and grain boundary ferrite. Finally, a small amount of martensite-austenite constituent "**M-A**" was present although not easily identified in these micrographs. Additionally, there was probably a small amount of retained austenite; however, the retained austenite phase is difficult to resolve with the use of the light microscope or SEM. For this study, this constituent is not evaluated primarily due to this difficulty in detection.

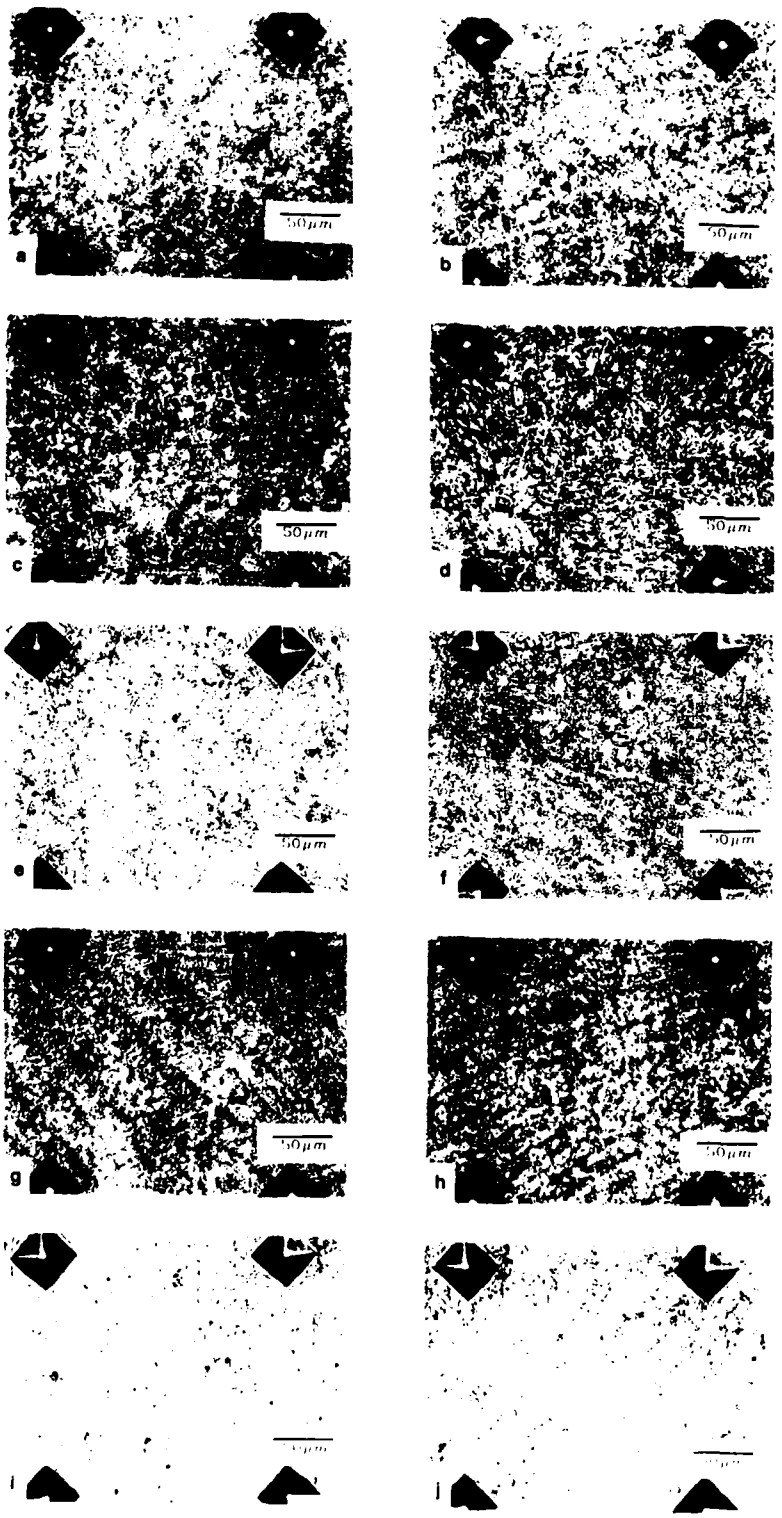

Figure 4.5 Optical micrographs at 400X magnification showing the weld metal microstructure. 2% nital etch. a) weld #1, b) weld #2, c) weld #3, d) Weld #4, e) weld #5, f) weld #6, g) weld #7, h) weld #8, i) weld #9, j) weld #10.

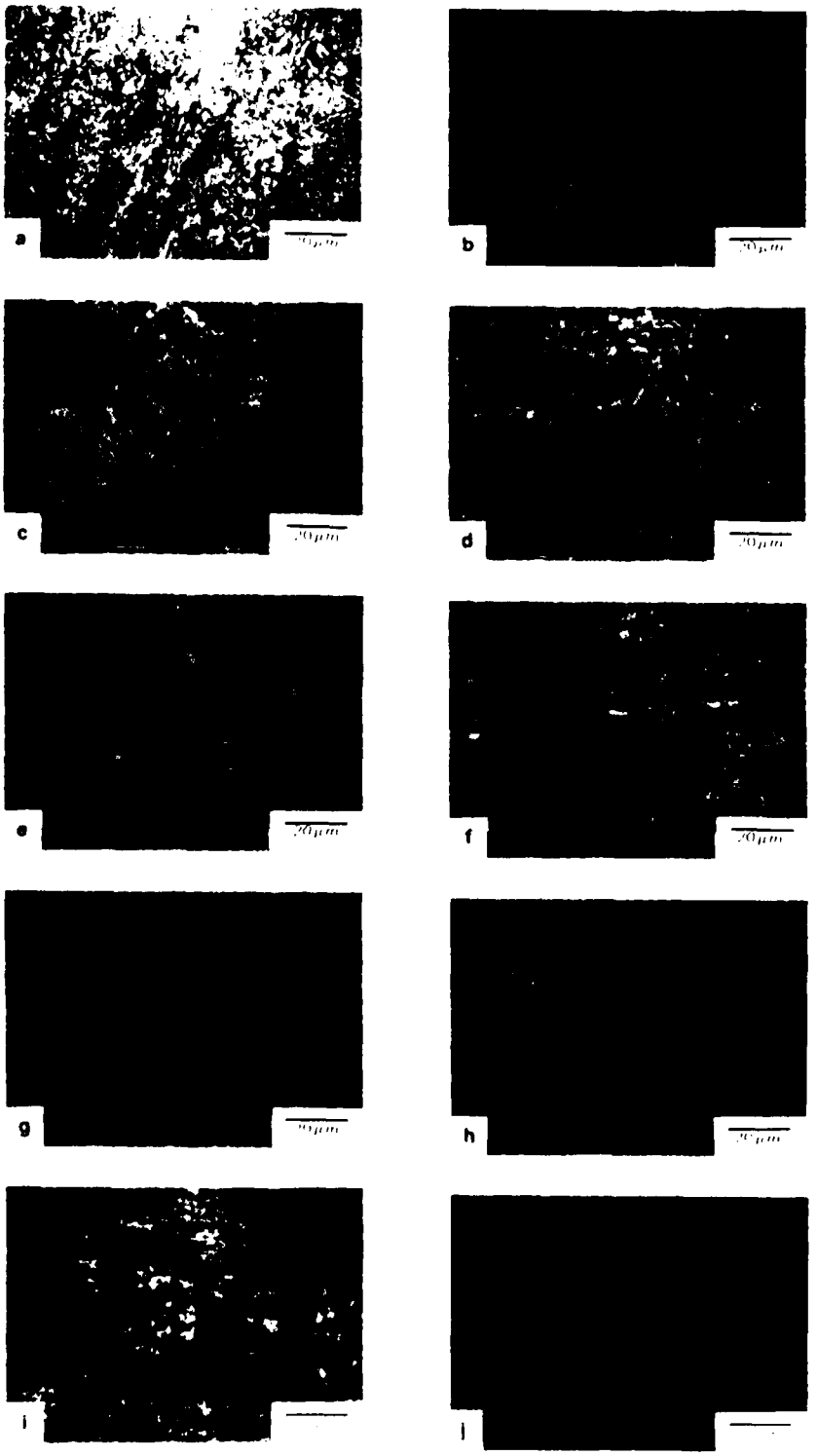

Figure 4.6 SEM micrographs at 1000X magnification showing the weld metal microstructure. 2% nital etch. a) weld #1, b) weld #2, c) weld #3, d) Weld #4, e) weld #5, f) weld #6, g) weld #7, h) weld #8, i) weld #9, j) weld #10.

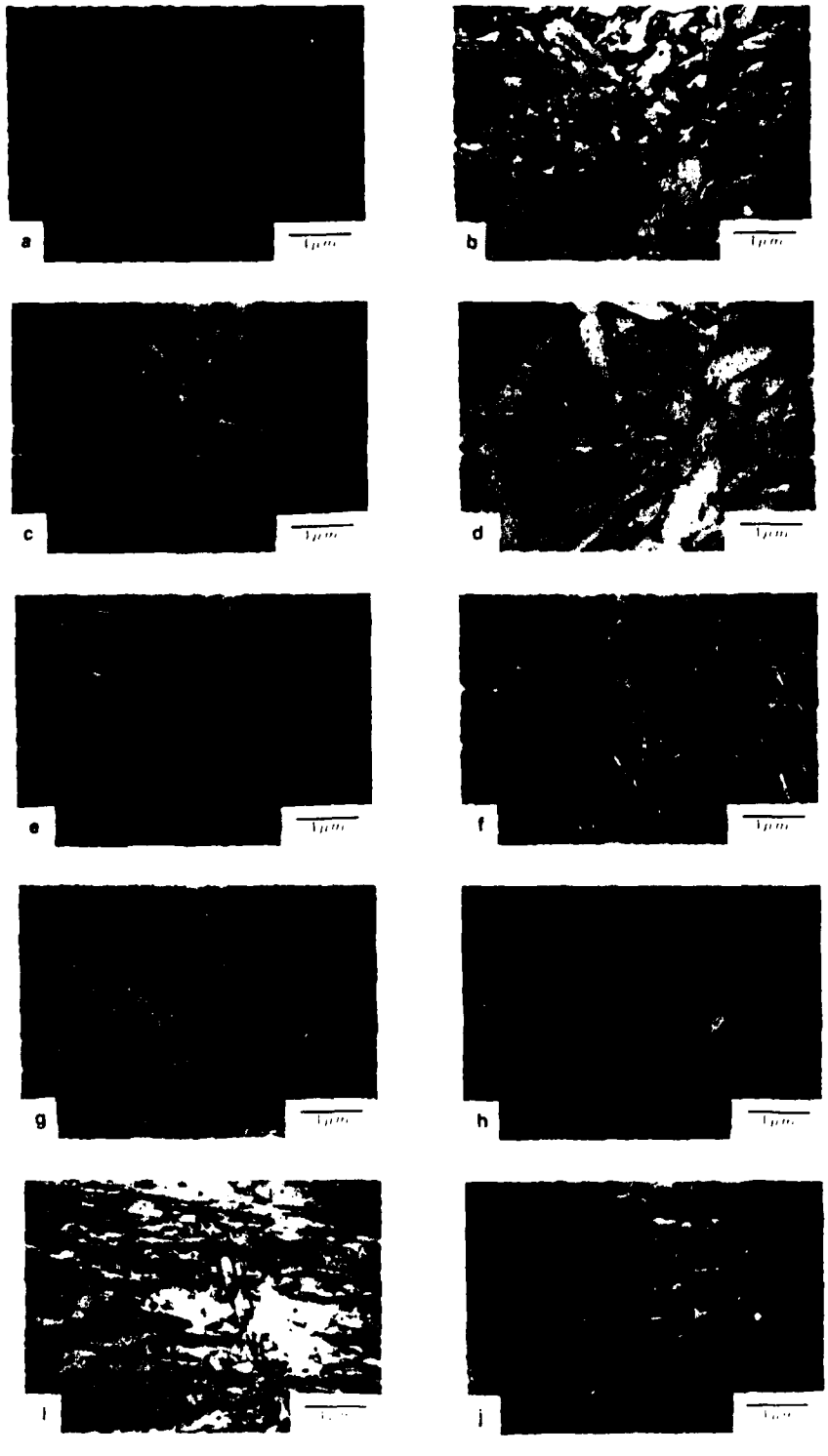

Figure 4.7 SEM micrographs at 5000X magnification showing the weld metal microstructure. 2% nital etch. a) weld #1, b) weld #2, c) weld #3, d) Weld #4, e) weld #5, f) weld #6, g) weld #7, h) weld #8, i) weld #9, j) weld #10.

4.3.3 Quantitative Metallography

The metallographic examination of each weld in this investigation provided quantification of the microstructural constituents, the prior austenite grain sizes, and the size, number and relative composition of the inclusions. The results of these quantitative analyses show trends that indicate significant correlations exists between the weld metal microstructural features, and the nitrogen and titanium compositional variations.

A systematic manual point counting technique proposed by ASTM Standard E562-83 [34] was used to determine the volume fraction of acicular ferrite, grain boundary ferrite, polygonal ferrite, ferrite with aligned M-A-C, and M-A constituent. Within the 150 μm by 150 μm area of each weld, nine micrographs were taken and later pieced together into a montage. All point counts were performed over the entire 150 μm by 150 μm region using a 1 mm by 1 mm grid overlaid on the nine 1000X micrographs. A sample size of nine fields for each test weld was considered to provide a representative statistical sampling. Additionally, no less than 1000 points per micrograph were counted.

According to the ASTM standard [34], the average percentage of grid points on the features of interest provides an unbiased statistical estimator for the volume percentage within the three dimensional microstructure. The average, $\overline{P}_p$, the standard deviation estimator, $\hat{S}$, and the 95% confidence interval, CI, were calculated and recorded for each set of nine fields. The equations for calculating these values are as follows:

$$\overline{P}_p = \frac{1}{n}\sum_{i=1}^{n} P_{p_i} \qquad (4.3)$$

In this equation, P_{p_i} equals the percentage of grid points in the ith field and n equals the number of fields counted.

$$\hat{S} = \left\{ \frac{1}{(n-1)} \sum_{i=1}^{n} \left[P_{p_i} - \bar{P}_p \right]^2 \right\}^{0.5} \tag{4.4}$$

$$CI = 2.26 \times \frac{\hat{S}}{\sqrt{n}} \tag{4.5}$$

The volume percentage estimate V_v is calculated as:

$$V_v \doteq \bar{P}_p \pm CI \tag{4.6}$$

The estimate of the percent error associated with the estimate is calculated as:

$$\% \text{ error} = \frac{CI}{\bar{P}_p} \times 100 \tag{4.7}$$

The results of the quantitative point count for volume percents of the various weld metal microstructural constituents are presented in Table 4.3.

The method outlined in the ASM Handbook [32] was used to calculate the prior austenite grain size. This standard defines a mean intercept length, L_γ, to represent the average statistical grain size or diameter.

For space-filling grains, the ASM Handbook defines mean intercept length as:

$$L_\gamma = \frac{L_T}{(P \times M)} \tag{4.8}$$

In this equation, the mean intercept length, L_γ, equals the total test-line length, L_T, divided by the magnification, M, and the number of grain boundary interceptions, P. In order for this to be considered statistically representative of the weld, at least 50 grains within each weld need to be measured [32]. However, do to problems in etching the grain boundaries; only an average of 12 grains per weld were measured.

Thus, the accuracy of the values obtained for prior austenite grain size was not well defined. The prior austenite grain size calculated for each weld is shown in Table 4.4.

Finally, a magiscan image analyzer was used to quantify the shapes, sizes, total numbers and area fractions of inclusions. The image analyses were conducted on the same micrographs which were produced for microstructural examination. The image analyzer provided the best method for an accurate and rapid inclusion quantification. In conjunction with this inclusion count, an energy dispersive X-ray spectrometer associated with the Cambridge SEM was used to qualitatively evaluate the compositions of the inclusions. The results of the inclusion quantification for each weld is shown in Table 4.5.

Table 4.3 Fractions of microstructural constituents within each weld sample, volume percent ± 95% confidence interval.

DESCRIPTION		WELD #1	WELD #2	WELD #3	WELD #4	WELD #5	WELD #6	WELD #7	WELD #8	WELD #9	WELD #10
NITROGEN (wgt %)		.0054	.0.052	.0066	.0120	.0180	.0330	.0053	.0049	.0051	.0170
TITANIUM (wgt %)		.0090	.0090	.0090	.0090	.0090	.0100	.0140	.0200	.0370	.0140
AF	Vol%	69.61	68.38	44.02	40.30	36.39	36.14	62.28	53.06	37.92	32.41
	95% CI	2.71	2.56	2.97	3.33	4.20	3.52	2.11	1.26	2.90	2.05
	% Error	3.89	3.74	6.75	8.26	11.54	9.74	3.39	2.37	7.65	6.33
AC	Vol %	17.67	17.53	37.15	38.13	40.22	41.28	24.17	32.29	47.04	48.97
	95% Ci	1.99	2.27	2.51	3.02	2.77	4.12	1.91	2.38	3.11	3.25
	% Error	11.26	12.95	6.76	7.92	6.89	9.98	7.90	7.37	6.61	6.64
GF	Vol %	6.65	5.84	10.48	12.34	12.66	12.51	5.15	6.89	7.81	5.86
	95% CI	0.91	1.40	1.09	1.52	1.25	1.14	1.08	0.98	0.87	1.63
	% Error	24.93	20.47	10.40	12.32	9.87	9.11	17.56	14.22	11.13	27.82
PF	Vol %	2.79	2.49	3.81	5.11	5.55	4.75	1.81	2.38	3.46	8.52
	95% CI	0.25	0.34	0.78	1.06	0.95	1.12	0.92	1.20	0.82	1.80
	% Error	13.97	22.82	20.47	20.74	17.12	23.58	19.13	27.40	23.70	21.13
M-A	Vol %	3.11	2.73	3.52	3.96	4.32	4.84	2.98	3.33	3.55	3.65
	95% CI	0.17	0.25	0.29	0.32	0.28	0.34	0.15	0.22	0.40	0.18
	% Error	5.48	9.26	8.29	8.21	6.48	7.02	5.03	6.67	11.27	5.00

Table 4.4 Prior austenite grain size calculated for each weld sample.

DESCRIPTION	WELD #1	WELD #2	WELD #3	WELD #4	WELD #5	WELD #6	WELD #7	WELD #8	WELD #9	WELD #10
Prior Austenite Grain size (μ m)	65	69	67	62	59	60	61	59	53	63

Table 4.5 Quantification of inclusions by number, size and area fraction for each weld sample.

DESCRIPTION	WELD #1	WELD #2	WELD #3	WELD #4	WELD #5	WELD #6	WELD #7	WELD #8	WELD #9	WELD #10
Total Inclusions	405	387	447	435	428	460	442	551	670	594
Inclusions <1.0 μm	381	368	420	399	405	419	397	487	582	522
Inclusion >1.0 μm	24	19	27	36	23	41	45	64	88	72
Area % Inclusions	.4937	.3884	.5271	.5132	.4986	.5506	.5221	.6657	.8439	.6412

4.3.3.1 Acicular Ferrite and Ferrite With Aligned M-A-C

The mechanism for acicular ferrite formation has been linked to the nucleation of AF on fine inclusions trapped within the weld metal during solidification or nucleation of AF at dislocation substructure sites. The maximum acicular ferrite volume fraction has been shown [35] to be most strongly associated with a high density of inclusions of a critical size (less than or equal to 1 μm diameter).

The formation of ferrite with aligned M-A-C has been linked with the presence of precipitated carbides, retained austenite and martensite along the ferrite plates [31]. Increased AC is often shown to be most strongly associated with faster weld metal cooling rates.

Of particular relevance to this investigation is the finding that the notch toughness is favorably influenced by increasing the amount of AF and decreasing the amount of AC. Specifically, the good low temperature toughness of acicular

ferrite weld metal arises from the very fine effective ferrite grain size which exist without preferential fracture paths. Furthermore, the finer and more interlocking the individual AF laths, other factors held constant, the better the effect of AF on toughness. Conversely, the poor low temperature toughness of ferrite with aligned M-A-C weld metal arises from the larger effective grain sizes due to ferrite plates being separated by low angle grain boundaries. Additionally, AC exhibits high crystallographic orientation which provides a lower energy path for crack propagation.

Since the only parameters that were varied in this investigation were the weight percent nitrogen and the weight percent titanium, the separate influence of these elemental changes on volume percent acicular ferrite and ferrite with aligned M-A-C can be individually quantified, as shown in figures 4.8 and 4.9 for incremental increases in nitrogen and 4.10 and 4.11 for incremental increases in titanium.

Figure 4.8 shows that an increase in the weld metal nitrogen concentration from 0.0054 to 0.033 weight percent resulted in a decrease in fine intragranular acicular ferrite from 69.61 ± 2.71 to 36.14 ± 3.52 volume percent. The implication is that nitrogen has a strong deleterious effect on the amount of acicular ferrite microstructure present in the weld metal.

Figure 4.9 shows that an increase in the weld metal nitrogen concentration from 0.0054 to 0.033 weight percent resulted in an increase in the amount of ferrite with aligned M-A-C from 17.67 ± 1.99 to 41.28 ± 4.12 volume percent. Converse to its influence on the volume percent AF, nitrogen promotes the formation of AC.

Qualitatively it was observed that with increased nitrogen content, less acicular ferrite microstructure was formed and what did form was coarser than the acicular ferrite in the low nitrogen welds. Additionally, the interlathed matrix of ferrite with aligned M-A-C became more aligned and needle shaped as the nitrogen level increased. This can be seen in the micrographs of figure 4.7.

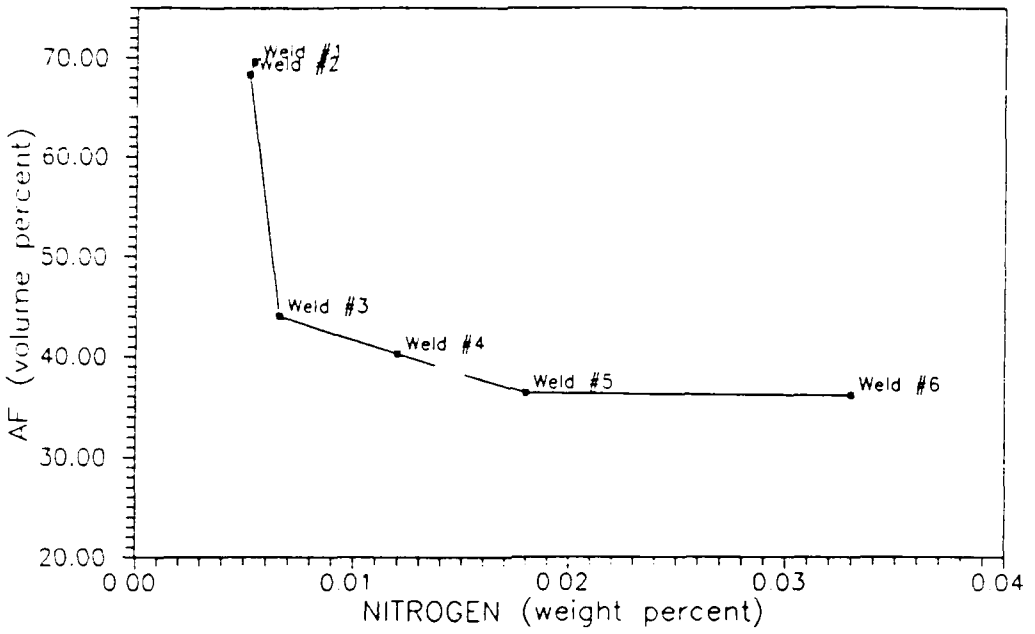

Figure 4.8 Weight percent nitrogen versus the volume percent acicular ferrite.

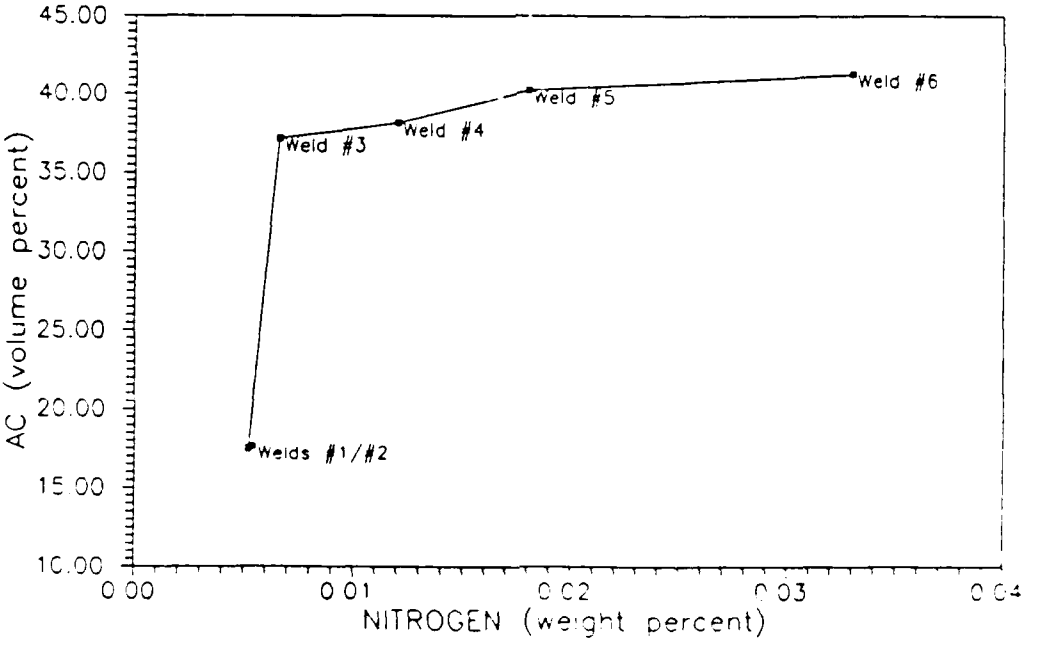

Figure 4.9 Weight percent nitrogen versus the volume percent ferrite with aligned M-A-C.

The means by which nitrogen inhibits formation of acicular ferrite and enhances formation of ferrite with aligned M-A-C can be related to nitrogen's influence on the CCT diagram. The influence of chemical composition is expressed by a change in shape and a shift of the CCT diagram to shorter or longer times as discussed in chapter 3. In this respect, the interaction of nitrogen is especially important in terms of its affect on the development of acicular ferrite. Nitrogen results in a shift in the CCT diagram to the left which correlates with a longer transformation time. This results in the reduction of fine, interlocking AF and the increase in highly aligned, needle-like AC as the nitrogen content increases.

With a high volume of aligned, needle-like AC microstructure, toughness is expected to decrease as the energy to propagate a crack in the aligned direction decreases. This is supported by Tweed and Knot [4] who show that a low ductile-brittle transition temperature, i.e., a high resistance to cleavage, will occur when the proportion of acicular ferrite is high and that of grain boundary ferrite and ferrite with aligned M-A-C are correspondingly low. However, they also propose that an increase in the amount of AF in the microstructure is not always beneficial to weld metal toughness, if the deposited yield strength increases too much as a result of phenomena like solid solution hardening or precipitation hardening. The net effect of these factors may even be negative, and so toughness decreases.

Figure 4.10 shows that an increase in the weld metal titanium concentration from 0.009 to 0.037 weight percent resulted in a decrease in the volume percent acicular ferrite from 69.61 ± 2.71 to 37.92 ± 2.90 volume percent.

Conversely, figure 4.11 shows that as titanium was increased from 0.009 to 0.037 weight percent, the volume percent of ferrite with aligned M-A-C increased from 17.67 ± 1.99 to 47.04 ± 3.11 volume percent.

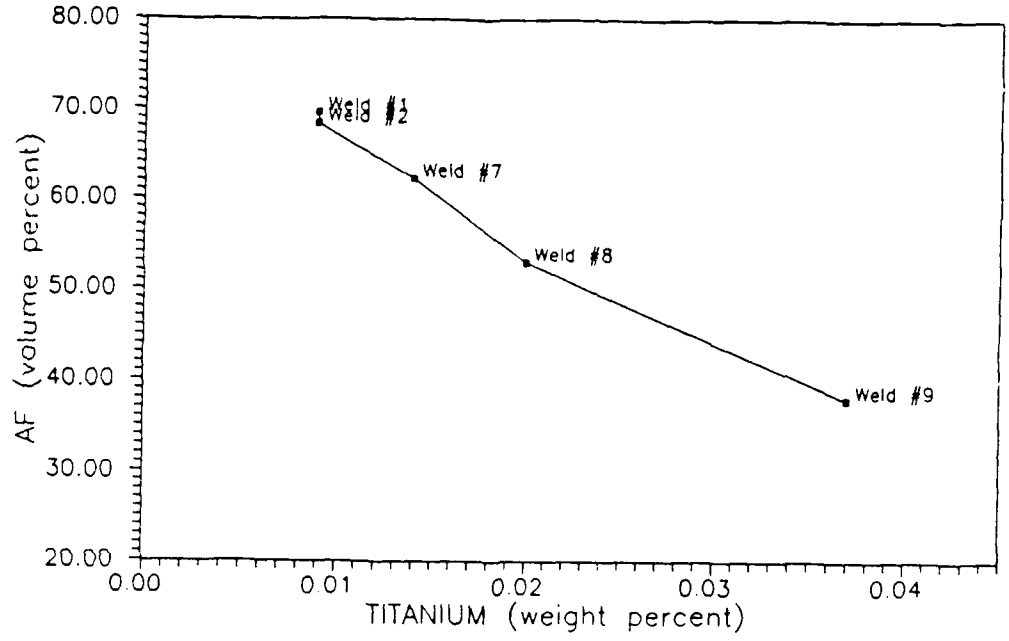

Figure 4.10 Weight percent titanium versus the volume percent acicular ferrite.

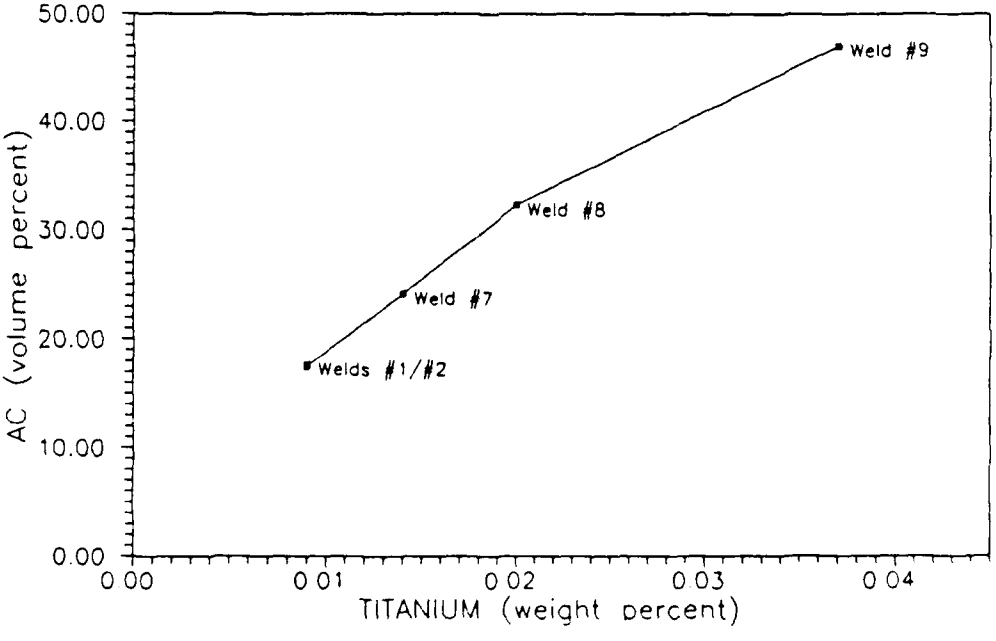

Figure 4.11 Weight percent titanium versus the volume percent ferrite with aligned M-A-C.

Titanium in small amounts has been shown to promote the formation of AF due to an increase in the TiO and TiN nucleation sites for AF and due to a shift in the CCT diagram to the right which results in shorter transformation times. However, this investigation showed that above 0.009 weight percent titanium; the acicular ferrite volume percent decreased, much of the microstructure coarsened and became more aligned, and there was a significant increase in the amount of ferrite with aligned M-A-C.

From figures 4.10 and 4.11 we can see that the baseline welds (#1 and #2) indicate that the optimum concentration for titanium is less than or equal to 0.009 weight percent. A titanium concentration in this range is believed to be optimum in terms of obtaining a high acicular ferrite content and a low ferrite with aligned M-A-C content through a proper balance between titanium, boron, aluminum, oxygen, and nitrogen.

It is believed that any titanium increase up to 0.009 weight percent would result in more nitrogen combined as TiN, which would leave less nitrogen free to shift the C-curves towards longer transformation times. Thus, more AF and less AC would be transformed.

A 0.009 weight percent titanium may provide the best titanium/oxygen ratio to satisfy complete TiO formation demands and tie up nitrogen as finely dispersed TiN particles. This would mean that there is effectively no titanium left over to form embrittling carbides and no nitrogen left over to shift the C-curves towards more AC formation and less AF formation. Additionally, boron is left to segregate to the prior austenite grain boundaries.

Above 0.009 weight percent titanium, excess titanium has a marked influence on the microstructure as evidenced by the high content of ferrite with aligned M-A-C. Although the exact mechanism for this is not clearly understood, other works have observed the same occurrence in response to increasing titanium concentrations, [22] and [25]. In the case of Synder and Pense [25], they describe this coarse, needle-like

and aligned microstructure in terms of a ferrite veining phenomena which they show to increase with higher levels of titanium. They also correlate this high content of ferrite veining with a decrease in fracture toughness in the weld metal.

4.3.3.2 Grain Boundary Ferrite and Polygonal Ferrite

When the transformation from austenite to ferrite occurs in weld metal, grain boundary ferrite appears first at the grain boundary of prior austenite. Grain boundary ferrite grows in either elongated or granular form along the grain boundary of austenite. Polygonal ferrite also appears, but it exists as aggregate, blocky, intragranular ferrite. In most weld metals, the transformation to grain boundary ferrite at the austenite grain boundary precedes that of intragranular polygonal ferrite. When the cooling rate is slow or alloying additions are not closely balanced, increasing amounts of grain boundary ferrite and polygonal ferrite are observed. Both grain boundary ferrite and polygonal ferrite are detrimental to weld metal toughness.

Figures 4.12 and 4.13 show that an increase in the weld metal nitrogen concentration from 0.0054 to 0.033 weight percent resulted in an increase in grain boundary ferrite from 6.65 ± 0.91 to 12.51 ± 1.14 volume percent; and an increase in polygonal ferrite from 2.79 ± 0.25 to 4.75 ± 1.12 volume percent, respectively.

Thus, both grain boundary ferrite and polygonal ferrite contents increase as the weight percent nitrogen increases. Once again, this affect can be related to nitrogen's influence on the C-curves. Specifically, nitrogen pushes the C-curves to longer transformation times which promotes the formation of both GF and PF.

Figure 4.14 shows that an increase in weld metal titanium concentration from 0.009 to 0.037 weight percent resulted in a slight increase in the volume percent of grain boundary ferrite from 6.65 ± 0.91 to 7.81 ± 0.87 volume percent.

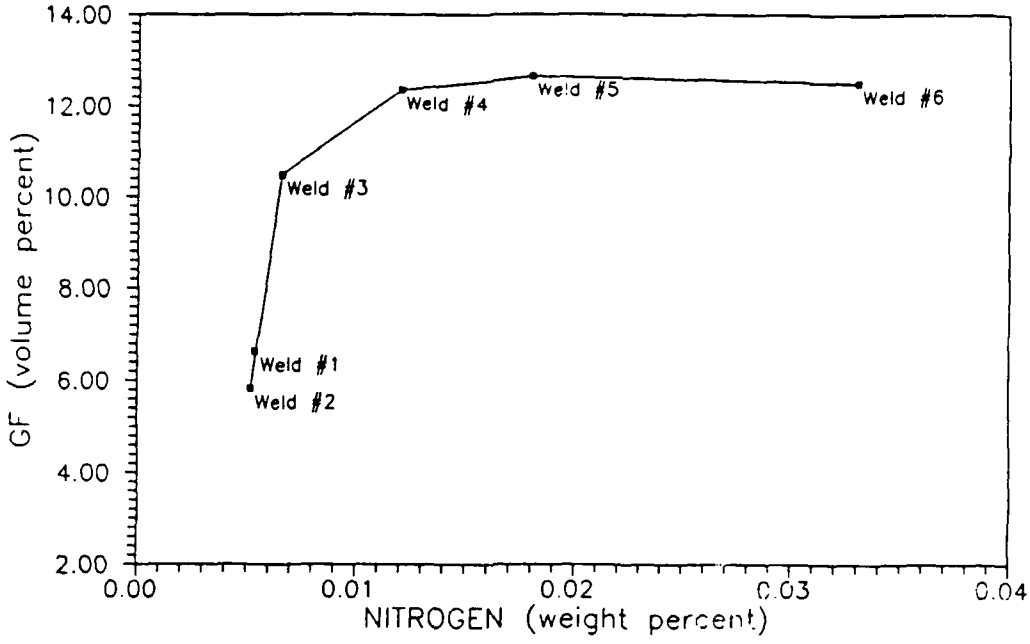

Figure 4.12 Weight percent nitrogen versus the volume percent grain boundary ferrite.

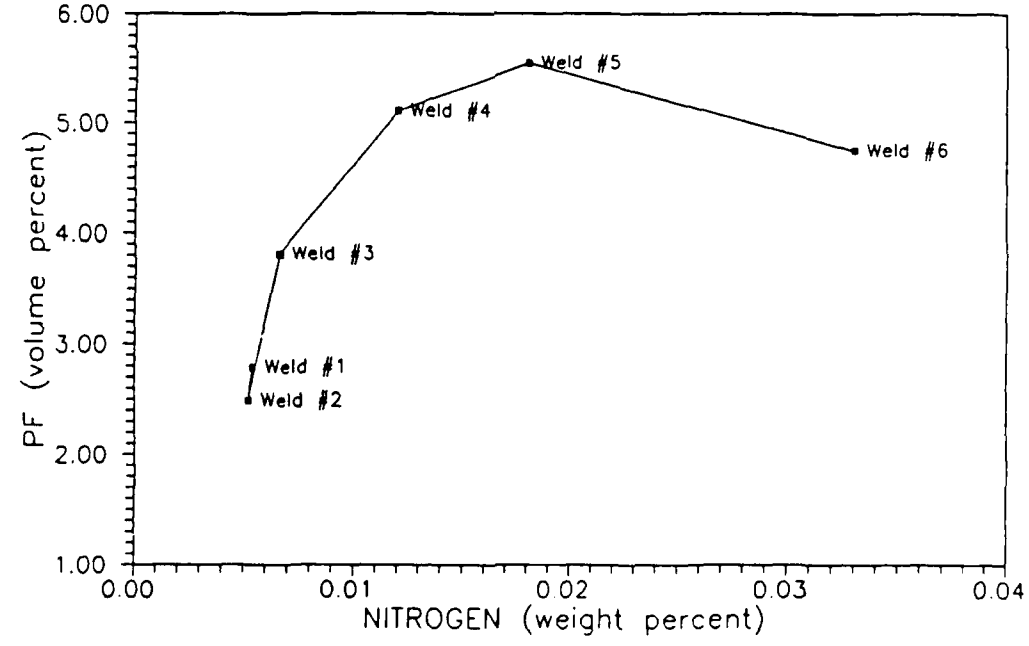

Figure 4.13 Weight percent nitrogen versus the volume percent polygonal ferrite.

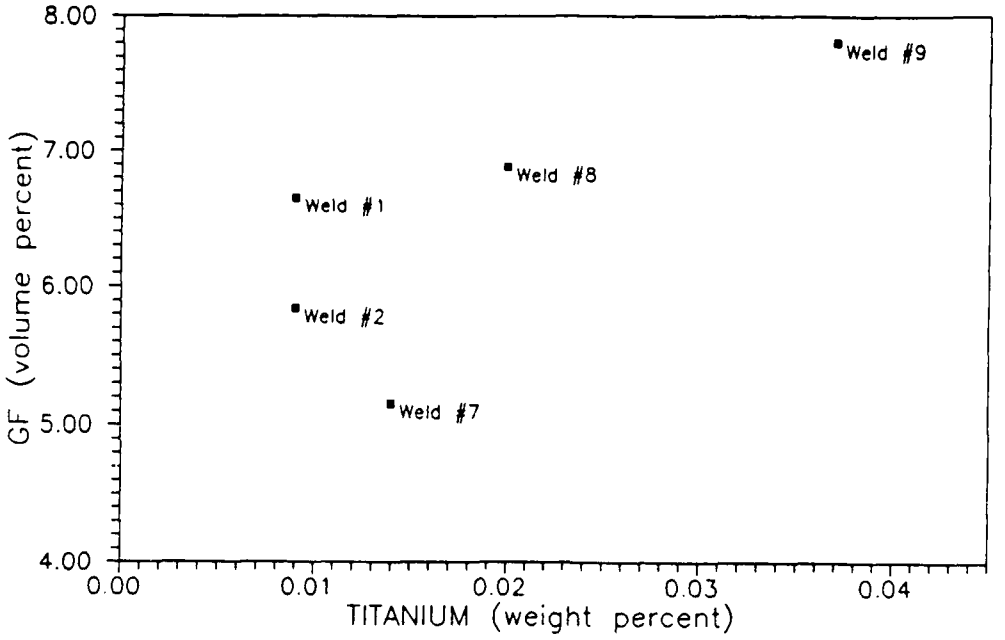

Figure 4.14 Weight percent titanium versus the volume percent grain boundary ferrite.

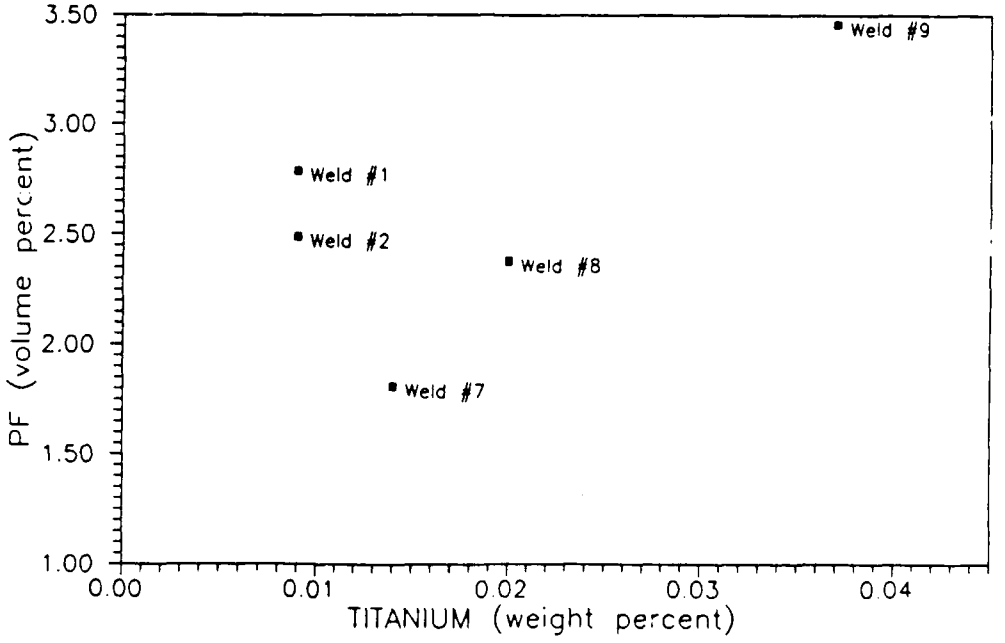

Figure 4.15 Weight percent titanium versus the volume percent polygonal ferrite.

Figure 4.15 shows that an increase in weld metal titanium concentration from 0.009 to 0.037 weight percent resulted in a slight increase in the volume percent PF from 2.79 ± 0.25 to 3.46± 0.82 volume percent.

In general, figures 4.14 and 4.15 indicate that titanium variations had minimal impact on the volume percents of GF and PF.

4.3.3.3 M-A Constituent

Figure 4.16 shows that an increase in weld metal nitrogen content from 0.0054 to 0.033 weight percent resulted in an increase in M-A constituent from 3.11 ± 0.17 to 4.84 ± 0.34 volume percent. This data indicates that nitrogen variations have a significant influence on the volume percent M-A.

Since M-A embrittlement is suspected to be a mechanism influencing the toughness properties of the weld, the Charpy V-notch ductile-to-brittle transition temperature (DBTT) is plotted against the corresponding change in M-A content among all the welds as shown in figure 4.17. This figure shows a significant trend as demonstrated by a decrease in the Charpy V-notch transition temperature of 78.96 ℃ as the volume percent M-A constituent increased from 3.11 ± 0.17 to 4.84 ±0.34 volume percent.

These results are supported in a study done by Lau et al [23]. In their study, they show that the M-A constituent is an important phase which contributes to embrittlement of the weld and ultimately lowers fracture toughness. Additionally, they believe that the M-A constituent increases with an increase in the nitrogen content; and, except for the carbon and nitrogen contained in the M-A constituent, the content of other elements remains the same as that in the matrix. So, as nitrogen increases, the content of nitrogen in the M-A constituent increases by segregation of nitrogen to these carbon-enriched sites, which enhances the tendency of twinned martensite formation. This makes the M-A phase even more abundant and embrittling.

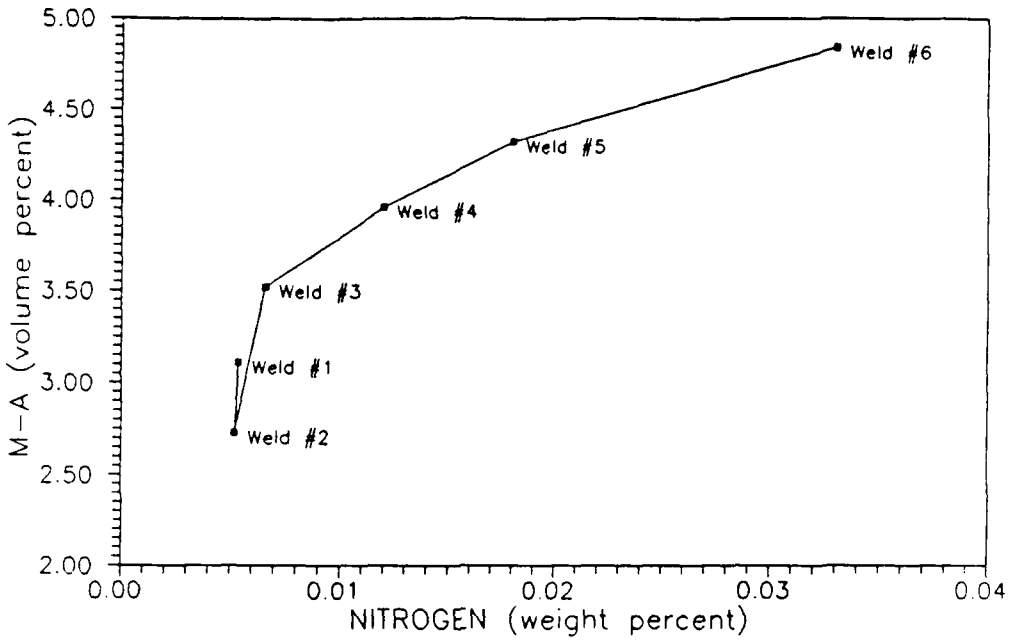

Figure 4.16 Weight percent nitrogen versus the volume percent of M-A constituent.

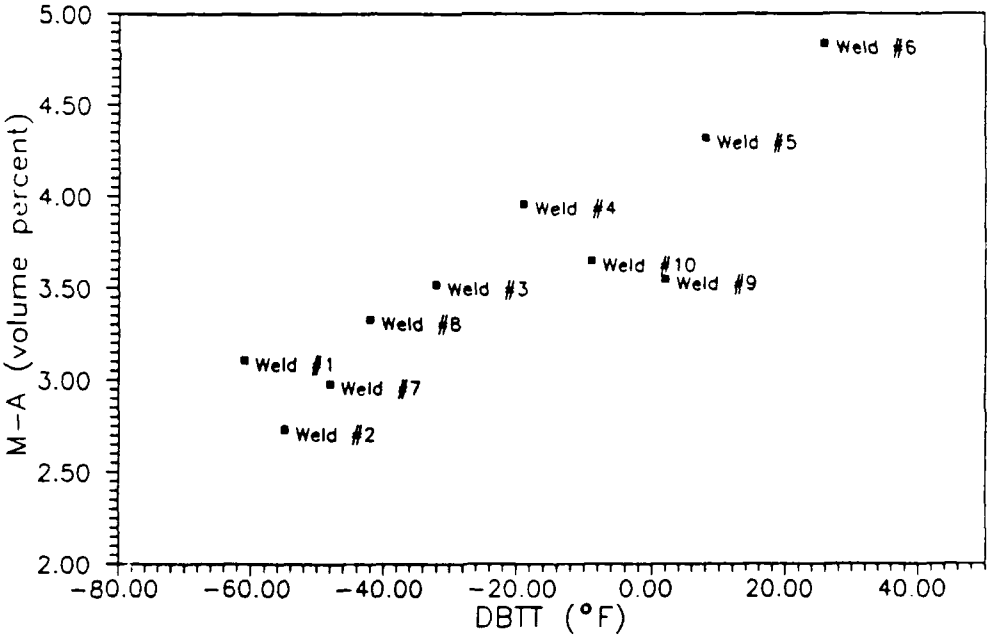

Figure 4.17 Charpy V-notched DBTT versus the volume percent M-A constituent.

As discussed in chapter 3, M-A islands are believed to be the site for crack initiation. Thus, as the M-A content increases, the fracture toughness is expected to deteriorate.

Figure 4.18 shows that as the titanium content increased from 0.009 to 0.037 weight percent, the volume percent M-A constituent increased from 3.11 ± 0.17 to 3.55 ± 0.40 volume percent. This plot indicates that titanium added to the weld slightly increased the volume percent M-A. However, this increase is much smaller than the increase in M-A observed from nitrogen additions. Additionally, there is no obvious mechanism to explain how titanium increased the content of M-A constituent in these welds.

Finally, it is worth noting that the M-A constituent observed in these welds consisted of blocky islands with an average grain size of 2 μm. The M-A constituent was blocky versus stringy due to the slow cooling rates experienced by the SAW process.

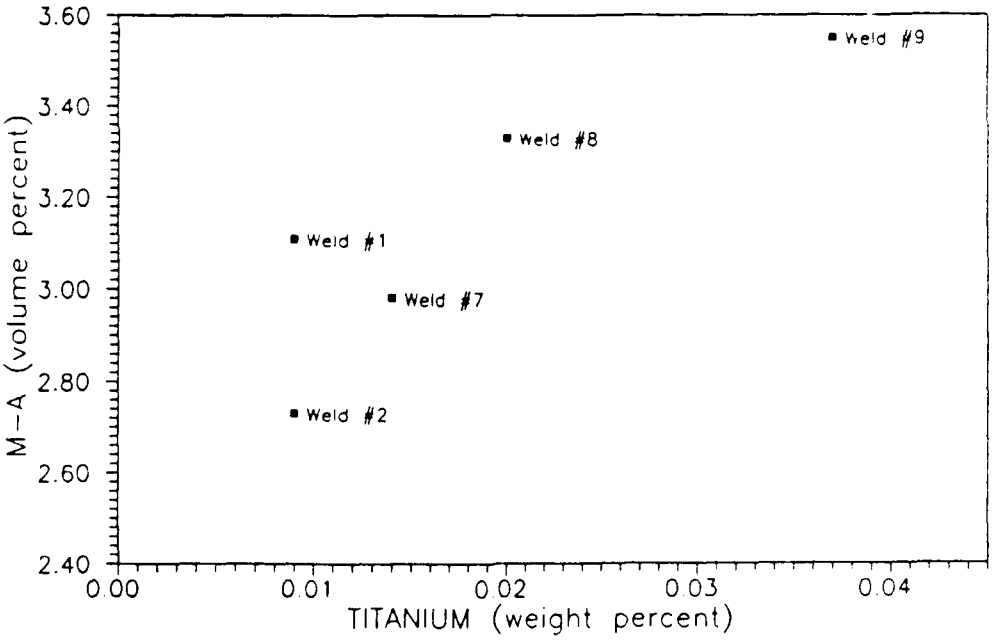

Figure 4.18 Weight percent titanium versus the volume percent M-A constituent.

4.3.3.4 Prior Austenite Grain Size

After solidification, austenite grain growth occurs during cooling from the peritectic temperature to 1200 ℃ because the mobility of grain boundaries is high. The extent of grain growth depends on several factors, the most important of which are the cooling rate above about 1200 ℃ and the volume fraction and size distribution of inclusions in the austenite. A smaller austenite grain size results as the mean particle size decreases or as the volume fraction increases, or both. The cooling rate above 1200 ℃ depends on the heat input, which governs the volume of the deposited nugget (i.e. the heat source during cooling); and the section thickness, which governs the efficiency of heat removal from the fusion zone. The time available for grain growth will increase with increasing heat input and decreasing section thickness [22].

It has been shown by Brownlee [22] that the prior austenite grain diameter in a series of SAW welds made on Q&T steel plate is a function of the weld metal oxygen content. For a given thermal cycle, the prior austenite grain size decreased with increasing weld metal oxygen concentration reflecting an increase in the number of grain boundary pinning sites.

According to Harrison and Farrar [3], the result of decreasing the prior austenite grain size is an increase in the amount of grain boundary ferrite in the final microstructure. Additionally, with smaller austenite grain size, it is easier for weld metal to transform to polygonal ferrite dominated structures, whereas with larger grain size, acicular ferrite is dominant.

Harrison and Farrar [3] also contend that the influence of prior austenite grain size on transformation temperature shows that the transformation temperature is depressed by some 10 ℃-20 ℃ per ASTM number increase, indicating the powerful effect of this variable. Thus, notch toughness is unfavorably influenced by reducing the average size of prior austenite grains.

Figure 4.19 shows that the prior austenite grain size decreased slightly from 65 μm to 60 μm as the nitrogen content increased from 0.0054 to 0.033 weight percent. This is most likely due to the pinning effect on the prior austenite grain boundaries from the increasing inclusion content observed at higher nitrogen concentrations. The increase in the grain boundary ferrite observed at higher nitrogen concentrations can be attributed to this reduction in size of the prior austenite grains.

Figure 4.20 shows that the prior austenite grain size was refined slightly from 65 μm to 53 μm as the titanium content increased from 0.009 to 0.037 weight percent. This indicates that the higher inclusion content due to the added titanium serves to pin the grain boundaries and limit the prior austenite grain size. This smaller prior austenite grain size accounts for the increasing content of grain boundary ferrite observed at higher titanium concentrations.

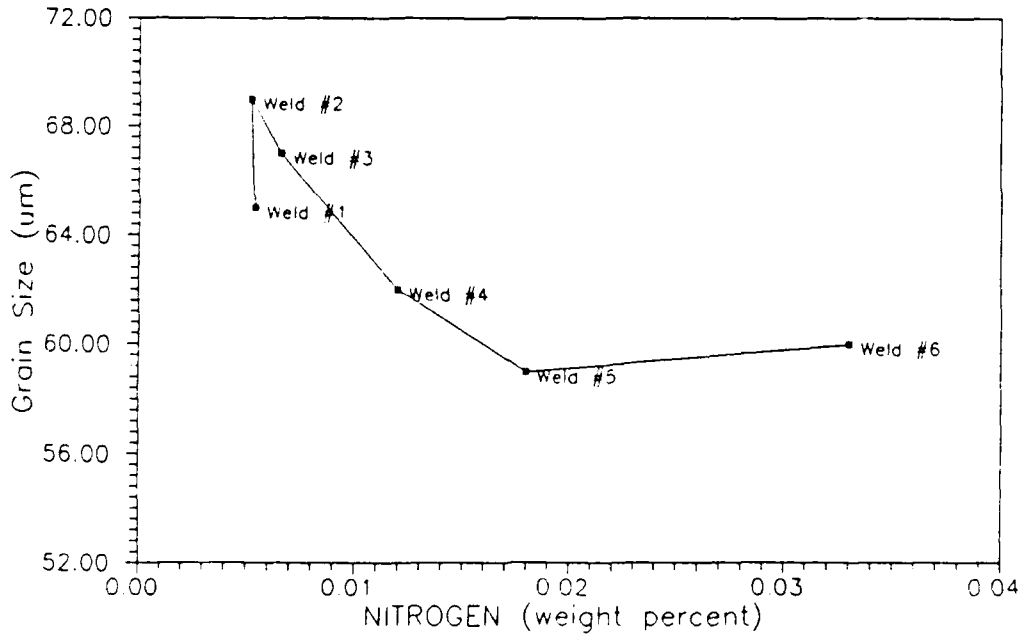

Figure 4.19 Weight percent nitrogen versus the prior austenite grain size.

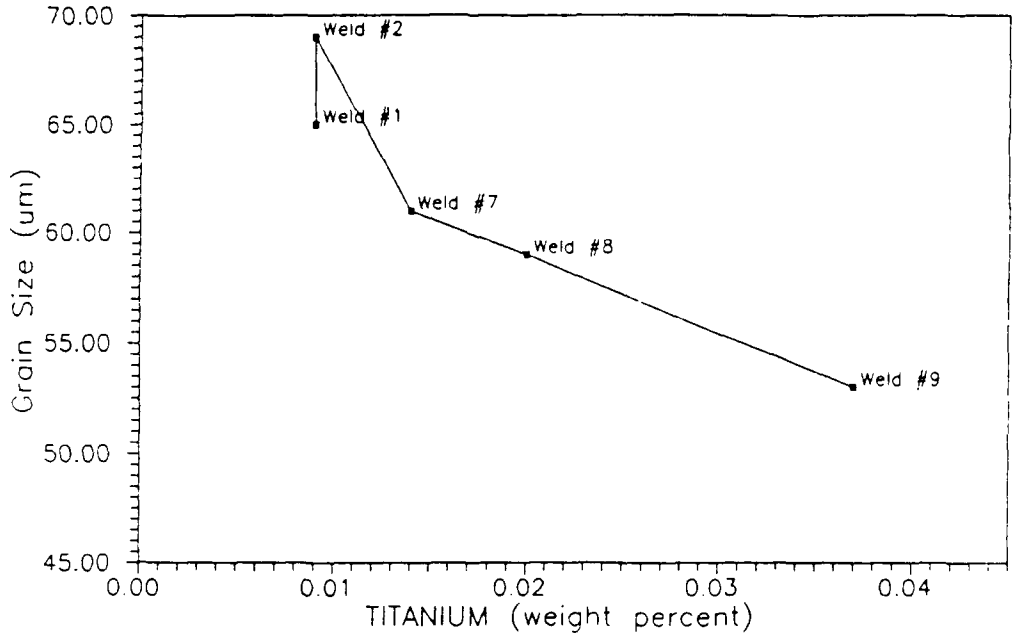

Figure 4.20 Weight percent titanium versus the prior austenite grain size.

However, the confidence level for this analysis is very low due to the small population sampled. Even with a 5% nital etch, an average of only 12 prior austenite grains per 150 μm by 150 μm weld metal sample area could be identified.

4.3.3.5 Inclusions

The inclusion distribution influences the austenite to ferrite transformation either directly by providing heterogeneous nucleation sites for ferrite during transformation or indirectly by pinning the prior austenite grain structure and thus promoting grain boundary nucleated transformation products.

Lau et al [14] feel that the critical balance between titanium, aluminum, boron, oxygen, and nitrogen has important consequences for the inclusion population of the weld and the resulting content of acicular ferrite. For a constant oxygen and aluminum content, higher deposit (plate) nitrogen levels require higher titanium/oxygen ratios

to satisfy oxide formation requirements, tie up the nitrogen as TiN, and prevent the effective boron content at prior austenite grain boundaries from being depleted. This insures that inclusion nucleation sites for AF will be optimized.

Figure 4.21 shows that as the nitrogen content is increased from 0.0054 to 0.033 weight percent, the inclusion content increases from 0.49 to 0.55 area percent. However, there is no apparent trend between the inclusion content and the nitrogen variations.

Figure 4.22 shows that as the titanium content is increased from 0.009 to 0.037 weight percent, the inclusion area percent increases from 0.49 to 0.85 area percent. This increase is in both the total number and net size of the inclusions which appear to have a strong influence on the weld metal properties. Specifically, the higher inclusion content is believed to contribute to an increase in precipitation hardening from nitride and carbide particles and dispersion hardening from titanium oxide and titanium-aluminum oxide particles, although the presence of these specific particles was not confirmed. However, this does provide an explanation for the higher hardness and lower toughness observed in these welds. Additionally, the work by Synder and Pence [25] in this area has shown that dispersion hardening does occur at higher titanium levels; and the work by Brownlee [22] supports the contention that precipitation hardening by nitride and carbide particles occurs with elevated titanium concentrations. Finally, it was observed that titanium's influence on promoting the formation of ferrite with aligned M-A-C seemed to have precedence over the tendency of fine inclusions to nucleate acicular ferrite.

The morphology of the inclusions were spheroidal as typified by the micrographs shown in figure 4.23. The inclusion size distributions were determined by measuring an average of 488 inclusions in the chosen area of each weld. The average inclusion diameter varied from 0.5 μm to 2.0 μm. However, fewer than 20 percent of the inclusions in any of the welds were greater than 1.0 μm diameter. In all welds, inclusions greater than 2 μm diameter were occasionally observed.

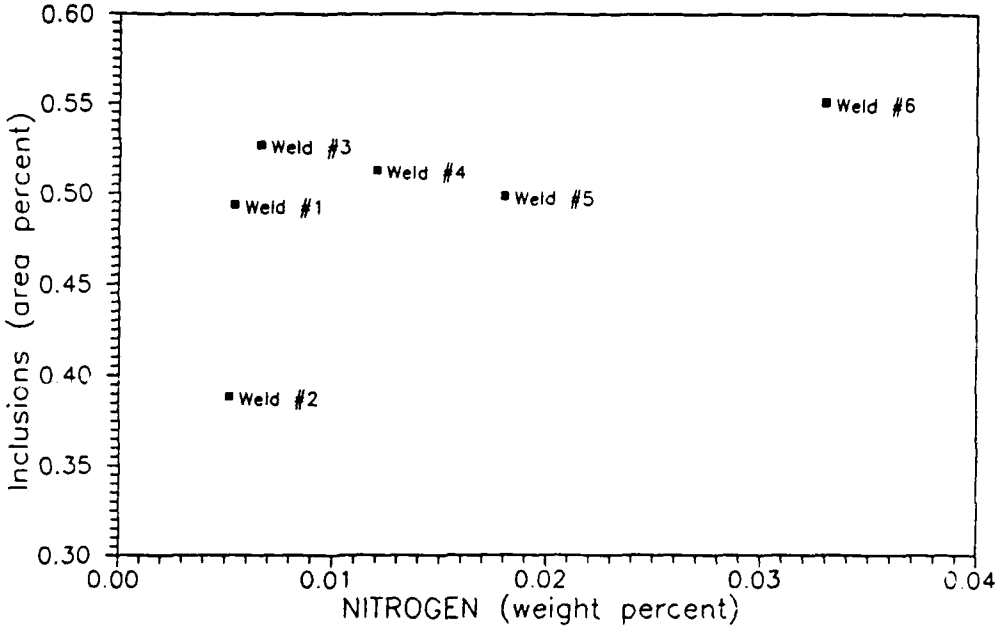

Figure 4.21 Weight percent nitrogen versus the area percent inclusion.

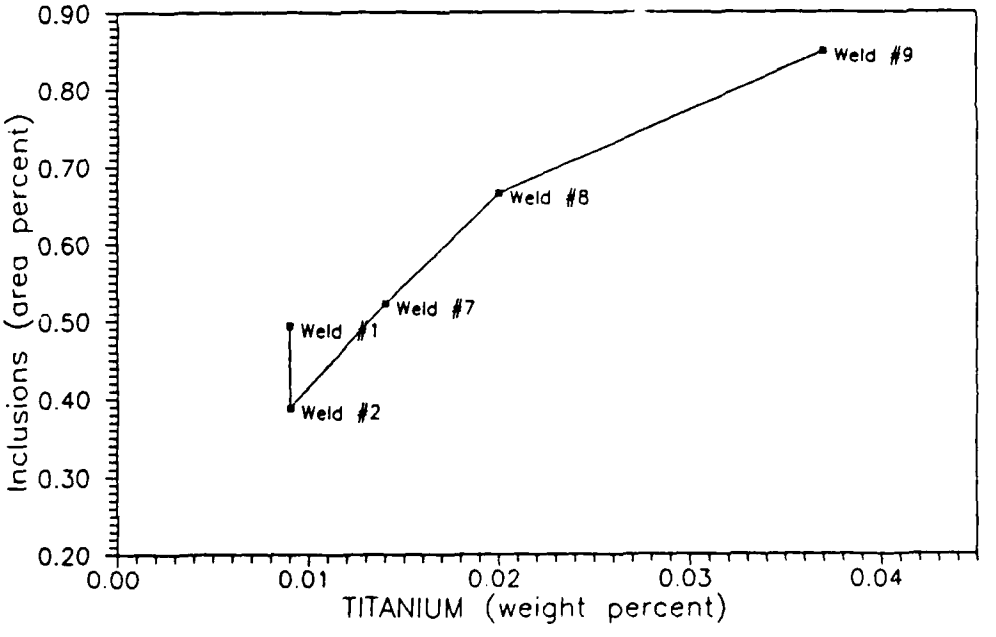

Figure 4.22 Weight percent titanium versus the area percent inclusions.

The inclusions were divided into two size ranges: 0-1 μm and greater than 1 μm. The main elements in the composition of the inclusions in each sample are given in Table 4.6 (in order of highest to lowest composition). From each weld, five inclusions were analyzed using the X-ray energy dispersive spectrometer attached to the SEM. Between the nitrogen varied welds, there appeared to be no significant difference in inclusion composition which supports the contention that changes in nitrogen levels had little influence on the content of the inclusions. When the inclusion composition of the titanium varied welds were analyzed, it was obvious that inclusions in these welds contain higher levels of titanium which provides an explanation for the increase in the total number and area fraction of inclusions observed with higher titanium levels. The indication is that as more titanium is added, more excess oxygen and nitrogen are tied up as TiO and TiN which serve as nucleating sites for inclusions.

Table 4.6 Inclusion compositions, in order of highest to lowest concentrations.

DESCRIPTION	INCLUSION COMPOSITION
WELD #1	Si, Al, Mn, Ti, Mg
WELD #2	Al, Mn, Si, Mg, Ti
WELD #3	Si, Mn, Al, Ti, Mg
WELD #4	Si, Mn, Al, Ti, Mg
WELD #5	Si, Mn, Al, Mg, Ti
WELD #6	Al, Si, Mn, Mg, Ti
WELD #7	Al, Si, Mn, Mg, Ti
WELD #8	Al, Si, Ti, Mn, Mg
WELD #9	Al, Si, Ti, Mn, Mg
WELD #10	Al, Si, Ti, Mn, Mg

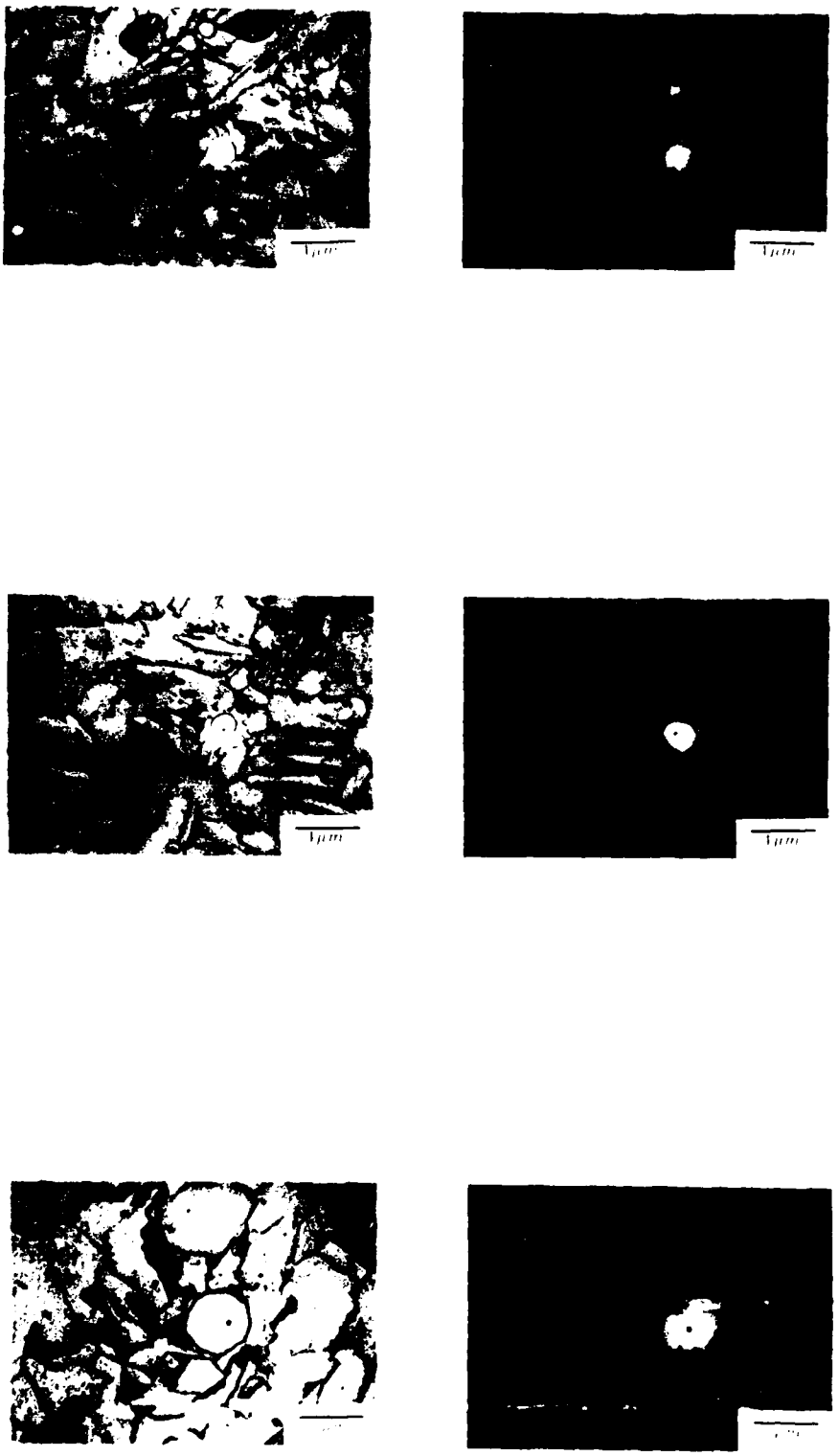

Figure 4.23 Typical morphology of the inclusions encountered in all ten test welds. 2% nital etch.

4.3.3.6 Porosity

Porosity is the result of gas being entrapped in solidifying weld metal. The discontinuity is generally spherical, but it may be elongated. In the case of uniformly scattered porosity distributed throughout the passes of a multiple pass weld, the cause is generally faulty welding techniques or defective materials.

Dissolved gases are usually present in molten weld metal. Porosity is formed as the weld metal solidifies if the dissolved gases are present in amounts greater than their solid solubility limits. The welding process, welding procedures and baseplate type directly affect the quantities and types of gases that are present in the molten weld pool.

There are numerous gases which may be present in the molten weld pool, the most important of which are hydrogen, carbon monoxide and nitrogen. Only these gases are soluble to any significant extent in the molten weld pool, and the solubility of these gases in solidified metal is significantly less than in liquid metal [44].

In this investigation, porosity due to nitrogen gas evolution is of most concern since oxygen and hydrogen contents in all the welds were maintained at very low levels as shown in Table 4.1. Nitrogen from several sources can cause porosity in steel. This gas may enter the molten weld pool from the atmosphere, or from contaminated shielding gas, or it may be in the base metal or filler metal in the form of dissolved nitrogen or nitrides. In this study, nitrogen contamination was closely regulated and the only significant source of this element came from the addition of manganese nitride powder.

At the highest level of this contamination (weld #6), the nitrogen gas evolution was great enough to cause porosity problems as shown in figure 4.24. This weld contained a high level of nitrogen (0.033 weight percent); although , this is still below the documented solid solubility limit of 0.045 weight percent in solidified steel weld

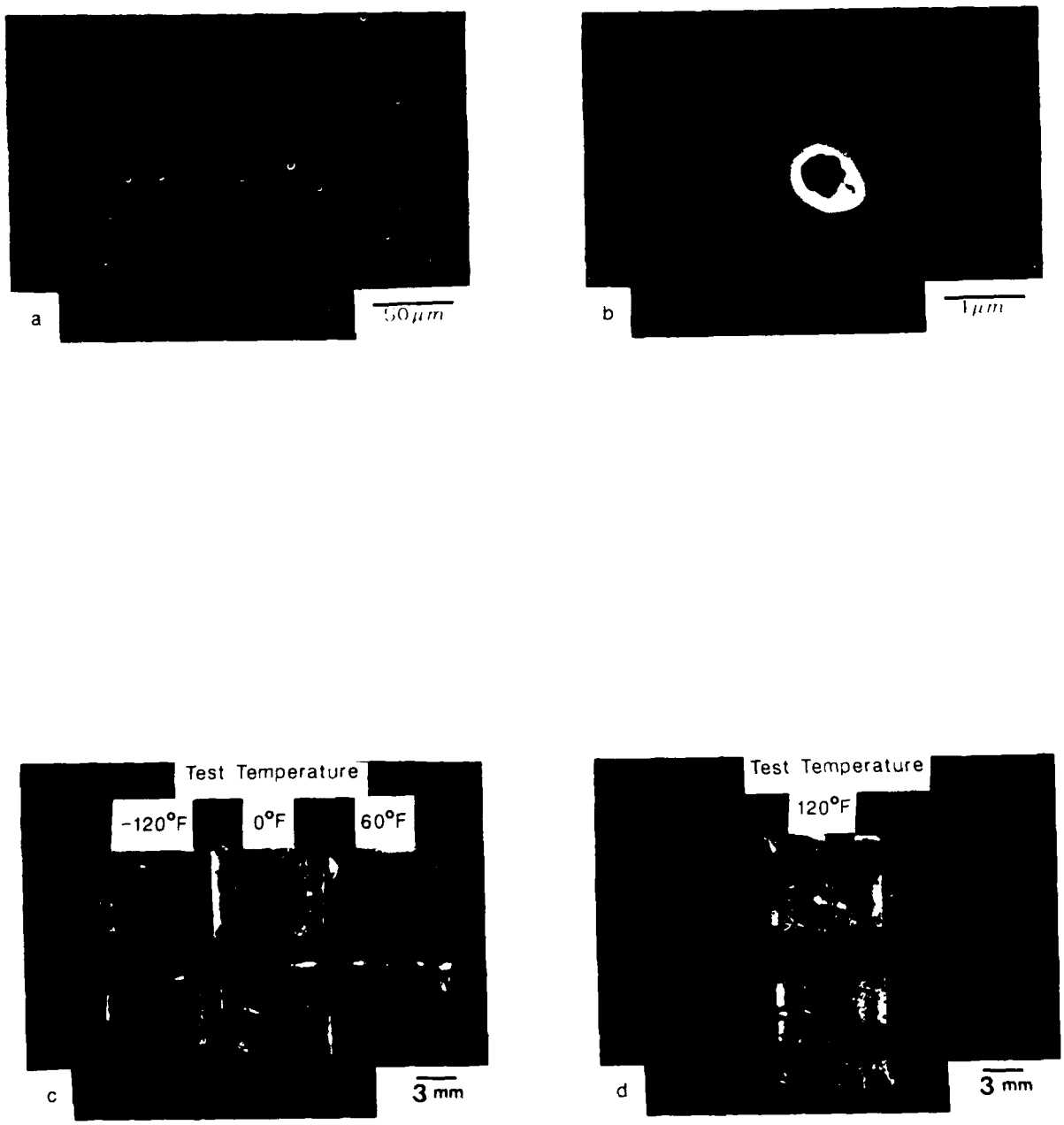

Figure 4.24 Micrographs showing the porosity observed in weld #6. a) weld #6 (400X), b) weld #6 (5000X), c) broken Charpy specimens illustrating porosity defects in weld #6, d) broken Charpy specimen showing how porosity degrades the fully ductile fracture behavior of weld #6.

metal [12]. Thus, it seems obvious that for the materials and procedures used in this investigation, the solid solubility limit of nitrogen in these welds is somewhat less than 0.033 weight percent. This type of porosity problem is often attributed to the lack of deoxidizer in relationship to the amounts of both oxygen and nitrogen in the solidified weld.

At the high level of nitrogen contamination contained in weld #6, porosity became the overriding factor controlling the mechanical properties of the weld. This was obvious through inspection of the broken Charpy specimens of weld #6, some of which are shown in figure 4.24. Also shown in figure 4.24 are micrographs illustrating the pinhole porosity observed in this weld. According to the American Welding Society [44], porosity's effect on mechanical properties is most pronounced for ductile fracture as opposed to brittle fracture. Additionally, the higher the yield strength of the metal, the greater is the adverse affect of porosity on ductility. This is illustrated in figure 4.24 which shows the influence of porosity on the fracture behavior as the mode of fracture transitions from brittle to ductile with increasing test temperature. This phenomena is verified and quantified in sections 4.4.2 and 4.4.3 which include the mechanical testing results for weld #6 in relationship to the other welds.

4.4 Mechanical Tests

The primary objective of this work is to quantify the influence of nitrogen and titanium on the toughness of HY-100 SAW weld deposits. In this effort, a full series of mechanical tests; including Vickers microhardness scans, sub-sized tensile tests and full sized Charpy tests, were conducted. The specific results of these tests are presented in the sections following this discussion.

From the previous discussion of the importance of microstructure, it becomes evident that achieving an optimum weld metal microstructure is necessary in order to provide adequate toughness for a specified application at an acceptable level of

strength. Additionally, compositional changes have a major influence on forming the microstructure and changing the mechanical properties. This is done beneficially through alloying additions to optimize the amount and fineness of acicular ferrite. However, in inappropriate proportions, elements such as nitrogen and titanium have been known to cause excessive increases in the strength of the weld at the expense of good toughness. Thus, the interaction between titanium, nitrogen, oxygen, boron, and aluminum, as discussed previously, is extremely important since the optimum ratios of these elements should provide good toughness properties while maintaining excellent strength of the weld.

4.4.1 Hardness Test

High hardness is generally desirable in weld metal because it indicates a corresponding high tensile strength. This becomes undesirable when the high hardness is coupled with a microstructure which is detrimental to the toughness.

In this regard, microhardness measurements give an indication of the microstructural differences within the weldment.

Grain boundary ferrite and polygonal ferrite exhibit the lowest hardness because of there relatively large grain size and low level of internal stress associated with the highest transformation temperatures of the decomposition products of austenite [38].

Ferrite with aligned M-A-C is usually produced at lower temperatures then grain boundary and polygonal ferrite. The higher hardness of this constituent is mainly caused by the martensite-austenite (M-A) or carbide microphases between the narrow ferrite plates. Acicular ferrite is formed at temperatures lower than ferrite with aligned M-A-C, and mostly exists in the interior of the prior austenite grains. The

small grain size, high dislocation density, and high angle grain boundaries are responsible for the higher hardness of acicular ferrite compared with the other two microstructural constituents [38].

Thus, high hardness with a corresponding microstructure high in acicular ferrite is most desirable with respect to good toughness and strength; while high hardness with a microstructure high in ferrite with aligned M-A-C or M-A constituent is not particularly desirable due to an anticipated low toughness.

In this investigation, the overall hardness of the weld metals were measured with a load of 200 grams at intervals of 0.5 mm. The weld samples were polished and then lightly etched prior to hardness testing. The reported microhardness values of Table 4.7 were the average of two diagonal measurements ("V" and "H" of figure 3.4) for each weld sample. Also shown in this table are the approximate tensile strengths that correspond to these hardness values.

As Table 4.7 shows, the weld metal Vickers hardness numbers range from 300.80 to 351.0 and increase with both titanium and nitrogen in roughly the same proportion.

Table 4.7 Average Vickers microhardness numbers and the corresponding average tensile strengths for all ten test welds.

DESCRIPTION	AVERAGE VICKERS (VHN)	AVERAGE TENSILE (KSI)
WELD #1	300.80	135.90
WELD #2	303.70	137.35
WELD #3	308.20	139.60
WELD #4	310.40	140.70
WELD #5	342.70	156.87
WELD #6	351.00	161.00
WELD #7	312.10	136.70
WELD #8	337.90	140.25
WELD #9	350.80	160.90
WELD #10	318.00	144.50
Base Plate	287.80	130.05

Figure 4.25 shows a plot of Vickers microhardness (VHN) versus the weight percent nitrogen. As expected, hardness increased from 300.80 to 351.0 VHN as nitrogen increased from 0.0054 to 0.033 weight percent.

Even though weld #6 (high nitrogen) exhibited the greatest hardness, the microstructure was high in ferrite with aligned M-A-C and M-A constituent and demonstrated poor toughness, as expected. Welds #1 and #2 (baseline) had lower hardness; but, demonstrated good toughness due to the high content of acicular ferrite.

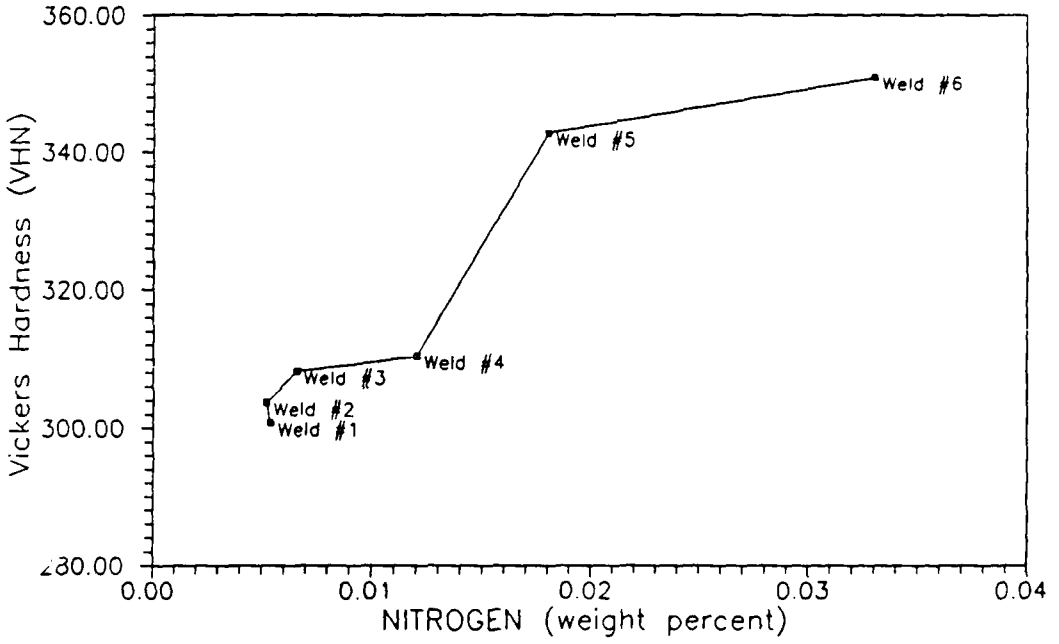

Figure 4.25 Weight percent nitrogen versus the Vickers microhardness numbers.

Nitrogen is believed to increase hardness through an increase in the amount of hardened M-A constituent, through interstitial solid solution hardening effects and through strain aging effects. All these items have a deleterious influence on the weld metal toughness.

Figure 4.26 shows a plot of Vickers microhardness (VHN) versus the weight percent titanium. In this case, hardness increased from 300.80 to 350.80 VHN as titanium increased from 0.009 to 0.037 weight percent.

In this case, hardness increases were believed due to carbide and nitride precipitation hardening as well as oxide dispersion hardening.

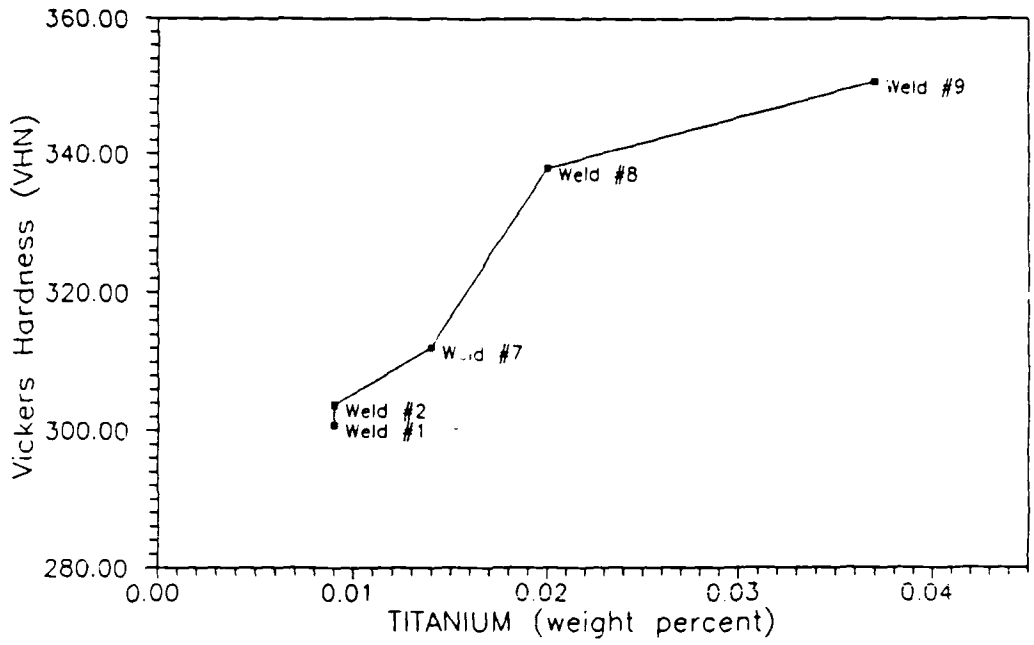

Figure 4.26 Weight percent titanium versus the Vickers microhardness numbers.

4.4.2 Tensile Test

Weld metal normally has higher tensile and yield strength than the equivalent plate material even when the carbon and/or alloy content is low. Excessive strength is a problem since excessively high strength often corresponds to low toughness and stress corrosion cracking susceptibility.

In general, the yield strength and ultimate tensile strength of weld metal increases as the ferrite grain size is reduced. This means that acicular ferrite is the most desirable microstructure in terms of strength while grain boundary and polygonal ferrite are not desirable. The specific gain in strength is the result of increasing the total number of high angle grain boundaries and a corresponding increase in the

interaction between dislocations and grain boundaries in the microstructure [22]. Oldland [39] has found that increasing amounts of grain boundary ferrite, polygonal ferrite, and inclusion volume fractions generally tend to reduce strength.

Generally, yield and tensile strengths correlate well with compositional changes. In addition to their influence on the microstructural features of the weld, nitrogen and titanium are believed to influence the strength properties through strain aging and solid solution hardening; and through precipitation and dispersion hardening effects, respectively.

The most widely used technique to evaluate the strength properties of welds is the standard tensile test. The dimensions of the test specimen are shown in figure 3.5. The purpose of the test is to measure the 0.2 percent yield strength, ultimate tensile strength, percent elongation, and percent reduction in area in order to quantify the strength properties of the welds.

For this investigation, two sub-sized, all-weld-metal tensile specimens were prepared from each test weld. The specimens were tested at room temperature with a Baldwin Universal tensile machine at a crosshead speed of 0.02 in./min. A summary of the data obtained from the all-weld-metal tensile testing is shown in Table 4.8.

Table 4.8 shows that the yield strength was unaffected and the tensile strength increased only slightly as the nitrogen content was increased. In this case, the increased strength from any solid solution hardening appeared to be offset by a decrease in strength associated with the higher content of ferrite with aligned M-A-C. For higher titanium levels, the yield and tensile strengths decreased as did the percent reduction of area. The high content of coarse ferrite with aligned M-A-C observed at higher titanium concentrations was believed to have the largest influence resulting in the lower strength properties of these weld deposits. Of special note is that at high levels of nitrogen and titanium additions, tensile specimen data was not obtained. For weld

#6, this was due to porosity which caused the specimens to fail while being machined. In the case of welds #9 and #10, the tensile specimens exhibited severe embrittlement and transverse cracking, and also failed while being machined.

Figures 4.27 and 4.28 are plots of the average yield strengths versus nitrogen and titanium compositional variations, respectively.

Table 4.8 Results of the all-weld-metal tensile testing.

Specimen I.D.	0.2% Offset Yield Strength (ksi)	Ultimate Tensile Strength (ksi)	Elongation (%)	Reduction of Area (%)
WELD #1	113 100	128 129	24 21	67 65
WELD #2	138 106	149 131	18 21	54 62
WELD #3	110 101	130 130	22 24	60 65
WELD #4	125 109	159 134	22 22	53 61
WELD #5	114 112	146 143	22 21	60 60
WELD #6	---	---	---	---
.WELD #7	96 100	130 116	11 7	21 19
WELD #8	98 76	132 76	19 5	60 10
WELD #9	---	---	---	---
WELD #10	---	---	---	---

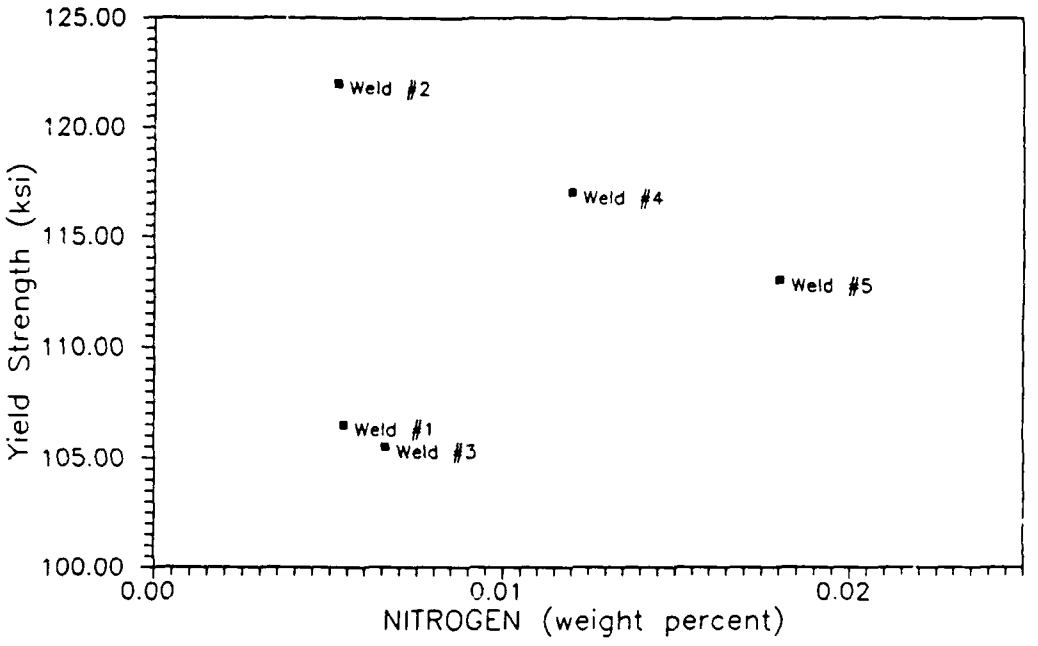

Figure 4.27 Weight percent nitrogen versus the weld metal average yield strength.

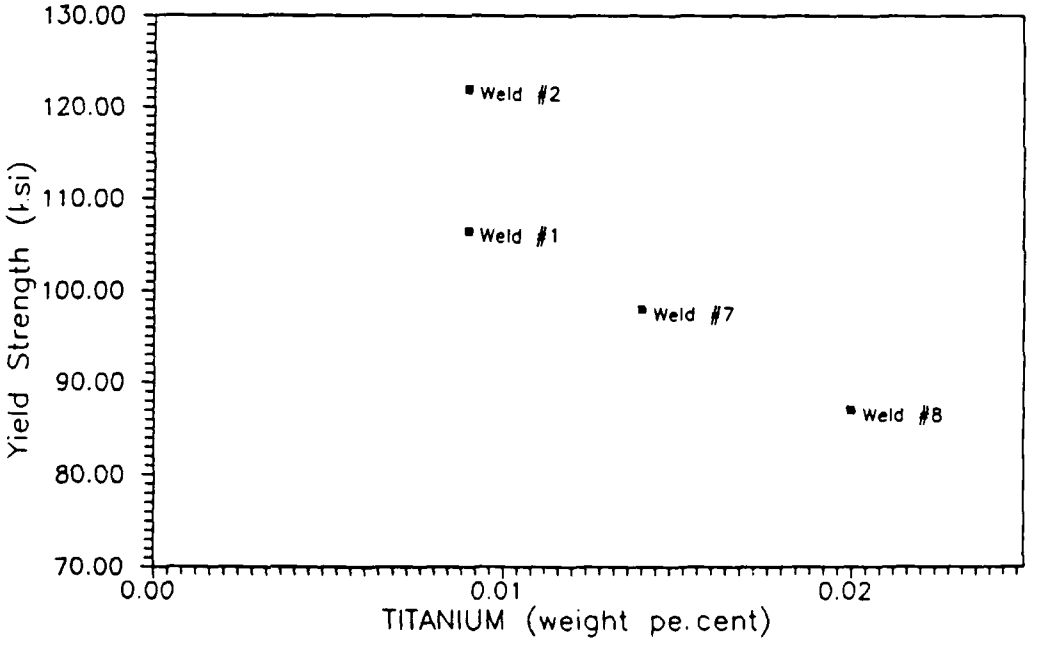

Figure 4.28 Weight percent titanium versus the weld metal average yield strength.

4.4.3 Charpy V-notched Impact Testing and Fractography

The notch-ductility of the weld metal samples as measured by impact testing, depends mainly on the compositional variations which influence the microstructure, grain size and inclusion content. Notch-ductility is reduced, other things being equal, by the presence of grain boundary ferrite, polygonal ferrite, and ferrite with aligned M-A-C in the structure; and particularly, when it is coarse and block-like in form. Ideally, the weld metal should consist entirely of fine acicular ferrite. The high resistance to cleavage due to acicular ferrite can be explained by the much smaller grain size of this constituent. The notch-ductility is also reduced as the amount of M-A constituent in the structure increases. The microstructure of HY-100 weld metal deposited by SAW process is such that the impact properties are usually adequate for the common run of applications, but where more stringent requirements prevail (such as impact testing at -60 °F) it is necessary to optimize the welding procedures and composition of the consumables.

Under circumstances where the origin of embrittlement is not related to a high proportion of a coarse GF, PF, or AC microstructure, or an increase in the amount and size of blocky M-A constituent; it is reasonable to assume that the observed deterioration in toughness arises either from strain ageing or solid solution hardening effects caused by free nitrogen; or precipitation hardening and dispersion hardening effects caused by excess titanium.

The most widely used technique to evaluate the impact properties or toughness of welds is the Charpy V-notched test. The dimensions of these test specimens are shown in figure 3.6. The purpose of the test is to plot the energy absorbed in fracturing a specimen using a pendulum hammer, and hence to relate the energy absorbed due to the impact with the specimen toughness. It is seen that there is a transition from low to high energy fracture over a relatively narrow temperature range and that this is associated with a change from transcrystalline cleavage to fibrous, or dimpled, ductile fracture. The weld's toughness quality can be defined in terms of this transition

temperature (DBTT), which in the literature [41] is usually specified as a certain minimum energy which has to be absorbed at a given test temperature. Other definitions include the temperature associated with half of the upper shelf energy and the temperature associated with the average of the upper and lower shelf energy. Conversely, the transition temperature is often simply defined in terms of a 50 percent crystalline fracture (FATT) as estimated from the broken Charpy specimen [41].

An average of 14 standard Charpy impact specimens were prepared from each weldment. All machined specimens were etched with 2% nital solution to reveal the weld metal so that the center of the weld could be located and marked for machining of the 45 degree V-notch. The specimens were then tested with a Tinius Olsen Impact Tester at temperatures of -180 °F, -120 °F, -60 °F, 0 °F, 60 °F, 120 °F and 180 °F. Standard ductile-to-brittle transition temperature (DBTT) curves were plotted from the tabular data. Finally, fracture surfaces from both ductile and brittle Charpy specimens were examined optically and by scanning electron microscopy to reveal the fracture mode.

4.4.3.1 Charpy Test Results

The complete results of Charpy V-notch measurements are tabulated in appendix A for each test weld. Included in appendix A are the CVN energy, lateral expansion and percent shear data for the Charpy specimens of each weld.

Table 4.9 is a summary of the data in appendix A showing the energy values obtained for each weld at each test temperature. Table 4.10. tabulates the ductile-to-brittle transition temperatures calculated by three popular criteria. Also shown in this table are the values for vTr45 which represents the temperature in the transition range associated with 45 ft-lbs for each test weld. Although several criteria are shown, the DBTT as derived from the average between the lower and upper shelf

energy is used in the subsequent comparative analysis. This is considered the most valid and representative criteria according to Deb et al [42]. However, worth noting is that the DBTTs based on the various criteria all show the same trends even if specific values vary.

Table 4.9 Charpy V-notched energy values obtained for each test weld.

TEST TEMP. (°F)	-180	-120	-60	0	60	120	180
WELD #1 (ft-lbs)	22 10	36 30	60 48 50	72 66 70	85 85	96 91	86 81
WELD #2 (ft-lbs)	12	16 20	37 55 39	66 59 62	71 63 68	75 82	74
WELD #3 (ft-lbs)	8	15 20	23 22 42 25	67 56 50*	71 82 76	70 80	77
WELD #4 (ft-lbs)	8	10 13 9	43 24 23 25	56 55 46	68 69 65	78 80 66	80
WELD #5 (ft-lbs)	8	9 10	19 20 15	37 27 24	49 55 41	57 70* 63	52 68
WELD #6 (ft-lbs)	---	5*	15 17 82*	23 27 14*	30* 32	43* 43	42
WELD #7 (ft-lbs)	6	16 21	39 48 23 44	60*** 64 64	71 76 68	71 78 75	52 78
WELD #8 (ft-lbs)	11	21 22	42 37 35	53 68 56**	60 71	73 70	73
WELD #9 (ft-lbs)	---	8	36** 59** 25 27	219** 129** 29 4***	96** 32**	59 118**	---
WELD #10 (ft-lbs)	5*	10**	16 17** 18	79** 36 48** 44*** 24	50 63	53 60	56

* Defect (pore)

** Defect (transverse split or crack)

*** Gross defect

Table 4.10 Ductile-to-brittle transition temperature calculated for each test weld.

DBTT CRITERIA	WELD #1 (°F)	WELD #2 (°F)	WELD #3 (°F)	WELD #4 (°F)	WELD #5 (°F)	WELD #6 (°F)	WELD #7 (°F)	WELD #8 (°F)	WELD #9 (°F)	WELD #10 (°F)
Half of the Upper Shelf CVN Energy	-82	-73	-41	-32	-11	3	-68	-64	-11	-27
Avg. of the Upper and Lower Shelf CVN Energy	-61	-55	-32	-19	8	26	-48	-42	2	-9
50% Shear (FATT)	-81	-63	-48	-40	6	35	-59	-55	0	-23
vTr45	-82	-56	-28	-16	47	125	-40	-34	-2	-15

Referring to Table 4.9, only the baseline welds (#1 and #2) are within the MILSPEC CVN energy requirements at 0 °F and 60 °F. All other welds failed to meet MILSPEC requirements. Additionally, there is an obvious trend indicating a degradation in CVN energy as the nitrogen and titanium contents were increased. In the case of weld #6, porosity defects were prevalent and in the case of welds #9 and #10, a transverse splitting phenomena and gross defects were common.

All the criteria in Table 4.10 verify a decrease in toughness as nitrogen and titanium contents increased. To illustrate this further, figure 4.29 shows the increase in the DBTT and figure 4.30 shows the decrease in the upper shelf energy as the nitrogen content increased. Additionally, figure 4.31 shows the increase in the DBTT and figure 4.32 shows the decrease in the upper shelf energy as the titanium content increased.

Referring to figures 4.29 and 4.30, we can see that the DBTT increased by 87°F and the upper shelf energy decreases by 46 ft-lbs as the nitrogen content increased from 0.0054 to 0.033 weight percent.

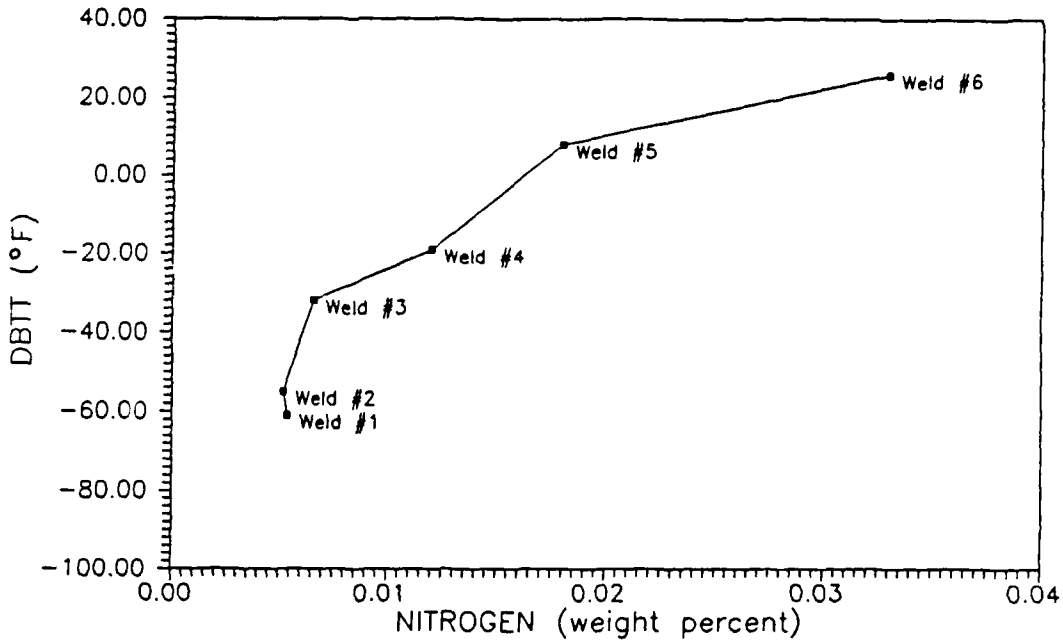

Figure 4.29 Weight percent nitrogen versus the ductile-to-brittle transition temperature.

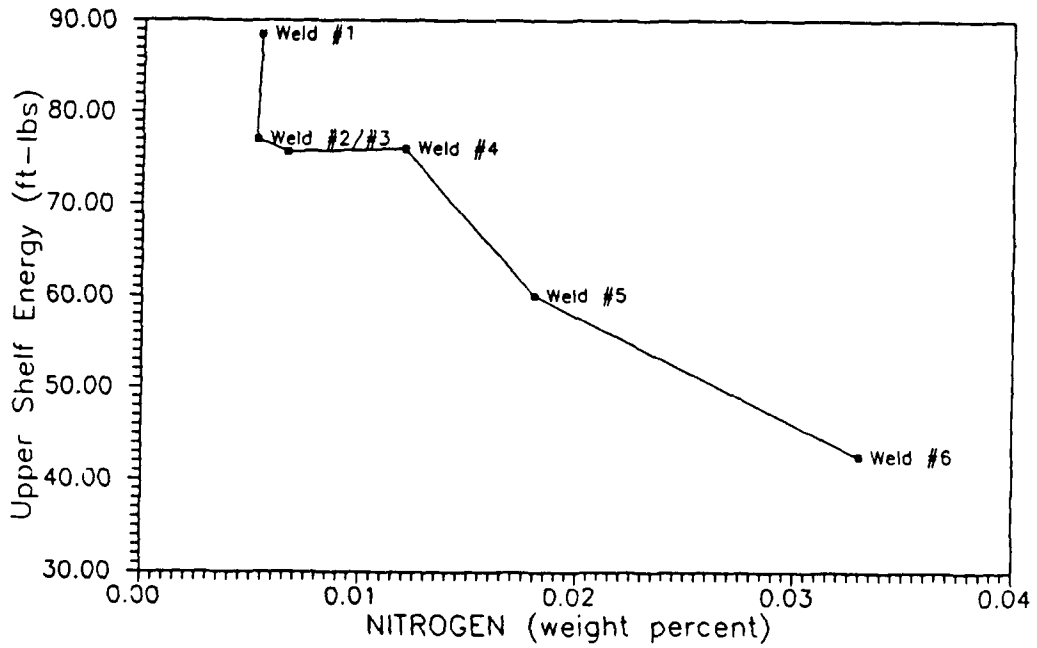

Figure 4.30 Weight percent nitrogen versus the upper shelf energy.

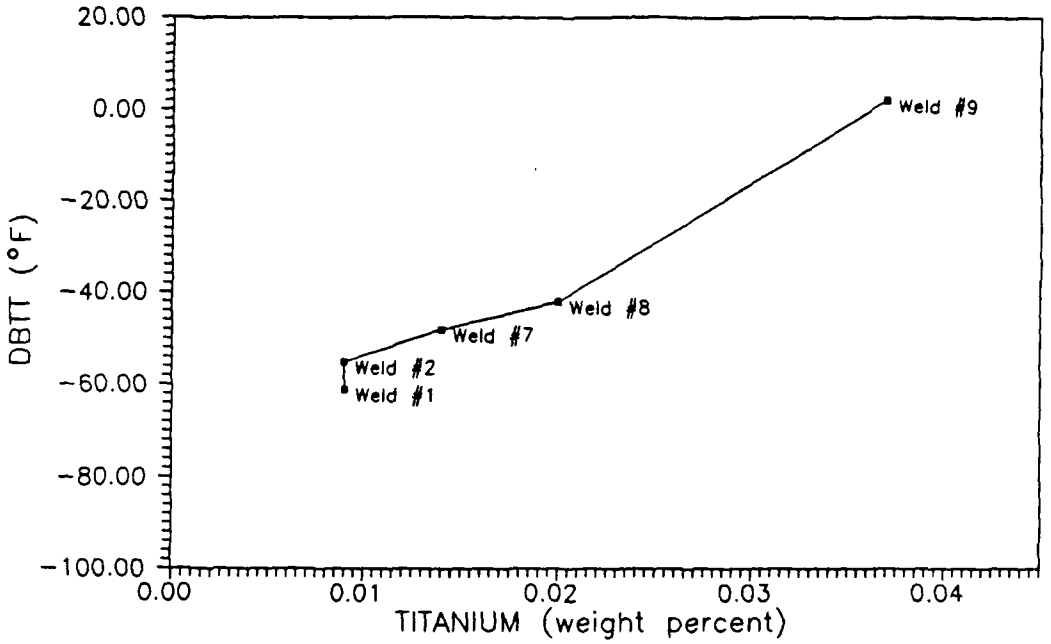

Figure 4.31 Weight percent titanium versus the ductile-to-brittle transition temperature.

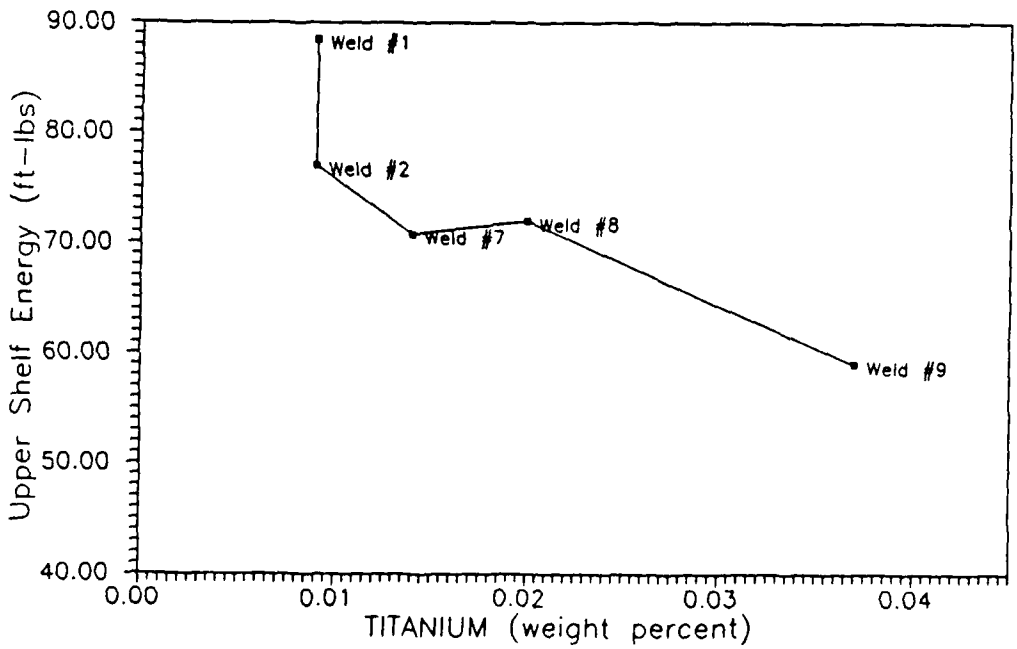

Figure 4.32 Weight percent titanium versus the upper shelf energy.

The difference in fracture properties between the high and low nitrogen welds is attributed to a combination of factors. This includes a reduction in the amount and fineness of the acicular ferrite and the increase in the amounts and grain sizes of the grain boundary ferrite, polygonal ferrite, ferrite with aligned M-A-C, and M-A constituent as the nitrogen content increased. Additionally, the increase in strain ageing and solid solution hardening effects as the nitrogen content increased is believed to further degrade the fracture toughness.

Figures 4.31 and 4.32 show that the DBTT increases by 63°F and the upper shelf energy decreases by 30 ft-lbs as the titanium content increases from 0.009 to 0.037 weight percent.

The best fracture properties occur at a titanium concentration of 0.009 weight percent. This corresponds to a microstructure high in finely dispersed acicular ferrite and low in grain boundary ferrite, polygonal ferrite, ferrite with aligned M-A-C, and M-A constituent. At titanium concentrations above 0.009 weight percent, the fracture toughness degradation appears to be most strongly influenced by a sharp increase in coarse needles of highly aligned ferrite with aligned M-A-C. An additional strong influence on the fracture toughness is believed to come from the increasing size and content of inclusions associated with higher titanium concentrations. These inclusions appear to further embrittle the weld deposit and may be responsible for precipitation and dispersion hardening, as described by Synder and Pense [25], although hardening effects from such mechanisms were not proven. This embrittling affect became so severe in the high titanium welds that transverse cracking occurred which resulted in the splitting phenomena observed in the fracture surfaces of these Charpy specimens.

For comparative purposes, the Charpy V-notch energy curves are plotted together in figure 4.33 and 4.34 for nitrogen and titanium variations, respectively. This serves to illustrate the trends in toughness as nitrogen and titanium contents were varied.

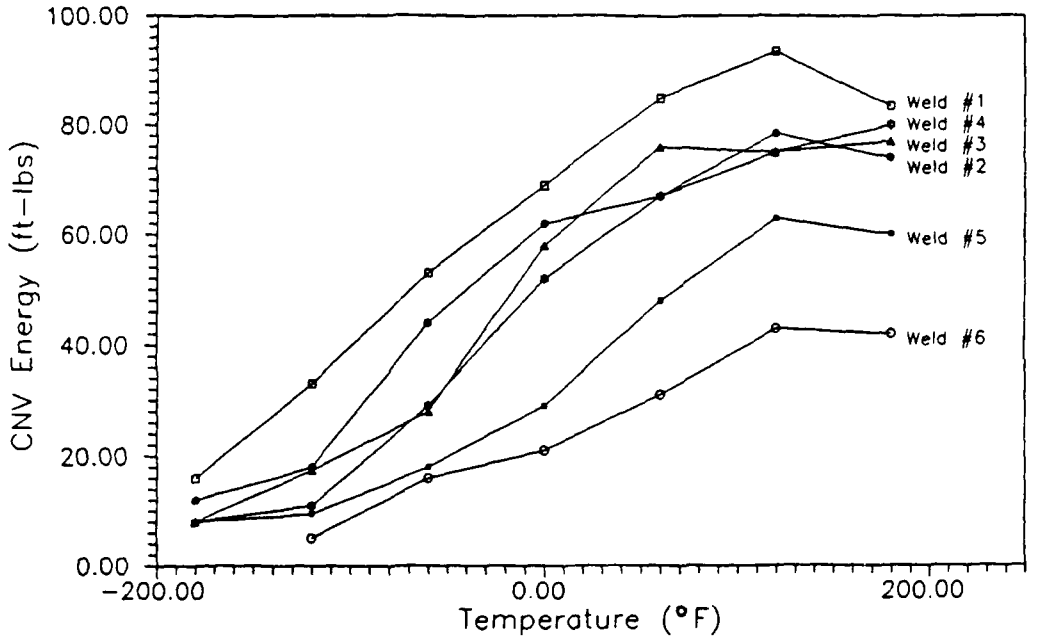

Figure 4.33 CVN energy versus temperature as nitrogen content increases.

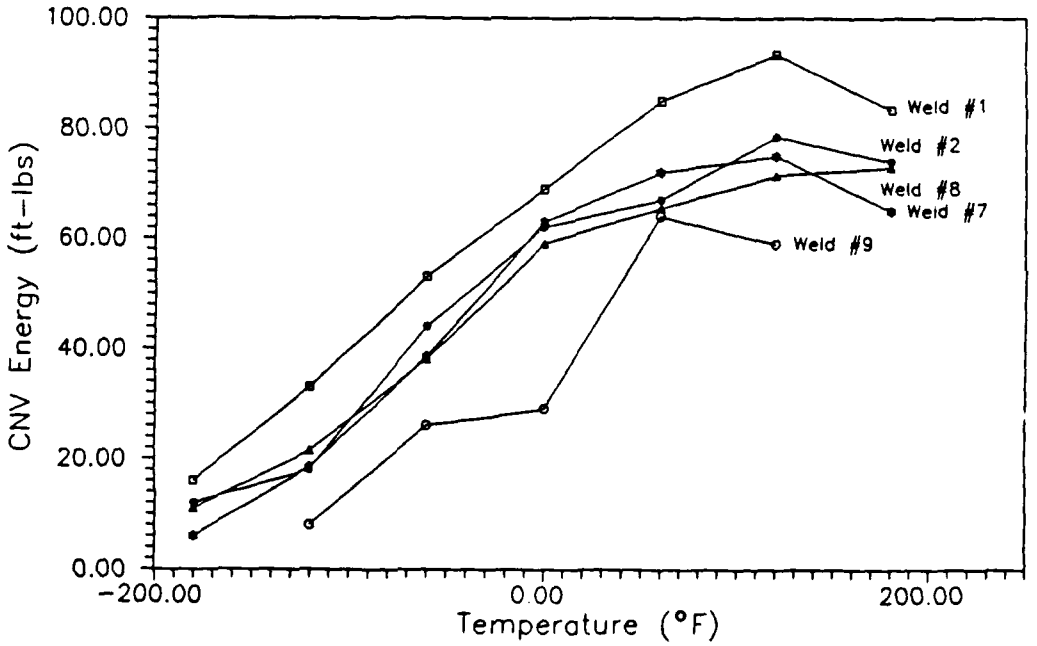

Figure 4.34 CVN energy versus temperature as titanium content increases.

Based on Charpy testing, it is found that nitrogen degrades toughness, as measured by the DBTT, at a rate of 26°F for every 0.01 weight percent increase. Furthermore, titanium above 0.009 weight percent degrades the DBTT at a rate of 20°F for every 0.01 weight percent increase.

4.4.3.2 Fractographic Analysis

The purpose of fractographic analysis is to identify the types and features of the fracture surfaces resulting from Charpy and tensile specimen testing in the hope of correlating these fracture characteristics to a specific microstructure feature, inclusion or defect which is indicative of nitrogen or titanium additions. The ultimate goal is to better understand the mechanisms by which nitrogen and titanium degrade toughness in these weld deposits.

In this endeavor, optical and SEM analyses were done on the fracture surface of all ten test welds to identify the mode of fracture. This required analysis of both the ductile and brittle fracture characteristics in all the welds in order to understand the overall fracture behavior.

Figure 4.35 shows the typical microvoid coalescence at inclusions and dimple features indicative of a ductile fracture. Ductile fracture occurs by microvoid initiation, growth and coalescence. The fibrous regions are observed most predominantly in the free surface of the shear-lip zone and at the origin of fracture near the root of the notch. Microvoids are initiated at interfaces between the matrix and particles such as carbides, precipitates and inclusions, and also at imperfections such as microporosity and microcracks. They grow under the triaxial stress conditions ahead of the crack tip and expand until they coalesce to leave behind on the fracture surface the familiar hemispheroidal cavities that are known as dimples [45]. Within all ten welds, there were no significant difference in these ductile features.

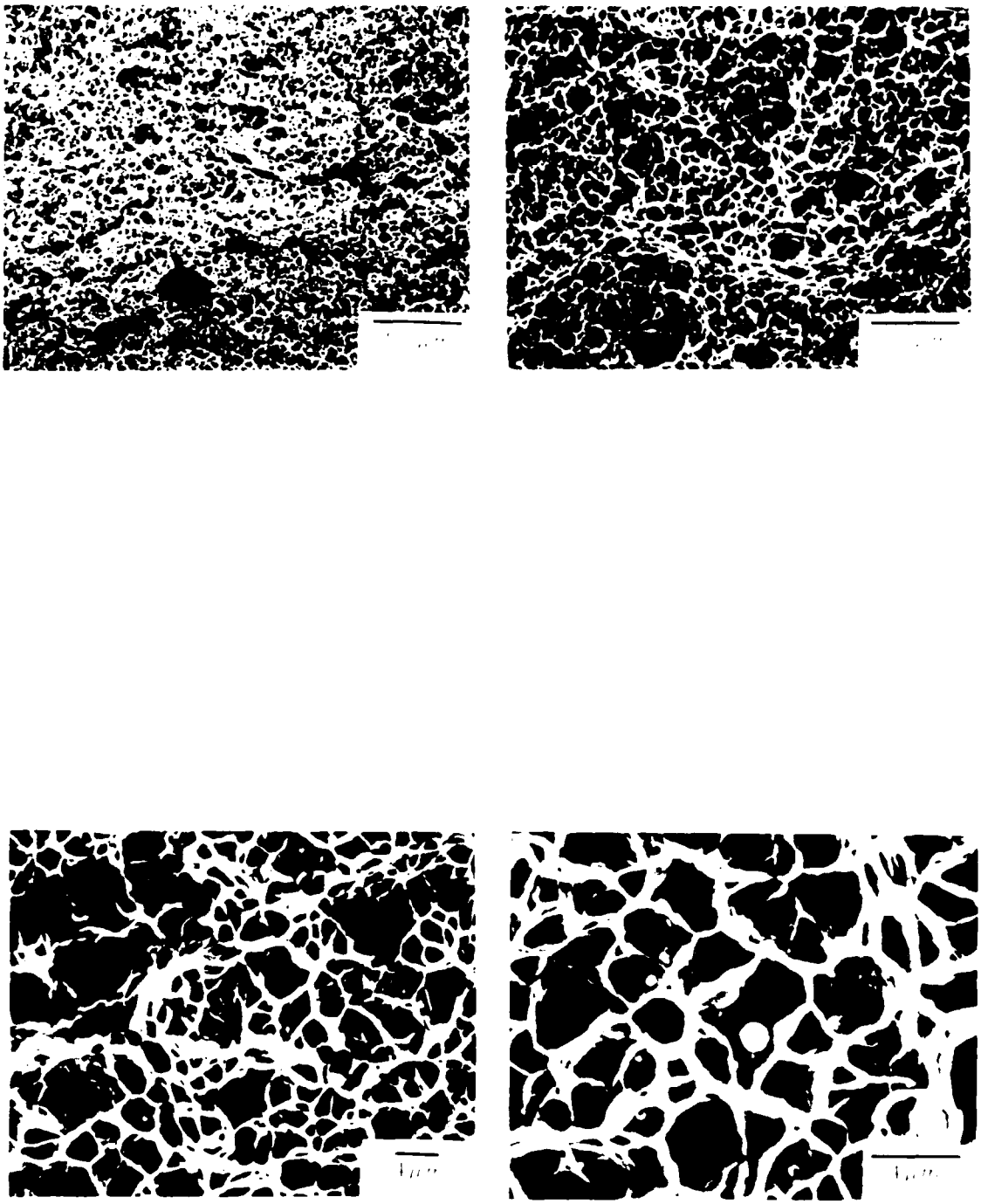

Figure 4.35 SEM micrographs showing the typical microvoid coalescence at inclusions which form the dimples indicative of the ductile fracture behavior seen in all ten welds.

However, an attempt was made to correlate toughness with the volume fraction and size distribution of non-metallic inclusions in these ductile fracture surfaces. Grong et al [40] have done much work in identifying the role of non-metallic inclusions in microvoid coalescence fracture mechanisms. They have shown that large inclusions tend to form voids first as the stresses required for initiation are proportional to $\sqrt{d}$ (where d denotes particle diameter). Thus, microvoid nucleation would be expected to occur preferentially at particles of diameter greater than 1 μm, thereby reducing the CVN upper shelf energy absorption. Comparison of Table 4.5 (inclusion composition) and Table 4.9 (CVN energy) tends to confirm this phenomena. Specifically, as nitrogen and titanium contents are increased, the number of inclusions greater than 1 μm diameter increase and there is a corresponding decrease in the upper shelf energy.

Figure 4.36 shows the typical features of cleavage fracture which occurred in all ten test welds. In these Charpy specimens, cleavage fracture was produced at low temperature under a condition of high triaxial stress and a high deformation rate due to the impact loading. In cleavage fracture, the fracture path follows a transgranular plane that is usually a well defined crystallographic plane. It is apparent that the fracture path changes orientation from grain to grain. This change of orientation from grain to grain leads to a branching of the crack along different planes and to a very chaotic over-all appearance of the fracture surface. However, at high magnification, many features typical in these cleavage fractures become apparent. This includes the river patterns which indicate the direction of crack propagation. Also seen are ductile ligaments and tearing ridges which connect the cleavage planes. The tearing ridges in the SEM micrographs of figure 4.36 are the bright contrast areas between the cleavage planes which get there appearance due to the sharp ridges formed subsequent to plastic flow or necking.

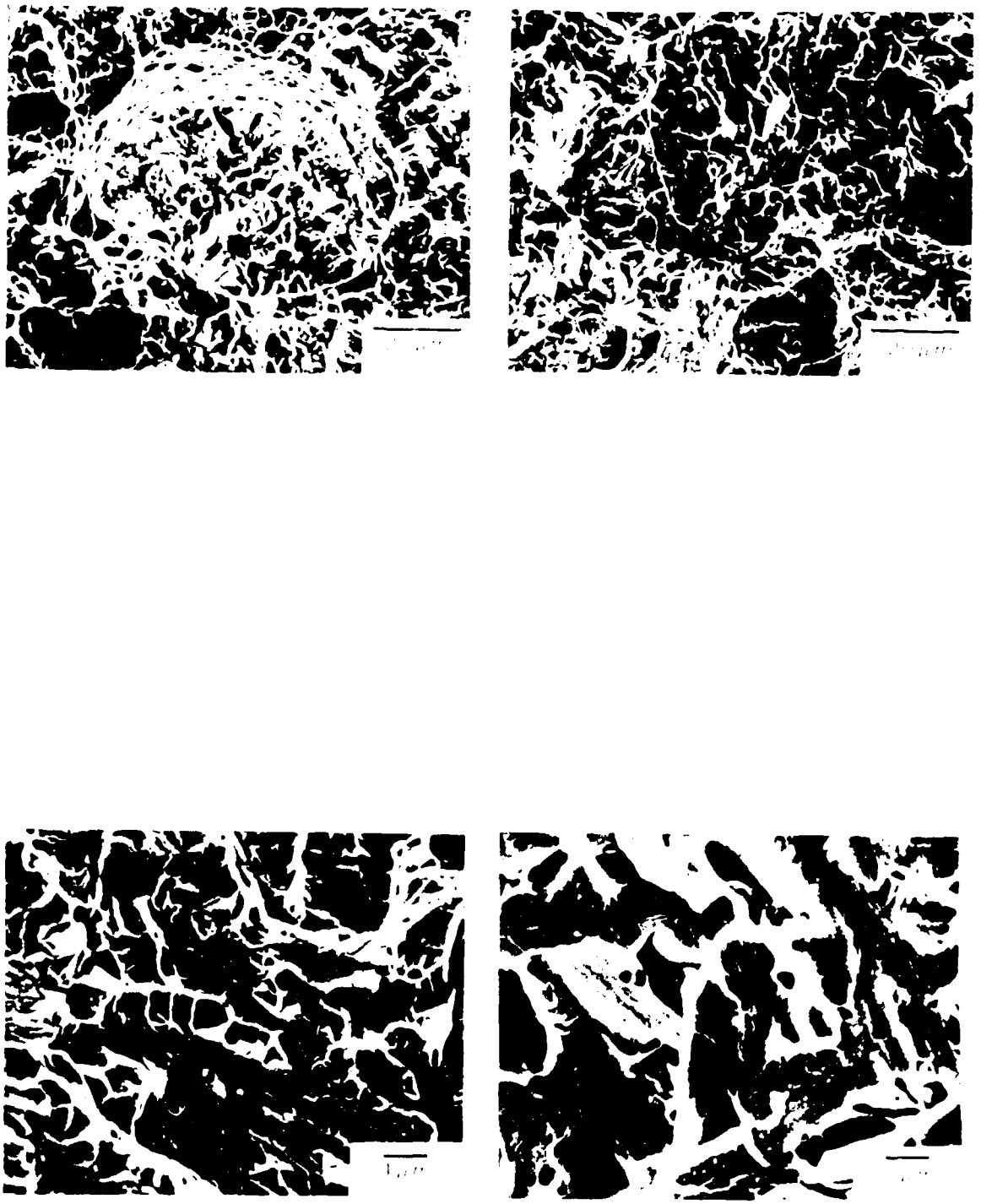

Figure 4.36 SEM micrographs showing the cleavage fracture behavior observed in all ten test welds.

In all the broken Charpy specimens, the cleavage regions show successive fracture mechanisms; that is, the fracture features are composed of cleavage facets and connected by ligaments most often consisting of ductile dimples or tears.

The most significant difference in fracture behavior among the ten test welds occurred in these cleavage regions. In an attempt to quantify this difference, the mean fracture length was measured as tabulated in Table 4.11. This data is plotted in figure 4.37 for nitrogen variations and figure 4.38 for titanium variations.

Figure 4.37 shows that the mean fracture length increased from 17 μm to 25 μm as nitrogen increased from 0.005 to 0.033 weight percent.

Additionally, figure 4.38 shows that the mean fracture length increased from 17 μm to 28 μm as titanium increased from 0.009 to 0.037 weight percent.

Table 4.11 Mean fracture length calculated for each weld.

DESCRIPTION	WELD #1	WELD #2	WELD #3	WELD #4	WELD #5	WELD #6	WELD #7	WELD #8	WELD #9	WELD #10
Mean Fracture Length (μm)	17	19	22	20	24	25	21	23	28	26

To better illustrate the variations in fracture features as the nitrogen and titanium contents were varied, figure 4.39 shows the fracture features for all ten test welds at the test temperatures of -120 °F, -60 °F, 0 °F, 60 °F and 120 °F.

Qualitatively, we can see that as the nitrogen content increased, the fracture behavior shifted towards a more brittle cleavage appearance with a higher orientation among the cleavage planes. Additionally, at the highest nitrogen level of 0.033 weight percent, porosity in the weld metal fracture surface is apparent.

Thus, nitrogen is shown to promote cleavage fracture and reduce toughness as indicated by the increase in the mean fracture length and the increase in the cleavage fracture appearance with increased nitrogen content.

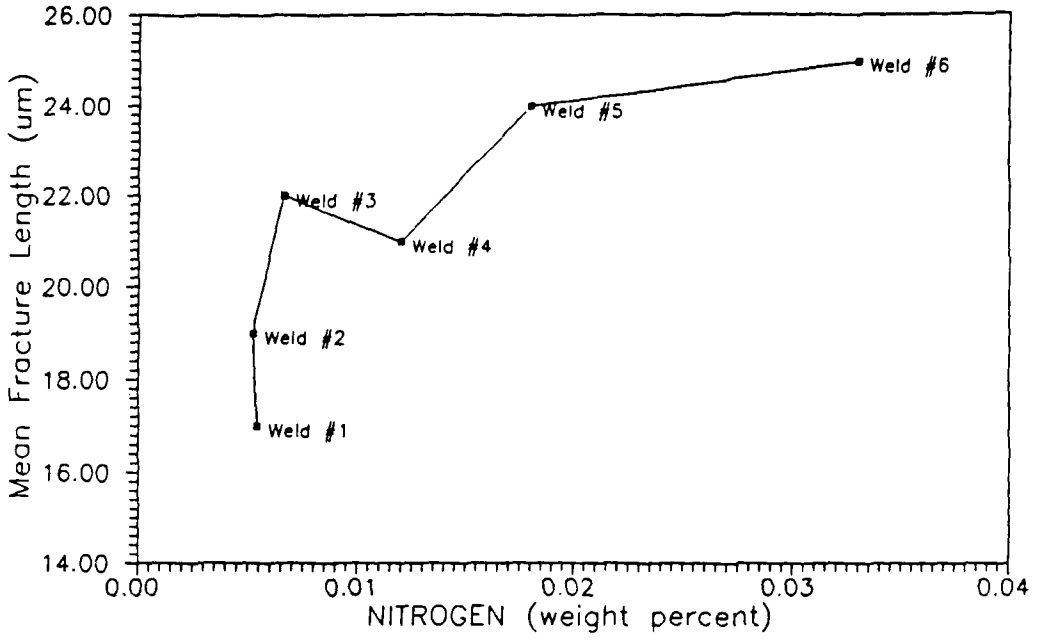

Figure 4.37 Weight percent nitrogen versus the mean fracture length.

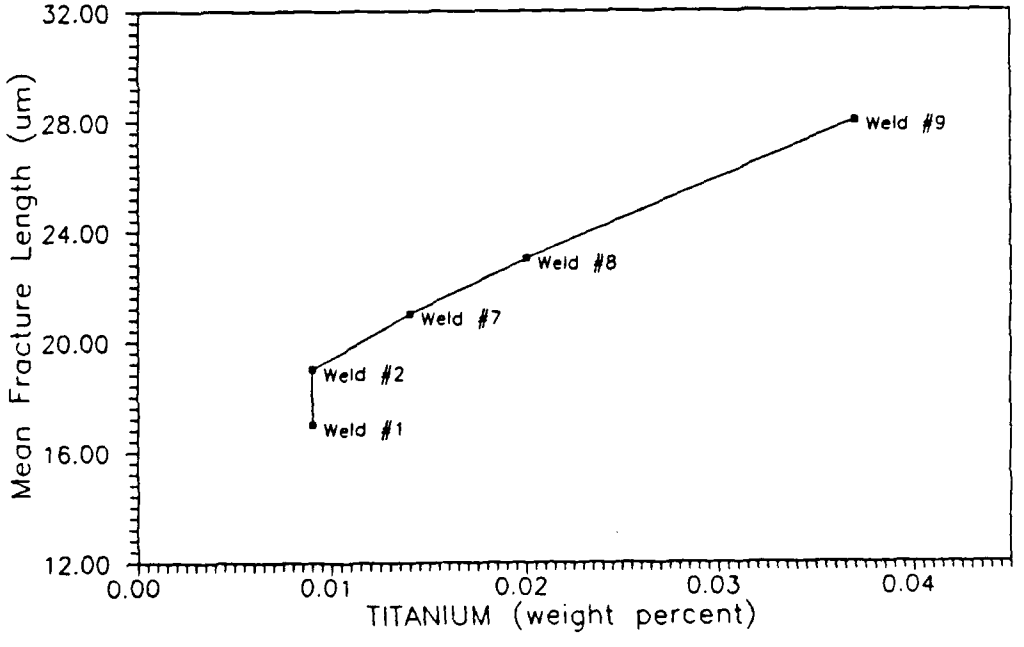

Figure 4.38 Weight percent titanium versus the mean fracture length.

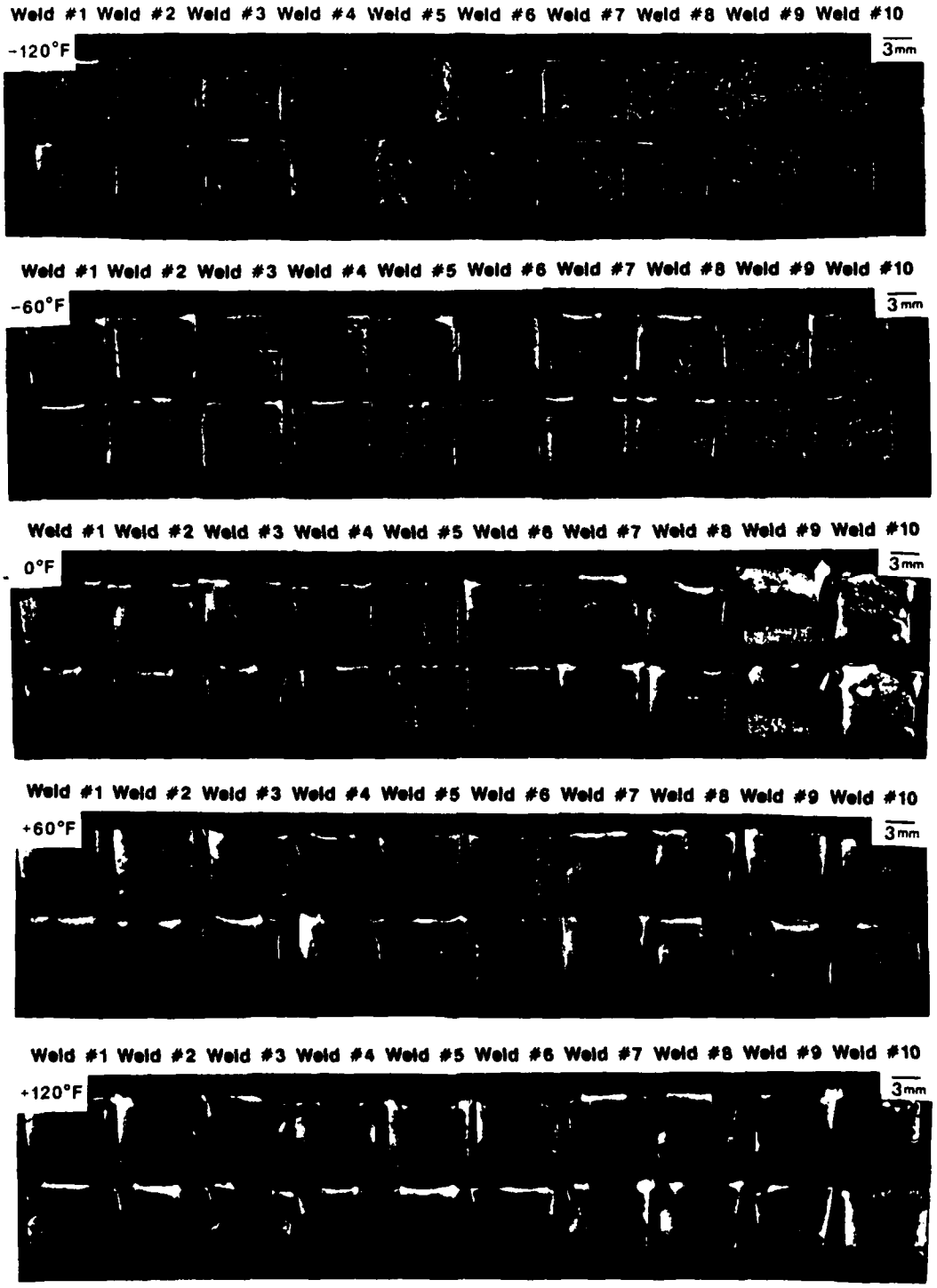

Figure 4.39 Optical micrographs of the broken Charpy specimens for all ten welds at the given test temperatures. This figure illustrates the change in fracture behavior in response to temperature and compositional variations.

Referring to figure 4.39 once again, qualitatively we can see that as the titanium content increased, the fracture behavior shifted towards a more torture cleavage appearance including the presence of transverse cracking phenomena called splits. At the highest titanium level of 0.037 weight percent, these splits dramatically influence the fracture behavior and toughness values for the weld metal.

Figure 4.40 illustrates in more detail the transverse cracking phenomena observed in the high titanium welds. The American Welding Society [44] states that this type of defect is characterized by cracks nearly perpendicular to the axis of the weld. This type of crack is effectively illustrated in figure 4.40, which includes a photograph of a large transverse crack observed in the metallography specimen of weld #9. Also shown in this figure are SEM micrographs showing micro-cracks which were very pervasive throughout the cleavage region of the high titanium welds. Finally, the optical micrographs in this figure show the transverse splitting which characterized the brittle fracture behavior of the high titanium welds.

According to the American Welding Society [44], cracking occurs in weld metal when the localized stresses exceed the ultimate tensile strength of the metal. Furthermore, in the case of transverse cracks, they are usually the result of shrinkage strains acting on weld metal of low ductility. A ductile weld, by localized yielding, is better able to withstand these stress concentrations and is thus less likely to fail then a brittle weld. Although transverse cracking has been related most often to hydrogen embrittlement, this does not appear to be the cause of transverse cracking observed in the low hydrogen welds of this investigation. In actuality, it is the higher titanium concentration which seems to cause the severe embrittlement leading to transverse cracking defects. This transverse cracking was further exasperated by the high degree of restraint on the joints during welding.

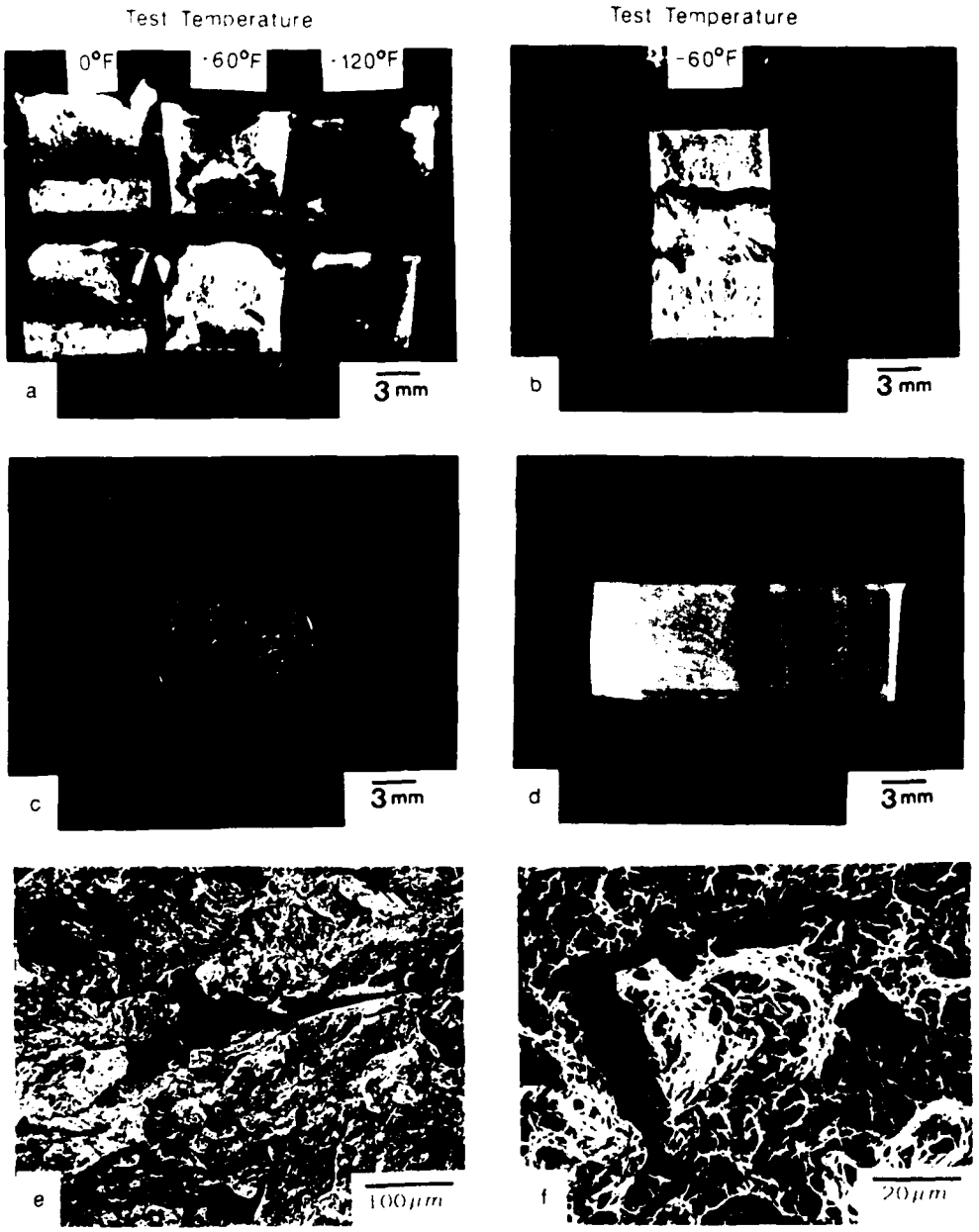

Figure 4.40 Micrographs showing the transverse cracking defects observed at the highest titanium concentration. a) Charpy specimens from weld #9 which illustrate the splitting behavior, b) Charpy specimen from weld #9 which did not break, c) fracture surface of a tensile specimen from weld #9, d) transverse crack observed in a section of weld metal removed from weld #9, e) secondary cracks seen in weld #9 (160X), f) secondary cracks seen in weld #9 (1000X).

Thus, titanium above 0.009 weight percent is shown to promote cleavage fracture and reduce toughness as indicated by the increase in the mean fracture length and the increase in the cleavage fracture appearance with increased titanium concentrations. Additionally, at titanium concentrations above 0.014 weight percent, the welds tend to become so embrittled that transverse cracking defects appear.

CHAPTER 5

CONCLUSIONS and FUTURE WORK

5.1 Conclusions

The influence of nitrogen and titanium on the microstructure and mechanical properties of HY-100 SAW weld deposits has been studied and quantified.

The following conclusions are made as a result of this research.

1. Nitrogen concentrations above 0.005 weight percent were shown to promote cleavage fracture and reduce toughness as indicated by the increase in the mean fracture length, the increase in the DBTT and the decrease in the upper shelf energy. For every 0.01 weight percent increase in nitrogen, the mean fracture length increased by 2.1 μm, the DBTT increased by 14°C and the upper shelf energy decreased by 19.0 joules.

2. The mechanisms by which nitrogen degrades toughness have been shown to be related to a sharp increase in coarse needles of highly aligned ferrite with aligned M-A-C, a corresponding decrease in fine acicular ferrite and a significant increase in the fraction of M-A constituent. Additionally, it is believed that the higher hardness coupled with lower toughness were partially due to interstitial solid solution and strain age hardening effects which increased with nitrogen.

3. Higher nitrogen concentrations have been shown to promote the formation of M-A constituent. It thus seems likely that nitrogen acts in the same manner as carbon by segregating to carbon-enriched areas; thus, effectively increasing the amount

of M-A constituent present and enhancing its embrittling influence. In this regard, it has also been shown that there exists a strong correlation between the increase in M-A constituent and the increase in the DBTT. The correlation, as quantified in this study, is a 18°C increase in the DBTT for every 1.0 percent increase in the volume percent of M-A constituent.

4. At high levels of nitrogen contamination, porosity due to nitrogen gas evolution becomes the overriding factor controlling the mechanical properties. This study showed that the effective solid solubility limit of nitrogen in these welds was near 0.033 weight percent. This differed from the 0.045 weight percent given for the solid solubility limit of nitrogen in steel by Lancaster [12].

5. Titanium concentrations above 0.009 weight percent were shown to promote cleavage fracture and reduce toughness as indicated by the increase in the mean fracture length, the increase in the DBTT and the decrease in the upper shelf energy. For every 0.01 weight percent increase in titanium, the mean fracture length increased by 2.7 μm, the DBTT increased by 11°C and the upper shelf energy decreased by 10.8 joules.

6. The mechanisms by which titanium degrades toughness have been shown to be related to a sharp increase in coarse needles of ferrite with aligned M-A-C which exhibited a high degree of crystallographic orientation and veining, a corresponding decrease in fine acicular ferrite, and a substantial increase in the size and content of embrittling inclusions which were believed to serve as stress concentration sites and crack initiators. Additionally, it is proposed that the higher hardness coupled with lower toughness were partially due to precipitation and dispersion hardening affects which increased with titanium.

7. At a titanium concentration of 0.037 weight percent, the weld deposit became so embrittled that transverse cracking defects formed and became the dominate factor controlling the mechanical properties of the weld.

8. It has been proven that the optimum toughness is achieved by maximizing the amount of acicular ferrite, and by minimizing the content of ferrite with aligned M-A-C and M-A. In this endeavor, it is believed that nitrogen concentrations need to be held as low as possible. Additionally, titanium concentrations should be held below 0.01 weight percent while the exact concentration needs to be based on a balance with boron, nitrogen, aluminum and oxygen.

5.2 Future Work

During the course of this study, a number of areas were found that suggested further investigation.

1. First, with regard to carbon equivalent indexes, it seems appropriate that a CE index needs to be developed to take into account the role of nitrogen and titanium on cold cracking susceptibility and hardening of weld metal. Although this investigation has helped to quantify the influence of nitrogen and titanium, more detailed work beyond the scope of this thesis needs to be accomplished to adequately address a CE index which includes both nitrogen and titanium. Maybe this work can serve as a basis for such an investigation.

2. Secondly, the microstructure and mechanical properties of weld deposits which contain nitrogen and titanium concentrations lower than those obtained in this study need to be investigated. The purpose here is to determine if superior weld deposit properties can be obtained at these lower levels of nitrogen and titanium. If these improvements in microstructure and properties are sufficiently significant, then an argument can be made to develop consumables and steel plate that contain lower levels of nitrogen and titanium. Of the two elements, reducing the amount of nitrogen

is much more difficult to achieve. However, improving argon shielding methods for steelmaking and the use of a vacuum degassing method for SAW electrode production are two possible approaches to reducing nitrogen levels.

3. Finally, further work is needed to adequately understand and quantify the complex interactions that occur among titanium, nitrogen, oxygen, boron, aluminum and other elements. Such knowledge would greatly simplify future endeavors at optimizing the welding consumables for SAW welding of high strength steels.

REFERENCES

[1] Military Specifications, *MIL-E-23765/2D(SH)*, Department of the Navy, Naval Sea Systems Command, 7 September 1984, 1-35.

[2] R.T. Brenna, R.A. Weber, and A. Pollack, *Development of a Welding Technology for HY-100 Steel*, Department of the Navy, Naval Research and Development Center Report 4155, 1-20.

[3] P. Harrison and R. Farrar, *Microstructural Development and toughness of C-Mn and C-Mn-Ni Weld Metals Part I - Microstructural Development*, Metal Construction, July 1987, 15-22.

[4] J.H. Tweed and J.F. Knott, *Micromechanisms of Failure in C-Mn Weld Metal*, Acta Metallurgica, Vol. 35 (7), July 1987, 1401-1414.

[5] S. Hoekstra, M.A. Munning Schmidt-vander Burg, and G. Den-Ouden, *Microstructure and Notch Toughness of Ferritic Weld Metal*, Metal Construction, December 1986, 771-774.

[6] International Institute of Welding, Compendium of Weld Metal Microstructures and Properties: Submerged Arc Welds in Ferritic Steel, The Welding Institute, Cambridge, UK, 1985.

[7] D.J. Abson and R.E.Dolby, *Microstructural Transformations in Steel Weld Metals - A Reappraisal*, Welding Institute Research Bulletin, Vol. 19, July 1978, 202-206.

[8] J.F. Lancaster, Metallurgy of Welding: Third Edition, Allen & Unwin Ltd., USA, 1986.

[9] J. Malcolm Gray, J.T. Hickey, and A.M. Gilroy-Scott, *Report on Effects of Nitrogen on the Weldability of Microalloyed Steels*, DTNSRDC/SME-CR-05-87, Contract No. N61533-86-M-5099, January 1987.

[10] T.W. Eagar, *Oxygen and Nitrogen Contamination During Arc Welding*, Proceedings of the Fifth Bolton Landing Conference, General Electric Company, August 1978, 31-41.

[11] J.J. Gullotti, A Study of Nitrogen Contamination During Submerged Arc Welding of Titanium, B.S. Thesis, M.I.T., Cambridge, Ma., 1978.

[12] J.F. Lancaster, Metallurgy of Welding: Fourth Edition, Allen & Unwin Ltd., USA, 1987.

[13] H.K.D.H. Bhadeshia, L.E. Svensson, and B. Gretoft, *Nitrogen in Submerged-Arc Weld Deposits*, Journal of Materials Science Letters 7, 1988, 610-612.

[14] T.W. Lau, M.M. Sadowski, T.H. North, and G.C. Weatherly, *Effect of Nitrogen on Properties of Submerged Arc Weld Metal*, Materials Science and Technology, Vol. 4, January 1988, 52-61.

[15] N. Mori, H. Homma, S. Okita, and K Asamo, *The behavior of B and N in Notch Toughness Improvement of Ti-B Bearing Weld Metals*, IIW Document IX-1158-80, International Institute of Welding, 1980.

[16] R. Okabe, N. Koshizuka, M. Tanaka, A. Katamine, and Y. Sannomiya, Transactions Iron Steel Institute, Japan, 1983, 23.

[17] M. Nakanishi, Y. Ito, and Y. Komizo, Sumitomo Search, 1979, 52.

[18] R.B. Oldland, Ph.D Thesis, Monash University, Australia, 1985.

[19] G. Den-Ouden, J.G. Verhagen, and G.W. Tichelaar, Welding Journal, 1975, 54.

[20] Y. Horii and K. Maiaki, Proceedings of the 4th International Symposium, Osaka, Japan, 1982, Japan Welding Society, 553.

[21] A.O. Oladipupo, Metallurgical Factors Influencing Charpy Energy of Submerged Arc Welded HY-80 Steel, S.M. Thesis, M.I.T. Cambridge, Ma., 1984.

[22] J.K. Brownlee, Effects of Aluminum and Titanium on the Microstructure and Properties of Microalloyed Steel Weld Metal, S.M. Thesis, Colorado School of Mines, Co., 1985.

[23] T. Lau, J. Burkhardt, T.H. North, and G. L'Esperance, *Effect of Aluminum on the Ti-O-B-N Balance in Submerged Arc Welding*, Welding Journal, August 1988, 25-30.

[24] R. Farrar and P. Harrison, *Microstructural Development and Toughness of C-Mn and C-Mn-Ni Weld Metals Part II - Toughness*, Metal Construction, August 1987, 39-42.

[25] J.P. Snyder II and A.W. Pense, *The Effects of Titanium on Submerged Arc Weld Metal*, Welding Research Supplement, July 1982, 201-211.

[26] N.A. Fleck II, The Effect of Filler Wire and Flux Compositions on the Microstructure and Properties of Microalloyed Steel Weld Metal, S.M. Thesis, Colorado School of Mines, Co., 1984.

[27] D.K. Matlock and G.R. Edwards, *The Metallurgy of HSLA Weld Metal Produced by the Submerged Arc Process; Semiannual Technical Report*, Department of the Navy, Office of Naval Research, Contract No. N00014-83-K-0779, March 1985.

[28] O. Grong and D.K. Matlock, *Microstructure Development in Mild and Low Alloy Steel Weld Metals*, International Metallurgical Reviews, Vol. 31 (1).

[29] H. Ikawa, H. Oshige, and T. Tanoue, *Effects of Martesite-Austenite Constituent on HAZ Toughness of a High Strength Steel*, Transactions of the Japan Welding Society, Vol. II (2), October 1980, 50-59.

[30] V. Biss and R.L. Cryderman, *Martensite and Retained Austenite in Hot-Rolled, Low-Carbon Bainitic Steels*, Metallurgical Transactions, Vol. 2, August 1971, 2267-2276.

[31] J.H. Chen, Y Kikuta, T. Araki, M. Yoneda, and Y. Matsuda, *Micro-fracture Behavior Induced by M-A Constituent (Island Martensite) in Simulated Welding Heat Affected Zone of HT80 High Strength Low Alloyed Steel*, Acta Metallurgica, Vol. 32 (10), 1984, 1779-1788.

[32] American Society for Metals, Metals Handbook: Ninth Edition, Vol. 9, Metallography and Microstructures, USA, 1986, 52-60 and 123-134.

[33] H. Suzuki, *Carbon Equivalent and Maximum Hardness*, Transactions of the Japan Welding Society, Vol. 15 (1), April 1984, 25-33.

[34] ASTM Standard Designation: E562-83, *Standard Practice for Determining Volume Fraction by Systematic Manual Point Count*, 1983.

[35] R.J. Pargeter, *Acicular Ferrite and Inclusions in C-Mn Steel Weld Metals*, Welding Research Supplement, July 1986, 207-215.

[36] C. Boli and Z. Yunhong, *Effects of Manganese and Nickel on Toughness and Strength of High Strength Steel Submerged-Arc Weld Metal of σ_s=550-800 MPa*, IIW Document II-1114-88, Tsinghua University, Beijing, China, 1-7.

[37] Y. Horii, S. Ohkito, M. Wakabayashi, and M. Namura, *Study on the Toughness of Large-Heat Input Weld Metal for Low Temperature Service TMCP Steel*, Nippon Steel Technical Report No. 37, April 1988, 1-9.

[38] M.A. Munnig, Schmidt-Vanderburg, S. Hoekstra, and G. Den-Ouden, *Influence of Microstructure on Mechanical Properties of Two Single-Bead Ferritic Weld Metals*, Welding Research Supplement, March 1985, 63-70.

[39] R.B. Oldland, *The Influence of Aluminum and Nitrogen on the Microstructures and Properties of Single Pass Submerged Arc Welds*, Welding Research Aboard, Vol. XXXIII (6/7), June/July 1987, 31-43.

[40] O. Grong, A.O. Kluken, and B. Bjornbakk, *Effect of Nitrogen on Weld Metal Toughness in Self-Shielded Flux-Cored Arc Welding*, Joining and Materials, October 1988, 164-169.

[41] K. Easterling, Introduction to the Physical Metallurgy of Welding, Butterworths Monographs in Materials, Buttersworth & Co. Ltd., 1983, 10-102.

[42] P. Deb, K.D. Challenger, and A.E. Therrien, *Structure-Property Correlation of Submerged Arc and Gas-Metal Arc Weldments in HY-100 Steel*, Metallurgical Transactions, Vol. 18A, June 1987, 987-999.

[43] J. Jang and J.E. Indacochea, *Inclusion Effects on Submerged-Arc Weld Microstructure*, Journal of Materials Science, Vol. 22, 1987, 689-700.

[44] American Welding Society, Welding Handbook: Eight Edition, Vol. 1, Welding Technology, USA, 1987, 354-365.

[45] American Society for Metals, Metals Handbook: Eighth Edition, Vol. 9, Fractography and Atlas of Fractographs, USA, 1974, 49-53, 64-78 and 93-103.

[46] K.E. Dorschu and A. Lesnewich, *Development of a Filler Metal For a High Toughness Alloy Plate Steel With a Minimum Yield Strength of 140 ksi*, Welding Research Supplement, December 1964, 564s.

[47] G.L. Franke, *Submerged Arc Welding Technology for HY-100 Steel*, Department of the Navy, David Taylor Research Center, DTRC/SME-84/70, March 1985, 1-79.

APPENDIX A

Charpy Specimen Test Results

Charpy Specimen Test Results

The complete results of Charpy V-notch measurements are tabulated in this appendix. This includes tabular data for the CVN energy, lateral expansion and percent shear for each test weld. Also included are the corresponding plots for CVN energy versus test temperature and percent shear versus test temperature.

The symbols located next to some of the entries in the tabular data are used to indicate specific defects observed in the fracture surface. The definitions of these symbols are as follows:

*	Defect (pore)
**	Defect (transverse split or crack)
***	Gross defect
(#)	Charpy specimen did not break when tested

Table A.1 CVN energy data for weld #1.

Temperature (°F)	Energy (ft-lbs)	Average Energy (ft-lbs)
-180	10	16
-180	22	
-120	36	33
-120	30	
-60	60	53
-60	48	
-60	50	
0	72	69
0	66	
0	70	
60	85	85
60	85	
120	96	93.5
120	91	
180	81	83.5
180	86	

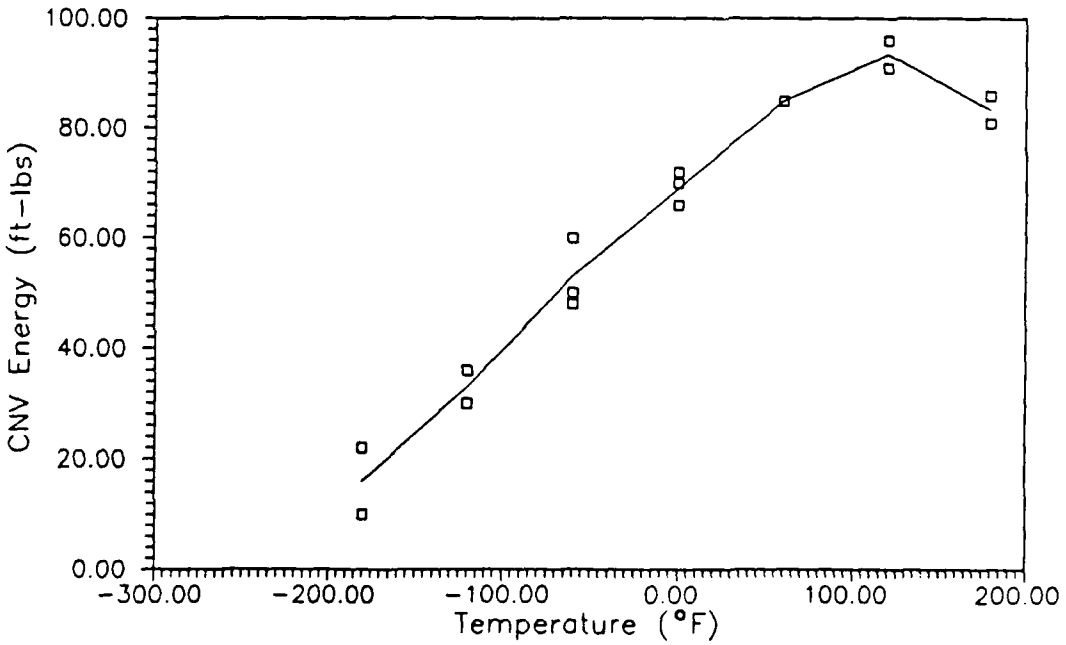

Figure A.1 Temperature versus the CVN energy for weld #1.

Table A.2 CVN lateral expansion and percent shear data for weld #1.

Temperature (°F)	Lateral Exp. (mils)	Shear (%)	Average Shear (%)
-180	8	10	10
-180	9	10	
-120	19	30	25
-120	20	20	
-60	28	70	63
-60	35	70	
-60	33	50	
0	35	90	83
0	45	80	
0	47	80	
60	42	95	92.5
60	50	90	
120	42	95	95
120	63	95	
180	49	100	100
180	52	100	

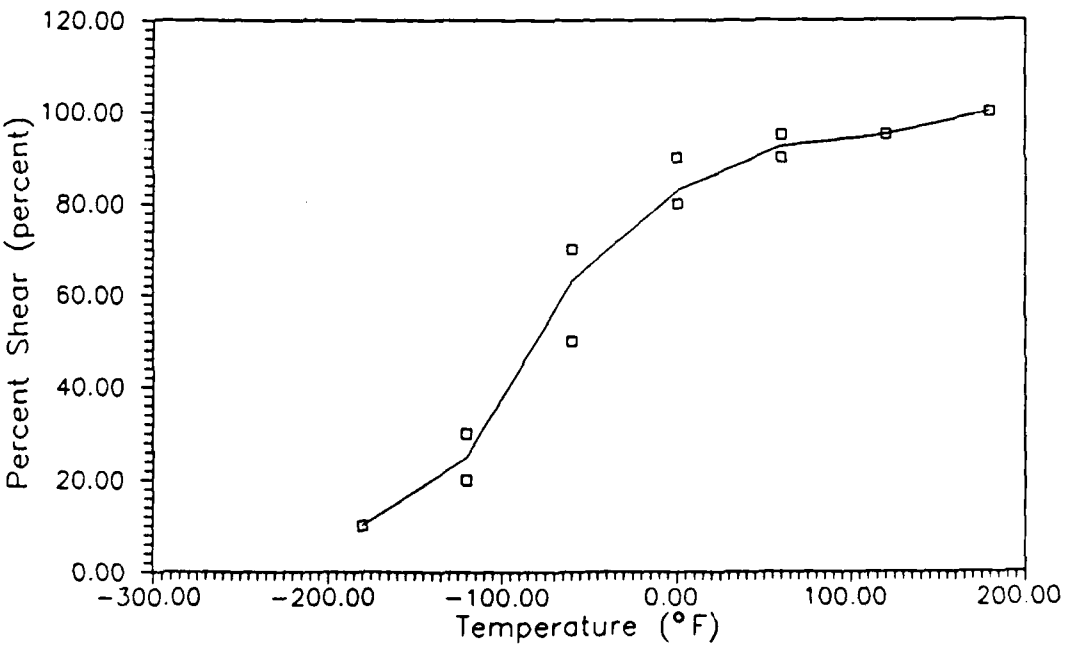

Figure A.2 Temperature versus the percent shear for weld #1.

Table A.3 CVN energy data for weld #2.

Temperature (°F)	Energy (ft-lbs)	Average Energy (ft-lbs)
-180	12	12
-120	16	18
-120	20	
-60	37	44
-60	55	
-60	39	
0	66	62
0	59	
0	62	
60	71	67
60	68	
60	63	
120	75	78.5
120	82	
180	74	74

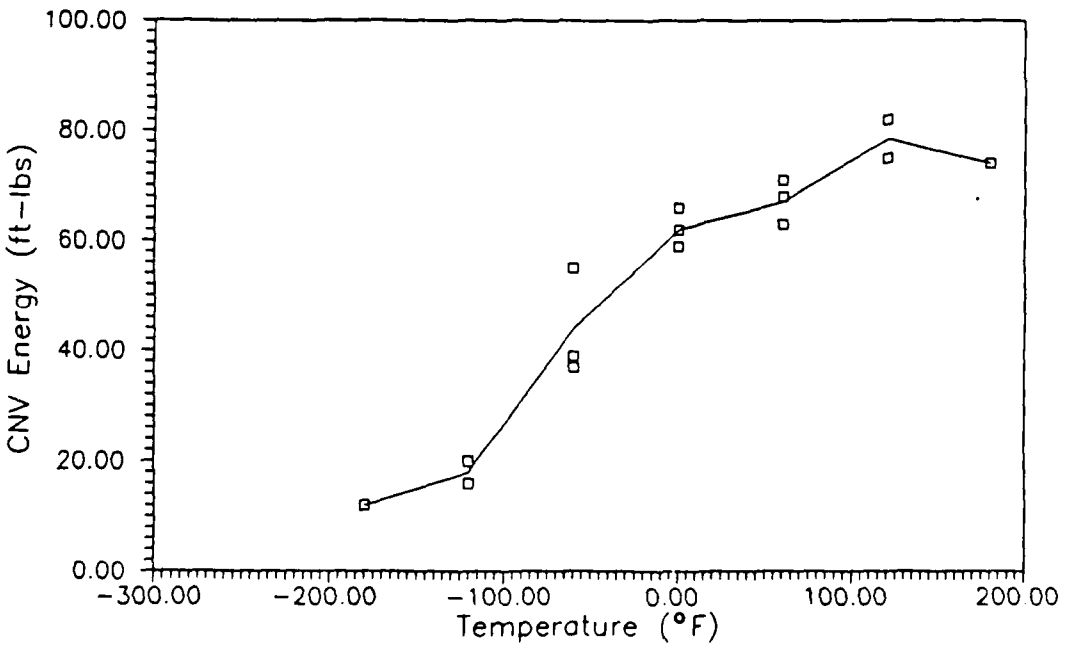

Figure A.3 Temperature versus the CVN energy for weld #2.

Table A.4 CVN lateral expansion and percent shear data for weld #2.

Temperature (°F)	Lateral Exp. (mils)	Shear (%)	Average Shear (%)
-180	15	10	10
-120	7	10	10
-120	15	10	
-60	23	30	33
-60	22	40	
-60	30	30	
0	51	90	83
0	30	80	
0	41	80	
60	53	90	92
60	51	90	
60	38	95	
120	54	100	100
120	40	100	
180	39	100	100

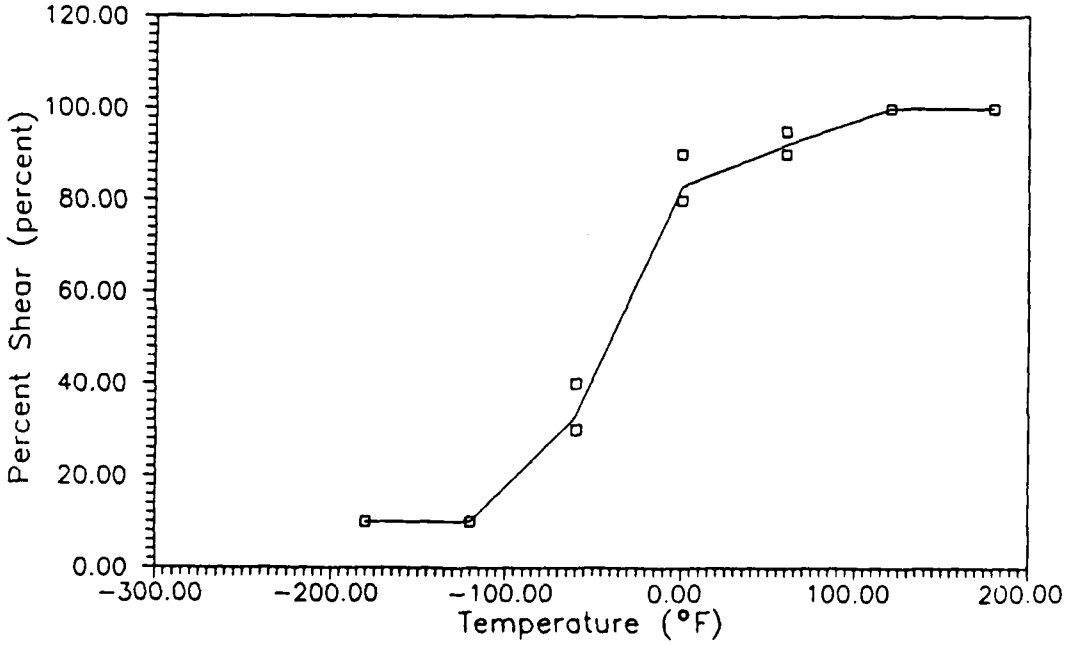

Figure A.4 Temperature versus the percent shear for weld #2.

Table A.5 CVN energy data for weld #3.

Temperature (°F)	Energy (ft-lbs)	Average Energy (ft-lbs)
-180	8	8
-120	15	17.5
-120	20	
-60	25	28
-60	23	
-60	22	
-60	42	
0	67	58
0	56	
0	50*	
60	76	76
60	71	
60	82	
120	70	75
120	80	
180	77	77

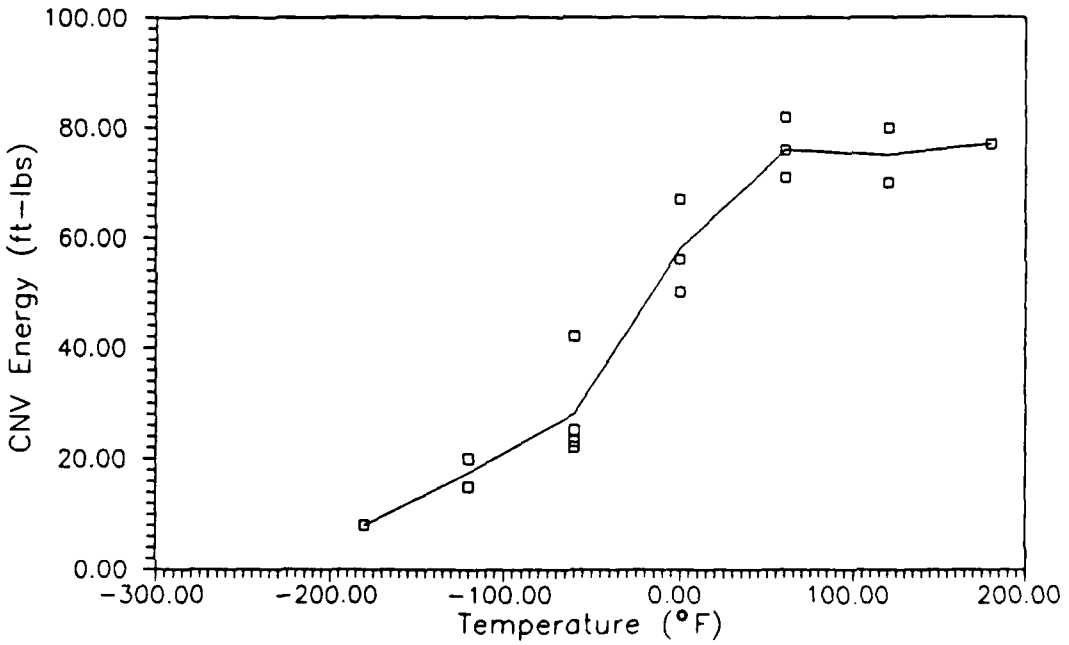

Figure A.5 Temperature versus the CVN energy for weld #3.

Table A.6 CVN lateral expansion and percent shear data for weld #3.

Temperature (°F)	Lateral Exp. (mils)	Shear (%)	Average Shear (%)
-180	0	5	5
-120	10	30	30
-120	23	30	
-60	19	40	42.5
-60	17	40	
-60	20	30	
-60	34	60	
0	47	80	80
0	42	80	
0	49	80*	
60	52	90	93
60	55	95	
60	58	95	
120	54	100	100
120	67	100	
180	55	100	100

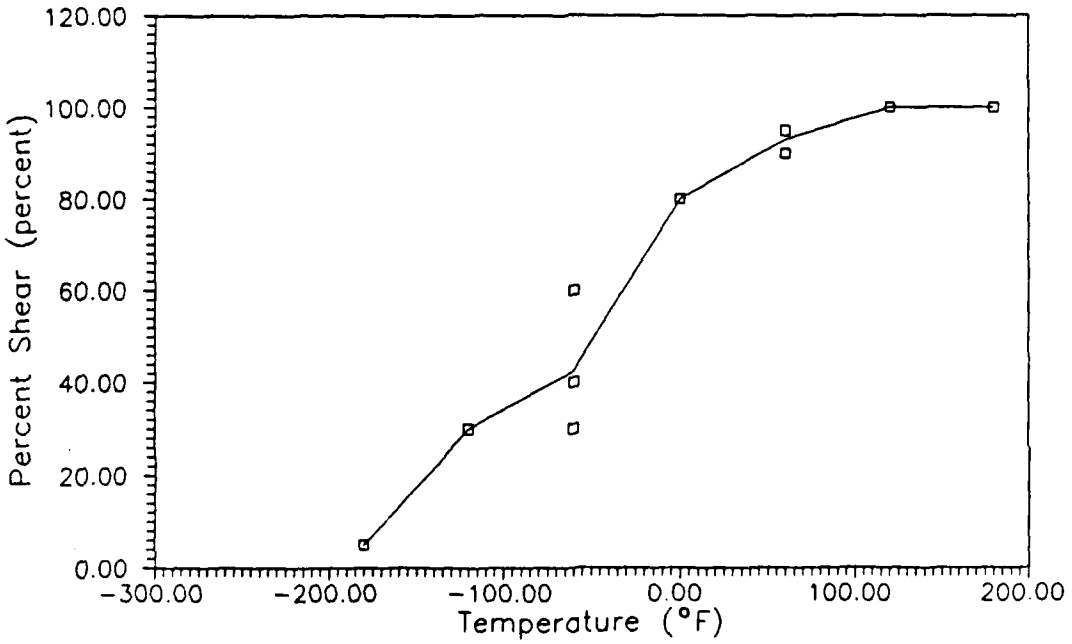

Figure A.6 Temperature versus the percent shear for weld #3.

Table A.7 CVN energy data for weld #4.

Temperature (°F)	Energy (ft-lbs)	Average Energy (ft-lbs)
-180	8	8
-120	9	11
-120	10	
-120	13	
-60	43	29
-60	24	
-60	25	
-60	23	
0	56	52
0	55	
0	46	
60	68	67
60	65	
60	69	
120	78	75
120	66	
120	80	
180	80	80

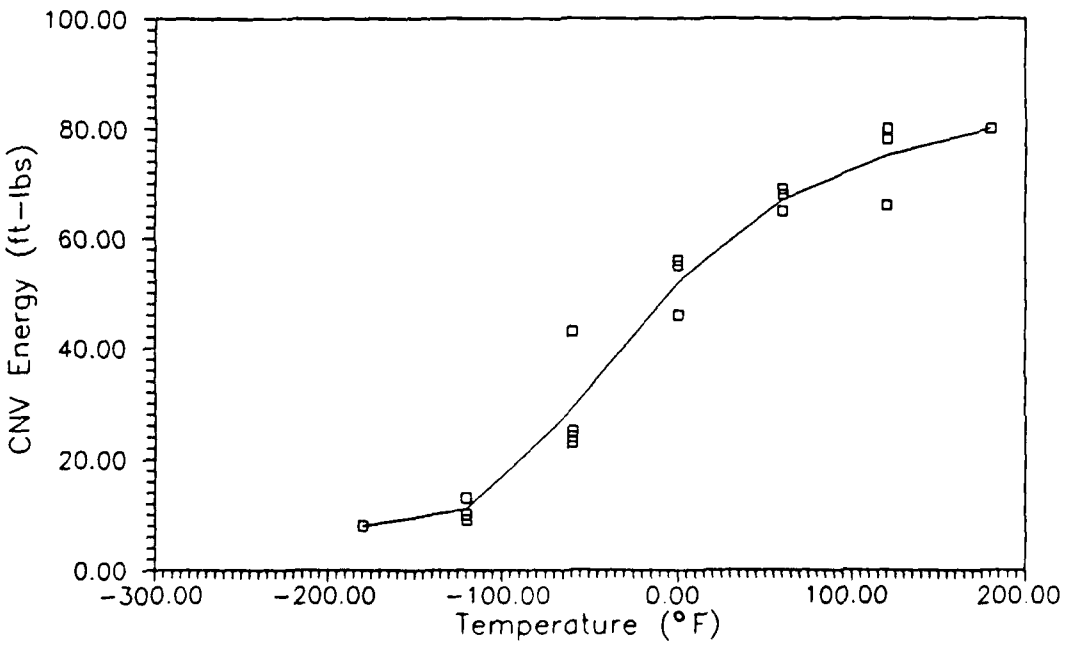

Figure A.7 Temperature versus the CVN energy for weld #4.

Table A.8 CVN lateral expansion and percent shear data for weld #4.

Temperature (°F)	Lateral Exp. (mils)	Shear (%)	Average Shear (%)
-180	0	5	5
-120	12	20	20
-120	6	10	
-120	9	30	
-60	17	40	50
-60	25	70	
-60	18	40	
-60	18	50	
0	38	80	80
0	37	80	
0	35	80	
60	44	95	95
60	51	90	
60	35	100	
120	32	100	100
120	52	100	
120	61	100	
180	55	100	100

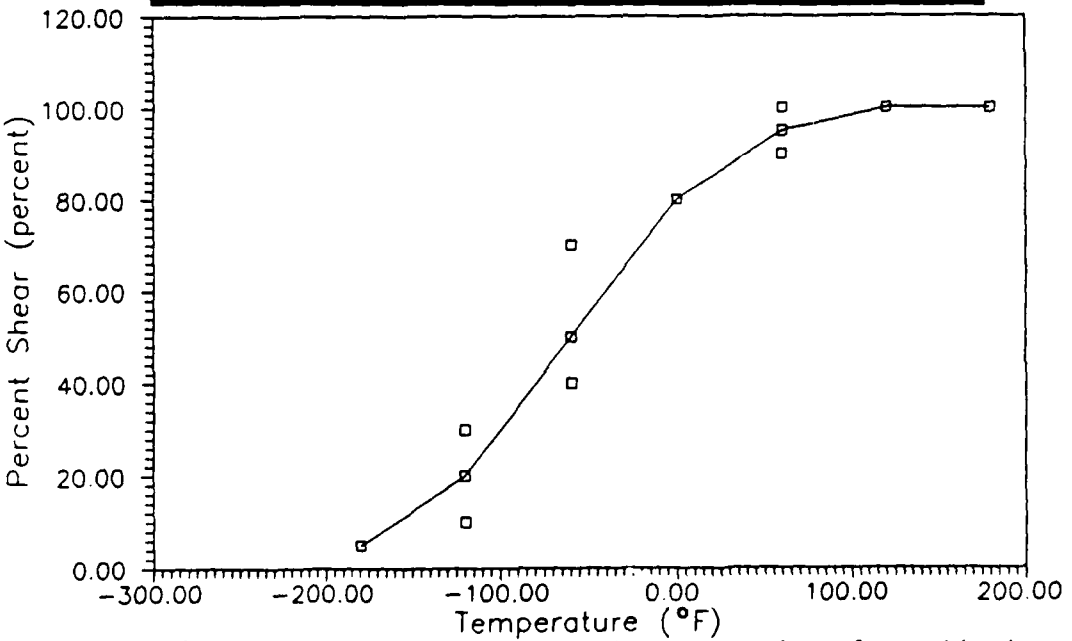

Figure A.8 Temperature versus the percent shear for weld #4.

Table A.9 CVN energy data for weld #5.

Temperature (°F)	Energy (ft-lbs)	Average Energy (ft-lbs)
-180	8	8
-120	9	9.5
-120	10	
-60	19	18
-60	20	
-60	15	
0	37	29
0	27	
0	24	
60	49	48
60	41	
60	55	
120	63	63
120	57	
120	70*	
180	68	60
180	52	

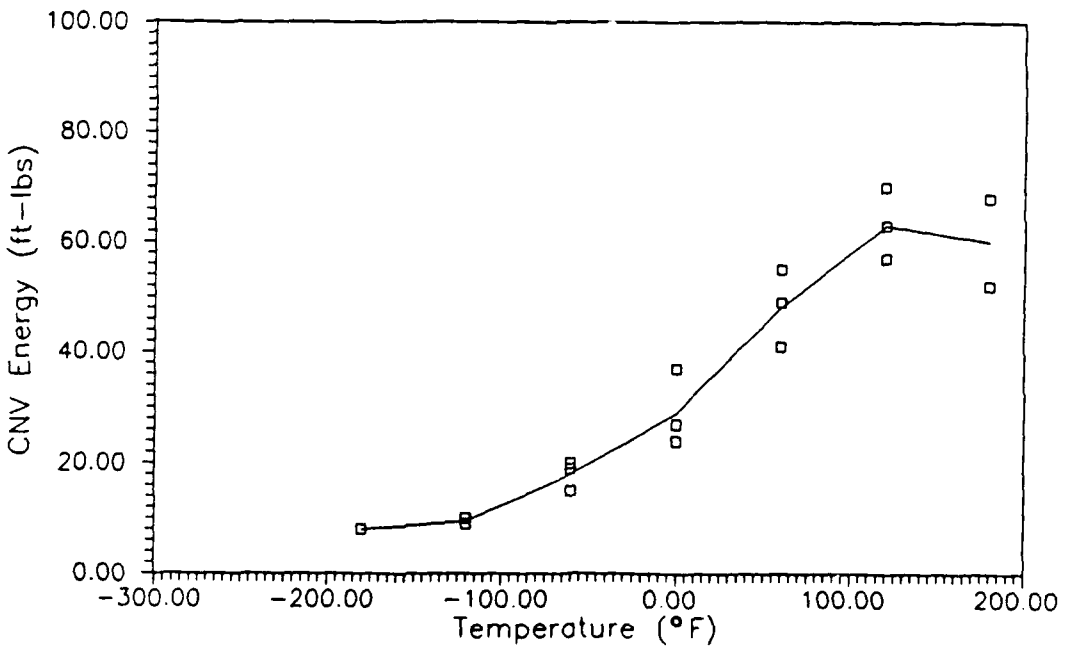

Figure A.9 Temperature versus the CVN energy for weld #5.

Table A.10 CVN lateral expansion and percent shear data for weld #5.

Temperature (°F)	Lateral Exp. (mils)	Shear (%)	Average Shear (%)
-180	0	5	5
-120	6	20	15
-120	7	10	
-60	12	40	37
-60	12	40	
-60	3	30	
0	24	50	47
0	18	40	
0	15	50	
60	31	80	77
60	21	70	
60	40	80	
120	44	95	97.5
120	30	95	
120	49	100*	
180	49	100	100
180	36	100	

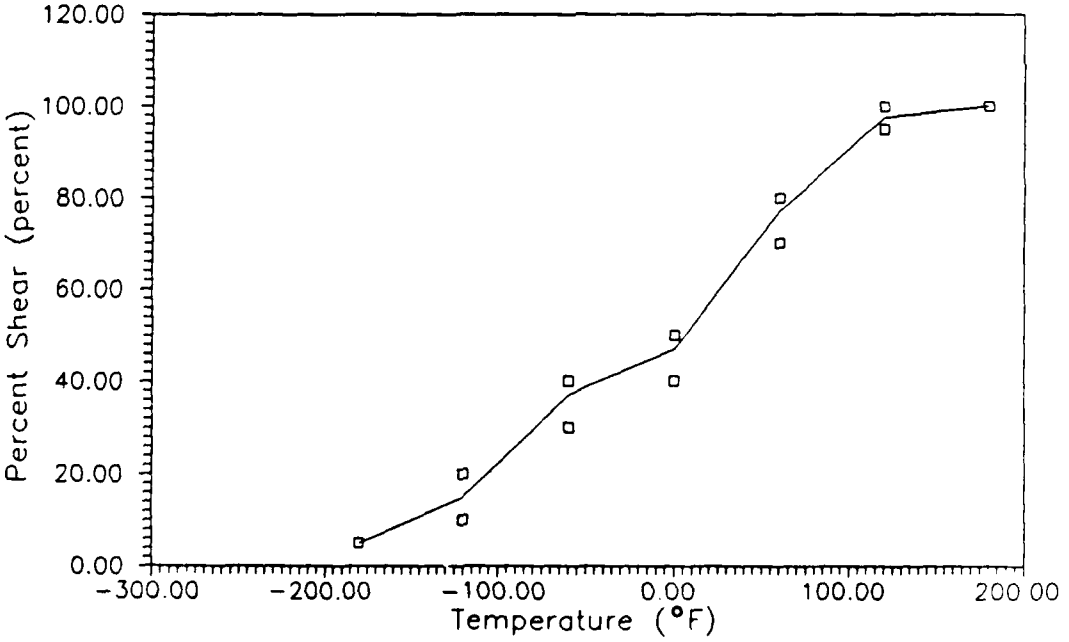

Figure A.10 Temperature versus the percent shear for weld #5.

Table A.11 CVN energy data for weld #6.

Temperature (°F)	Energy (ft-lbs)	Average Energy (ft-lbs)
-120	5*	5
-60	15	16
-60	17	
-60	82*	
0	23	21
0	27	
0	14*	
60	30*	31
60	32	
120	43*	43
120	43	
180	42	42

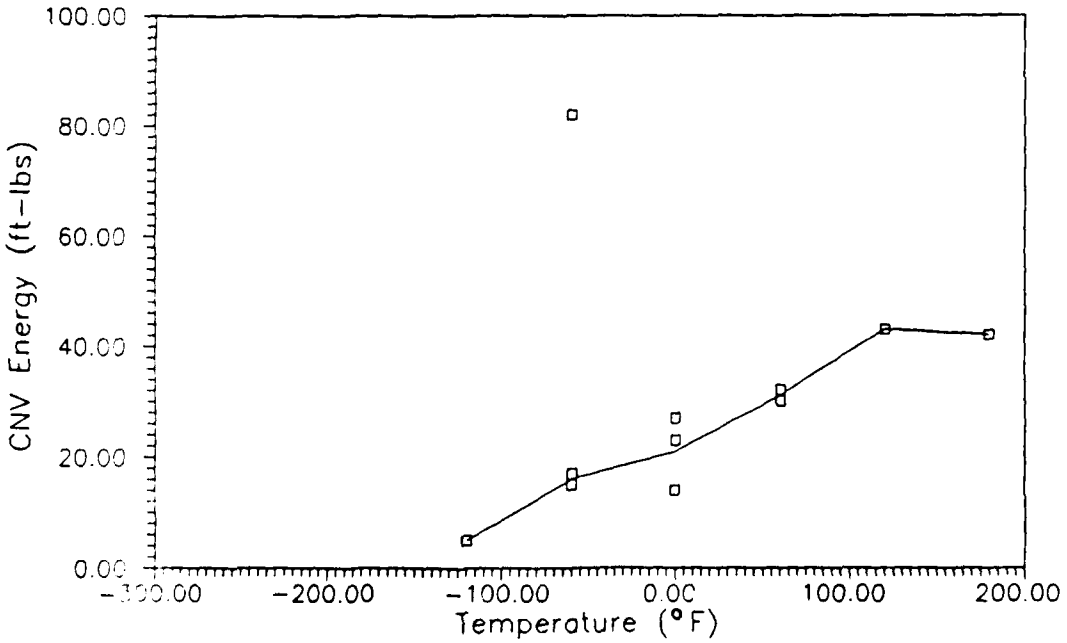

Figure A.11 Temperature versus the CVN energy for weld #6.

Table A.12 CVN lateral expansion and percent shear data for weld #6.

Temperature (°F)	Lateral Exp. (mils)	Shear (%)	Average Shear (%)
-120	6	10*	10
-60	8	20	30
-60	20	40	
-60	32	*	
0	19	40	37
0	16	50	
0	18	20*	
60	20	60*	70
60	27	80	
120	22	*	95
120	31	95	
180	31	100	100

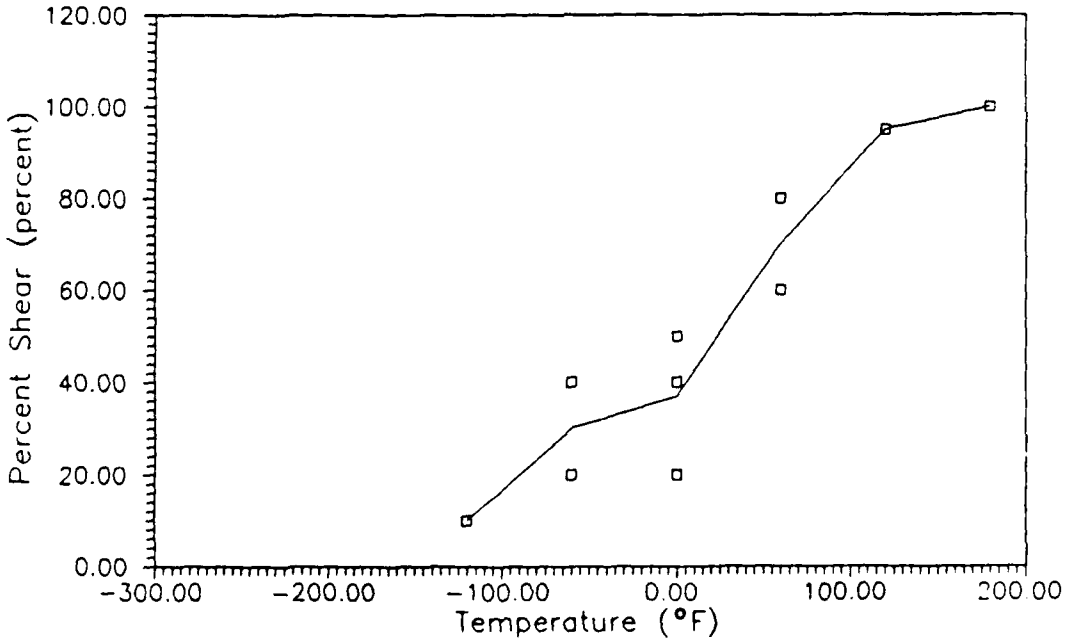

Figure A.12 Temperature versus the percent shear for weld #6.

Table A.13 CVN energy data for weld #7.

Temperature (°F)	Energy (ft-lbs)	Average Energy (ft-lbs)
-180	6	6
-120	16	18.5
-120	21	
-60	39	38.5
-60	48	
-60	23	
-60	44	
0	60***	63
0	64	
0	64	
60	71	72
60	68	
60	76	
120	71	75
120	75	
120	78	
180	78	65
180	52	

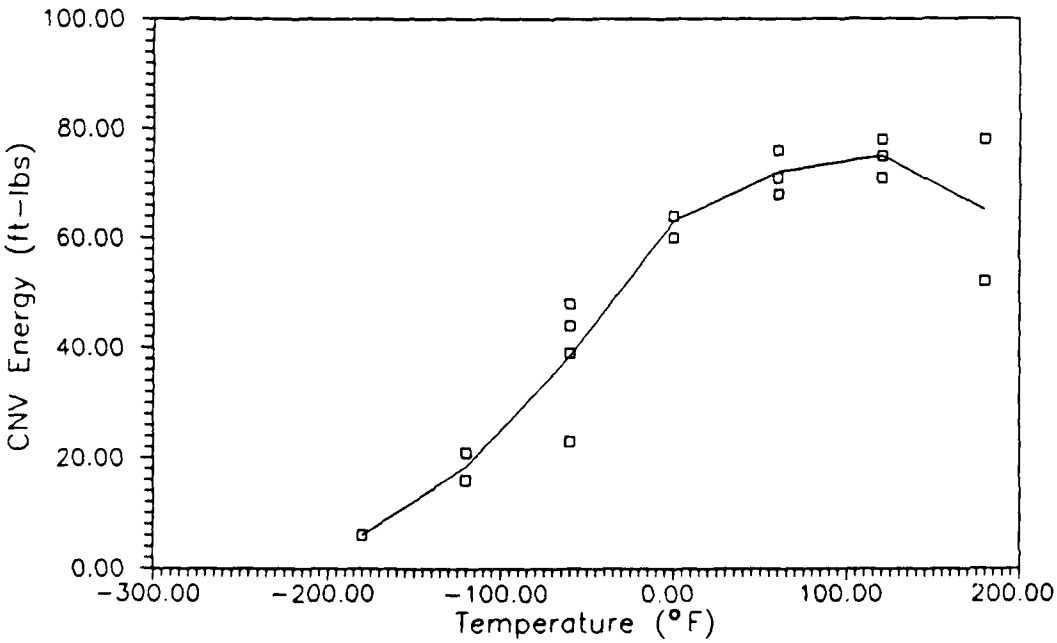

Figure A.13 Temperature versus the CVN energy for weld #7.

Table A.14 CVN lateral expansion and percent shear data for weld #7.

Temperature (°F)	Lateral Exp. (mils)	Shear (%)	Average Shear (%)
-180	6	0	5
-120	12	20	20
-120	16	20	
-60	20	50	55
-60	34	50	
-60	20	50	
-60	30	70	
0	38	80***	83
0	32	90	
0	40	80	
60	47	100	100
60	50	100	
60	45	100	
120	54	100	98
120	46	100	
120	44	95	
180	59	100	100
180	48	100	

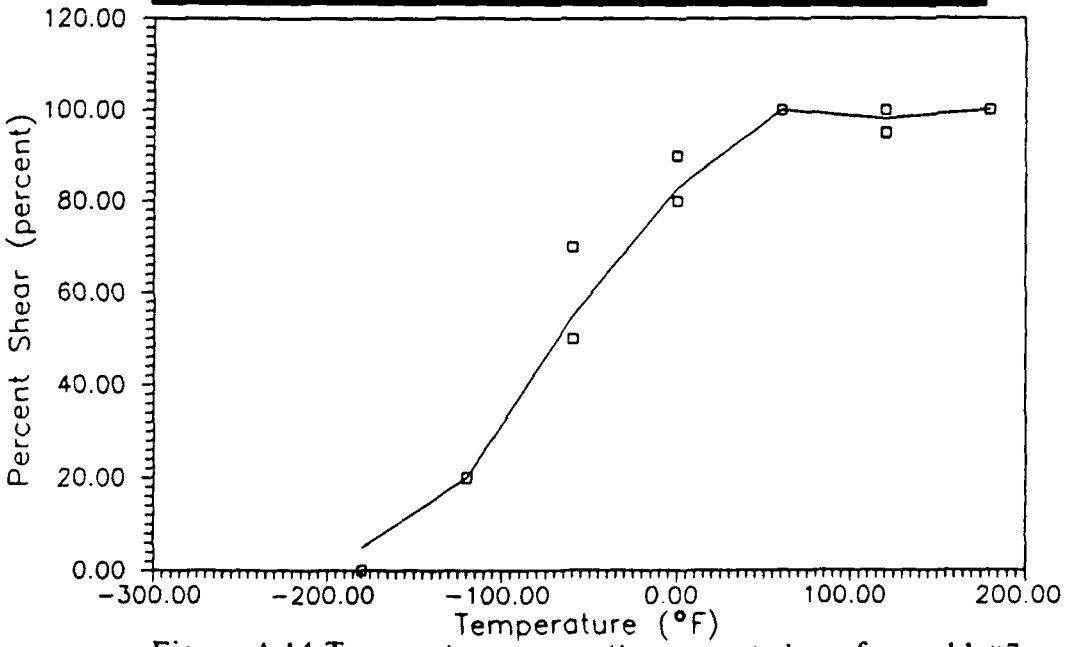

Figure A.14 Temperature versus the percent shear for weld #7.

Table A.15 CVN energy data for weld #8.

Temperature (°F)	Energy (ft-lbs)	Average Energy (ft-lbs)
-180	11	11
-120	21	21.5
-120	22	
-60	42	38
-60	37	
-60	35	
0	53	59
0	68	
0	56**	
60	60	65.5
60	71	
120	73	71.5
120	70	
180	73	73

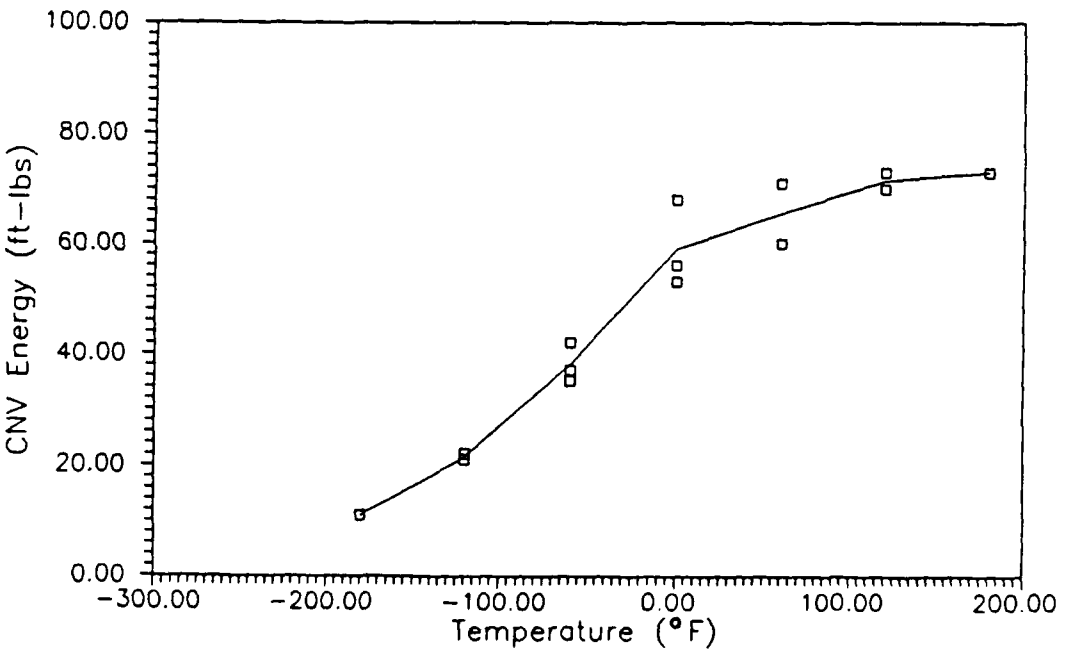

Figure A.15 Temperature versus the CVN energy for weld #8.

Table A.16 CVN lateral expansion and percent shear data for weld #8.

Temperature (°F)	Lateral Exp. (mils)	Shear (%)	Average Shear (%)
-180	2	0	0
-120	12	20	25
-120	16	30	
-60	32	50	47
-60	28	40	
-60	29	50	
0	50	95	88
0	48	90	
0	36	80**	
60	40	100	100
60	48	100	
120	56	100	100
120	53	100	
180	52	100	100

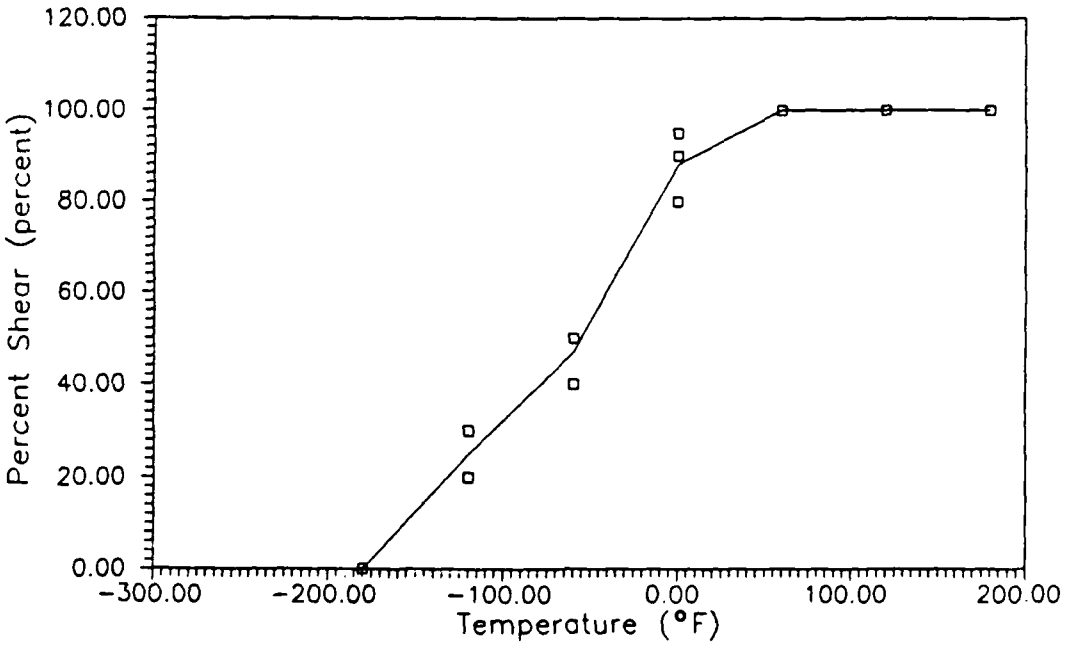

Figure A.16 Temperature versus the percent shear for weld #8.

Table A.17 CVN energy data for weld #9.

Temperature (°F)	Energy (ft-lbs)	Average Energy (ft-lbs)
-120	8	8
-60	36**	26
-60	59**	
-60	27	
-60	25	
0	219**	29
0	129**	
0	29	
0	4***	
60	96**	64
60	32**	
120	59	59
120	118**	

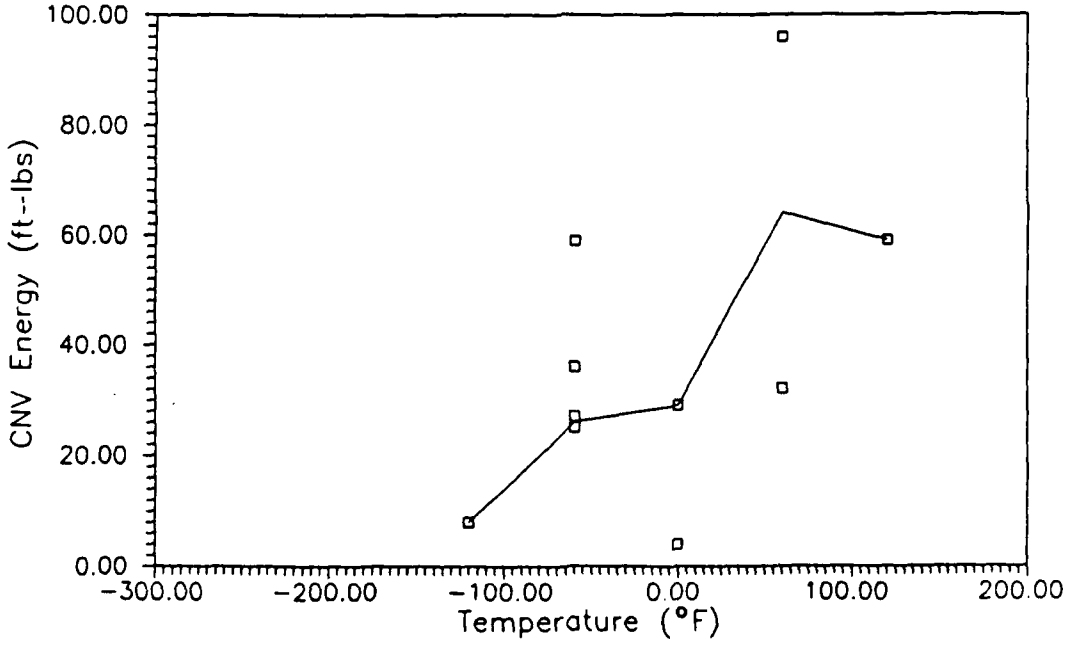

Figure A.17 Temperature versus the CVN energy for weld #9.

Table A.18 CVN lateral expansion and percent shear data for weld #9.

Temperature (°F)	Lateral Exp. (mils)	Shear (%)	Average Shear (%)
-120	9	10	10
-60	27	30**	23
-60	12	10**	
-60	22	30	
-60	10	** (#)	
0	85	**	50
0	53	**	
0	20	50	
0	11	** (#)	
60	63	80**	80
60	26	**	
120	46	100	100
120	83	**	

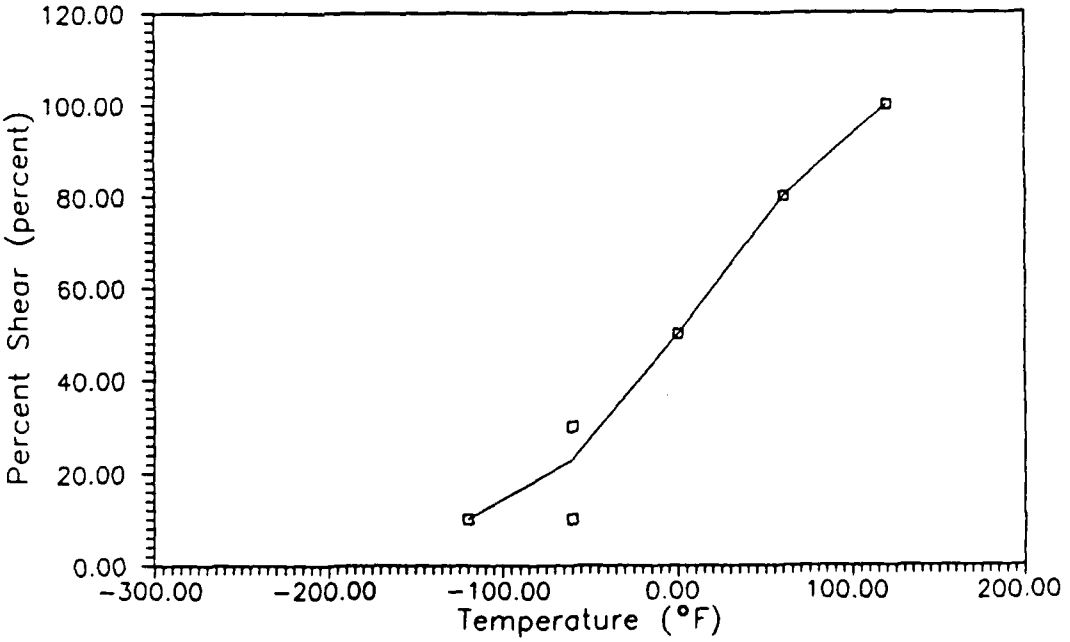

Figure A.18 Temperature versus the percent shear for weld #9.

Table A.19 CVN energy data for weld #10.

Temperature (°F)	Energy (ft-lbs)	Average Energy (ft-lbs)
-180	5*	5
-120	10**	10
-60	16	17
-60	17**	
-60	18	
0	79**	30
0	36	
0	48**	
0	24	
0	44**	
60	50	56.5
60	63	
120	53	56.5
120	60	
180	56	56

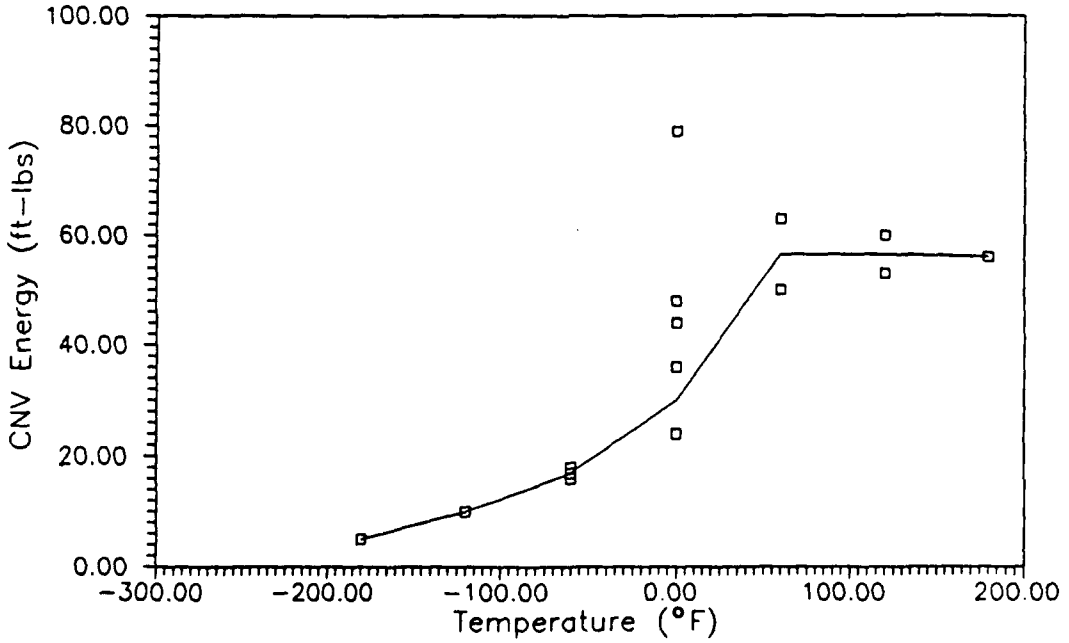

Figure A.19 Temperature versus the CVN energy for weld #10.

Table A.20 CVN lateral expansion and percent shear data for weld #10.

Temperature (°F)	Lateral Exp. (mils)	Shear (%)	Average Shear (%)
-180	0	0*	0
-120	5	10**	10
-60	14	20	25
-60	17	30**	
-60	18	30	
0	47	**	35
0	23	40	
0	34	90**	
0	15	30	
0	38	***	
60	21	80	85
60	42	90	
120	21	95	95
120	26	95	
180	42	100	100

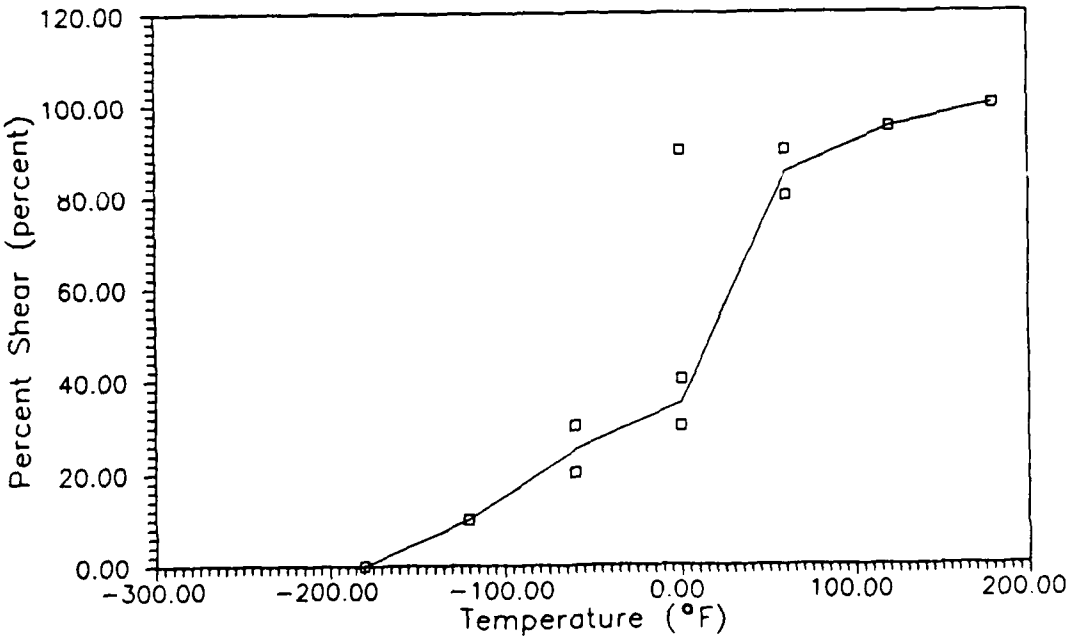

Figure A.20 Temperature versus the percent shear for weld #10.